Detection limits of tidal-wetland sequences to identify variable rupture modes of megathrust earthquakes

Ian Shennan[1]*, Ed Garrett[1,2] , Natasha Barlow[1]

[1] Sea Level Research Unit, Department of Geography, Durham University, Durham, DH1 3LE, UK

[2] Geological Survey of Belgium, Royal Belgian Institute of Natural Sciences, Rue Jenner, Brussels 1000, Belgium

* Corresponding author ian.shennan@durham.ac.uk

ABSTRACT

Recent paleoseismological studies question whether segment boundaries identified for 20th and 21st century great, >M8, earthquakes persist through multiple earthquake cycles or whether smaller segments with different boundaries rupture and cause significant hazards. The smaller segments may include some currently slipping rather than locked. In this review, we outline general principles regarding indicators of relative sea-level change in tidal wetlands and the conditions in which paleoseismic indicators must be distinct from those resulting from non-seismic processes. We present new evidence from sites across southcentral Alaska to illustrate different detection limits of paleoseismic indicators and consider alternative interpretations for marsh submergence and emergence. We compare predictions of coseismic uplift and subsidence derived from geophysical models of earthquakes with different rupture modes. The spatial patterns of agreement and misfits between model predictions and quantitative reconstructions of coseismic submergence and emergence suggest that no earthquake within the last 4000 years had a pattern of rupture the same as the Mw 9.2 Alaska earthquake in 1964. From the Alaska examples and research from other subduction zones we suggest that If we want to understand whether a megathrust ruptures in segments of variable length in different earthquakes, we need to be site-specific as to what sort of geological-based criteria eliminate the possibility of a particular rupture mode in different earthquakes. We conclude that coastal paleoseismological studies benefit from a methodological framework that employs rigorous evaluation of five essential criteria and a sixth which may be very robust but only occur at some sites: 1 – lateral extent of peat-mud or mud-peat couplets with sharp contacts; 2 – suddenness of submergence or emergence, and replicated within each site; 3 – amount of vertical motion, quantified with 95% error terms and replicated within each site; 4 – syncroneity of submergence and emergence based on statistical age modelling; 5 – spatial pattern of submergence and emergence; 6 – possible additional evidence, such as evidence of a tsunami or

liquefaction concurrent with submergence or emergence. We suggest that it is possible to consider detection limits as low as 0.1 to 0.2 m coseismic vertical change.

0. Introduction and structure of the paper

Coastal paleoseismology provides critical information that helps to improve understanding and modelling of seismic hazards, including associated tsunami, at all major subduction zones. Key contributions to practical earthquake hazard assessment include the identification of great (magnitude 8 or 9) earthquakes during the Holocene where there is no historical record (Atwater, 1987); earthquakes of substantially greater magnitude than directly observed (Minoura et al., 2001; Sawai et al., 2008); estimating recurrence intervals of great earthquakes (Atwater and Hemphill-Haley, 1997; Nelson et al., 1995); and defining different patterns of rupture along a subduction zone (Cisternas et al., 2005; Kelsey et al., 2002; Nelson et al., 2006; Sawai et al., 2004). Since publication of the seminal paper (Atwater, 1987), and widespread adoption of well-tested field and analytical methods (e.g. Atwater and Hemphill-Haley, 1997; Hayward et al., 2006; Kelsey, 2015; Nelson, 2015; Nelson et al., 1996; Witter, 2015) debate moved on to questions critical for hazard assessment, emergency planning and international building code design (Mueller et al., 2015; Wesson et al., 2007). Key questions include the extent of past great earthquake ruptures (a proxy for magnitude), the identification of the boundaries between rupture segments, the persistence of these boundaries over multiple earthquake cycles, recurrence intervals of great earthquakes in each segment, the role of aseismic slip, and whether segments of plate boundaries that are currently creeping can generate great earthquakes (Briggs et al., 2014; Goldfinger et al., 2012; Hayward et al., 2015; Kelsey et al., 2015; Mueller et al., 2015; Scholz, 2014; Witter et al., 2014).

In order to address these questions, coastal paleoseismology continues to seek evidence to discriminate between alternative hypotheses. This inevitably results in returning to the field evidence and the quantifiable resolution of the age, the extent, and the pattern of vertical surface displacement of each rupture. Tidal wetlands record evidence of relative sea-level change, whether submergence or emergence. Such evidence may reflect coseismic displacement of the Earth's crust, but this requires an evaluation of the evidence leading to one or more interpretations. Submergence is not a synonym for subsidence, or emergence for uplift. Typically, in areas of coseismic subsidence, freshwater peat rapidly submerges into the intertidal zone (Figure 1). This results in a peat-mud couplet, with a sharp boundary between the units (Atwater, 1987). In areas of coseismic uplift, where clastic tidal flat emerges above the local high tide limit, freshwater peat starts to form. This results in a mud-peat couplet, also with a sharp boundary (Figure 1). As the amount of coseismic surface displacement decreases, for example towards the periphery of uplift or subsidence, we expect to reach the point at which a line of evidence cannot distinguish between seismic and non-seismic explanations for the field stratigraphy. This is the detection limit for that type of evidence.

Similarly, the resolution of radiocarbon dating places an uncertainty on earthquake ages and correlations between sites.

With different interpretations possible from seemingly similar stratigraphic sequences, Nelson et al. (1996) suggested five criteria to distinguish peat-mud couplets that result from great earthquake subsidence from those produced by other processes. They suggested, 1 - lateral extent of peat-mud couplets with sharp contacts; 2 - suddenness of submergence; 3 - amount of vertical motion; 4 - presence of tsunami deposited sediments directly above the peat horizon, and, 5 - synchroneity with other sites. While these criteria were proposed with respect to tidal marsh sequences adjacent to the Cascadia subduction zone, they have proved valuable for numerous studies since (e.g. Briggs et al., 2014; Clark et al., 2015; Dura et al., 2015; Dura et al., 2016; Dura et al., 2011; Engelhart et al., 2013; Garrett et al., 2015b; Grand Pre et al., 2012; Hamilton and Shennan, 2005a; Hayward et al., 2015; Kelsey et al., 2015; Leonard et al., 2004; McCalpin and Carver, 2009; Nelson et al., 2009; Nelson et al., 2006; Shennan et al., 2009; Witter et al., 2003).

In this review, we first introduce general principles regarding indicators of relative sea-level change in tidal wetlands and the conditions in which paleoseismic indicators must be distinct from those resulting from non-seismic processes.

Section 2 summarises the tectonic setting and Holocene chronology of great earthquakes in the region of the 1964 Alaska M_w9.2 earthquake since we use evidence from this region to revisit the criteria recommended by Nelson et al. (1996) for identifying coseismic subsidence and use the evidence to test working hypothesis of variable rupture modes during the late Holocene.

In section 3, we consider developments over the past 20 years in popular methods of reconstructing relative sea-level change and their application to paleoseismic records from tidal wetlands.

Section 4 presents evidence from sites across southcentral Alaska to illustrate different detection limits and how these constrain alternative interpretations for marsh submergence and emergence. In section 5, we evaluate the predicted surface displacement of different rupture modes against the reconstructions of marsh submergence and emergence based on field data.

In the final sections, we consider the broader implications of detection limits of tidal wetland sequences at subduction zones around the world and suggest an expansion of the Nelson et al. (1996) criteria.

1. Indicators of coseismic displacement of tidal wetlands

The detection limits of tidal wetland sediment sequences that produce identifiable paleoseismic evidence depend upon two critical thresholds for each type of indicator that records relative sea-

level change: creation thresholds and preservation thresholds (McCalpin and Nelson, 2009). To exceed creation thresholds, paleoseismic indicators must be distinct from similar indicators that may result from non-seismic processes. We can formulate this in a general equation. For each geographical location (φ) the change in relative sea level (ΔRSL) at time t, where t is the time relative to present (Shennan et al., 2011):

$$\Delta RSL(\varphi,t) = \Delta EUS(t) + \Delta ISO(\varphi,t) + \Delta TECT(\varphi,t) + \Delta LOCAL(\varphi,t) + \Delta UNSP(\varphi,t) \quad [1]$$

- ΔEUS(t) is the time-dependent eustatic sea level, derived from a model of global ice history, that would result by distributing any meltwater evenly across a rigid, non-rotating planet and neglecting self-gravitation in the surface load.
- ΔISO(φ,t) is the total isostatic effect of the glacial rebound process including the ice load (glacio-isostatic), water load (hydro-isostatic) and rotational contributions to the redistribution of ocean mass.
- ΔTECT(φ,t), is the tectonic effect, which includes processes operating over long timescales such as plate motions, mountain building and dynamic topography, and short term such as uplift and subsidence during great earthquakes and through the interseismic period between great earthquakes.
- ΔLOCAL(φ,t) is the total effect of local processes within the coastal system. Since we use observations from the geological record to reconstruct relative sea-level elevation we can express these as the sum of ΔTIDE(φ,t) + ΔSED(φ,t), where ΔTIDE(φ,t) is the total effect of tidal regime changes and any other influences, such as dynamic oceanographic and atmospheric effects, that may change the reference water level of a sea-level index point. ΔSED(φ,t) is the total effect of sediment consolidation since the time of deposition. Numerous studies show that this can be both a major process in coastal evolution and a key variable in reconstructing relative sea-level change from index points taken from Holocene sediments (Brain, 2015).
- ΔUNSP(φ,t) is the sum of other unspecified factors, either not quantified or not thought of. Implicitly most studies assume their total effect close to zero and random.

In order to attribute a change in relative sea level the result of coseismic or interseismic vertical land motion we must demonstrate, for the relevant timescale:

$$\Delta TECT(\varphi,t) > (\Delta EUS(t) + \Delta ISO(\varphi,t) + \Delta LOCAL(\varphi,t) + \Delta UNSP(\varphi,t)) \quad [2]$$

As areas often dominated by net sediment accumulation, tidal-wetland environments provide the potential to preserve long records of relative sea-level change and multiple subduction earthquake cycles, more than 5000 years in the case of Copper River Delta, Alaska (Carver and Plafker, 2008) and

Cascadia (Nelson et al., 2006) and 7000 years in Hawkes Bay, New Zealand (Hayward et al., 2006; Hayward et al., 2015). The characteristics of a subduction earthquake cycle vary spatially; dependent upon factors that include rates of plate motion, angle of dip, roughness of the subducting plate, trench sediment properties, rupture length and coseismic slip (Wang, 2007; Wang et al., 2012). The idea of a cycle implies no suggestion of periodicity, with neither the time between earthquakes nor their magnitude deemed a constant. Recent modelling studies using GPS data from different subduction zones at different stages in their current cycle suggest four processes comprise a subduction earthquake cycle: rupture, afterslip, mantle relaxation and relocking of the fault (Wang et al., 2012). Coseismic surface deformation is limited to near the rupture zone, with maximum subsidence above the downdip end of the rupture (location b in figure 2). Afterslip, mantle relaxation and relocking all begin immediately after the earthquake but dominate at different times. Asiesmic afterslip occurs mostly around the rupture zone (figure 2), and earthquake-induced stress causes viscous relaxation of the mantle, leading to surface deformation across a wider area in the trench-normal direction. These dominate for years to decades after the earthquake, often called the postseismic phase (Figure 2), before the fault becomes fully locked, the decades to centuries interseismic period. Determining the duration of rapid, post-seismic deformation and the relative contributions of afterslip and viscoelastic relaxation remains a challenge (Wang, 2007; Wang et al., 2012). Timescales are related to along strike rupture length, and for great earthquakes the inland area a few hundred kilometres from the trench may continue to move seawards for decades after the earthquake (location d, figure 2). Where the coast lies above the rupture zone and the afterslip zone at the downdip end, tidal marshes at different distances from the trench have the potential to record vertical deformation in different parts of the earthquake cycle, including coseismic uplift and subsidence (locations a and b respectively, figure 2), rapid postseismic changes and slower interseismic changes. Beyond the coastal zone (locations c and d, figure 2), GPS observations show post-seismic and interseismic changes cover a much wider area than the area that records coseismic motions.

Tidal-wetland sediment sequences can register vertical land motions through changes in sediment lithology and biostratigraphy. Preservation of records of multiple subduction earthquake cycles, through stacked sequences of multiple peat-mud couplets or mud-peat couplets seen in outcrop or by coring, requires certain combinations of coseismic and interseismic land motions, non-seismic relative sea-level change, sediment accumulation and sediment compaction (Figure 2).

In general, relative sea-level rise over multiple earthquake cycles enhances the potential preservation of both types of couplet (Figure 2). For example, for the preservation of multiple peat-mud couplets beneath a marsh surface, without any non-seismic (i.e. eustatic or glacio-isostatic)

relative sea-level rise, interseismic uplift must be less than coseismic subsidence unless it is offset by sediment compaction (Scenario A, figure2). Otherwise, if interseismic uplift plus compaction equals coseismic subsidence, subsequent peat layers would be super-imposed on top of one another (Scenario C). Alternatively, if interseismic uplift was greater than coseismic subsidence (resulting in net uplift during the earthquake deformation cycle), it would lead to net emergence of marshes above present with potential oxidation and decay of peat. To allow preservation of buried peat-mud couplets where there is non-seismic relative sea-level rise, interseismic uplift can be less than, or equal to coseismic subsidence (Scenario B). Preservation of stacked mud-peat couplets, recording multiple earthquake cycles with coseismic uplift requires favourable combinations of sediment compaction and Holocene sea-level rise unless interseismic subsidence is greater than coseismic uplift (Scenarios D, E, F). In addition, coastal progradation can aid the preservation of sediments recording coseismic uplift along with net emergence over thousands of years although each outcrop or borehole may only record one earthquake (Plafker et al., 1982; Shennan et al., 2009).

Two of the original criteria suggested by Nelson et al. (1996), lateral extent of peat-mud couplets with sharp contacts and suddenness of subsidence, remain widely adopted, reflecting sound geological practice. They also apply when considering evidence for coseismic uplift (Shennan, 2009; Shennan et al., 2014c; Shennan et al., 2009). For the other three criteria, amount of vertical motion, synchroneity with other sites, and presence of tsunami sediments, numerous studies since the original publication present new approaches that improve our understanding of the paleoseismic record. We aim to illustrate a number of these in the following sections and then consider additions to the original criteria.

2. Tectonic setting and plate segmentation

The 1964 Alaska M_w 9.2 earthquake was the largest in a series of five earthquakes of M_w7.9 or greater between 1938 and 1965 along the Aleutian Peninsula and the coast of southcentral Alaska that helped define models of rupture segments along the Alaska – Aleutian megathrust (Davies et al., 1981; Nishenko and Jacob, 1990). The 1964 earthquake ruptured ~950 km of the megathrust, involving two main asperities focussed on Kodiak Island and Prince William Sound (Carver and Plafker, 2008; Suito and Freymueller, 2009) and crossed the Kenai segment that is currently creeping, producing coseismic uplift towards the trench and a zone of subsidence largely to the north and northwest (Figure 3).

Paleoseismic studies of coastal sediments currently provide a long record of previous large earthquakes only for the Prince William Sound (PWS) segment, with widespread evidence of seven great earthquakes in the last 4000 years (Shennan et al., 2014b; Shennan et al., 2014c) and more

restricted evidence for three earlier ones (Carver and Plafker, 2008). Shorter and more fragmentary records from the Kenai Peninsula, the Yakataga coast and Kodiak Archipelago raise the hypothesis of different patterns of surface deformation during past great earthquakes and hence differing coseismic slip at the plate boundary (Briggs et al., 2014; Hamilton and Shennan, 2005b; Hutchinson and Crowell, 2007; Kelsey et al., 2015; Shennan et al., 2014a; Shennan et al., 2014c; Shennan et al., 2009).

A Bayesian modeling approach (Bronk Ramsey, 2009; Lienkaemper and Bronk Ramsey, 2009) determines the best-fit ages and recurrence intervals of multiple great earthquakes. It allows us to combine the ages on earthquake horizons from all sites across the Prince William Sound segment, whether they record coseismic uplift or coseismic subsidence (Shennan et al., 2014c). This constitutes a fundamental difference to previous studies that first determine the chronology at each site, then compare the patterns between sites (Carver and Plafker, 2008; Shennan and Hamilton, 2006). The best-fit model gives the age of the penultimate great earthquake as 870 ± 34 BP (2σ) with decreasing precision for each older earthquake (Figure 4). This is a function of both the number of samples available, in part reflecting the limits to coring depth, and the number of sites that record the earthquake. The oldest three earthquakes are only constrained by samples from one site (Copper River Delta) and the precision of the estimated ages is poor, ± 180 to ± 300 years. In the following section, as we assess new data we use the best-fit age model as a test of the between-site synchroneity criterion.

Recent tsunami modelling studies use the results of paleoseismic studies to develop tectonic models for a range of credible scenarios of potential tsunamigenic earthquakes (Nicolsky et al., 2013; Nicolsky et al., 2014). In addition to tectonic models of the Mw 9.2 1964 earthquake, they consider scenarios that range from Mw 8.7 or 8.8 single segment earthquakes to Mw 9.3 multi-segment earthquakes, and a variety of different slip distributions. Here we take four of their scenarios (Figure 5 and Table 1) as examples to consider the extent to which paleoseismological constraints may discriminate between different rupture modes. Their coseismic deformation model of the Mw 9.2 1964 earthquake comes from a 3-D viscoelastic model, originally described by Suito and Freymueller (2009), of simultaneous rupture of the Prince Willian Sound, Kenai and Kodiak segments, and slip on the Patton Bay splay fault. The models for the Mw 8.8 earthquakes come from two theoretical scenarios for different slip distributions, distributed across 884 to 1068 sub-faults, in the Prince William Sound and Kenai segments (Nicolsky et al., 2013). The final scenario is for a hypothetical Mw 9.3 earthquake modelled as a simultaneous rupture of the Prince William Sound, Kenai and Kodiak segments, the western part of the Yakutat microplate and the Patton Bay splay fault (Nicolsky et al., 2013; Suito and Freymueller, 2009).

3. Approaches to reconstructing relative sea-level change, marsh submergence and emergence

Virtually all tidal-wetland paleoseismology studies use coastal morphology and sediment exposures or sediment cores to provide evidence of relative sea-level change, whether caused by seismic processes or not, and AMS radiocarbon dating of in situ herbaceous macrofossils, wood or shells to provide a chronology for each site. Many use microfossil evidence to provide either qualitative or quantitative estimates of the vertical motion, with quantitative approaches commonly based on transfer function methods.

Interest in the use of microfossil analyses within coastal paleoseismology developed quickly in the years following Atwater's 1987 paper, applying the approaches honed to study non-seismic relative sea-level change in numerous regions. At that time, such studies of relative sea-level change still used qualitative approaches in assessing microfossil evidence, many influenced by the meticulous work of Tooley (1974, 1976, 1978). These studies typically described changes in assemblages of pollen, diatoms or foraminifera in stratigraphic sequences and presented qualitative interpretations of relative sea-level change. In order to aid readers not familiar with taxonomy or ecology, authors used various types of summary classifications in microfossil diagrams to illustrate broad changes in microfossils. Quantitative estimates of past sea level came primarily from radiocarbon dated index points at major stratigraphic boundaries, such as the change from peat to mud or vice versa, and their analysis through age – elevation plots. Interpretation of changes in microfossil assemblages before or after dated index points comprised qualitative assessments of the trend, or tendency, of change, in terms of increasing or decreasing marine influence (Shennan, 1982, 1986). While this sea-level tendency approach introduced a hypothesis-testing route applicable to studies of both seismic and non-seismic relative sea-level change (Long and Shennan, 1993, 1994, 1998), numerical techniques started to appear in sea-level studies (Atwater et al., 1995; Guilbault et al., 1996; Guilbault et al., 1995; Horton et al., 1999; Shennan et al., 1996; Zong and Horton, 1999), much later than in some other fields (Imbrie and Kipp, 1971).

3.1 Approaches to quantitative microfossil-based reconstructions

The term transfer function does not imply a single numerical technique, but a common approach that draws from a suite of techniques to choose those most appropriate for the specific study (Kemp and Telford, 2015). Diatom and foraminifera based transfer functions are the most widely adopted approaches for quantitative reconstructions of both seismic and climate-driven relative sea level

changes, summarised in some comprehensive recent reviews (Barlow et al., 2013; Dura et al., 2016; Edwards and Wright, 2015; Kemp and Telford, 2015; Zong and Sawai, 2015) . Other microfossil groups used include pollen (Bernhardt and Willard, 2015; Hughes et al., 2002), ostracods (Cronin, 2015), mollusca (Pilarczyk and Barber, 2015) and testate amoebae (Charman, 2015), though these rarely appear in coastal paleoseismology studies with quantitative estimates of deformation.

Two of the first applications of microfossil techniques in Alaska, studying the sedimentary record of the 1964 earthquake (Shennan et al., 1999; Zong et al., 2003) found that diatoms provided a better resolution of elevation than pollen and better preservation through complete sedimentary couplets than foraminifera. Most studies in the area since then predominantly use diatom-based methods.

For the diatom analyses presented below, we illustrate quantitative methods using transfer function approaches based on weighted-averaging partial least squares, WA-PLS, developed and successfully applied at other sites in south central Alaska (Shennan et al., 2014b; Shennan et al., 2014c), the modern analogue technique, MAT, (Hamilton and Shennan, 2005a; Hamilton and Shennan, 2005b; Kemp and Telford, 2015), and qualitative approaches based on diatom summary classes. We use a regional-scale modern training set of surface samples collected from a wide range of marshes across ~1000 km of south central Alaska in order to seek the best fit between fossil and modern diatom assemblages (Watcham et al., 2013), with additional samples added during subsequent field seasons. New tide level data from Turnagain Arm (Bender et al., 2015) provide an improved calibration of the modern training set (data files in Supplementary Information), therefore the reconstructions presented below may differ from any previously published for the same sites. We use three WA-PLS models, constrained by the lithology of the Holocene sediment sequence: one for peat sediment, a second for organic mud units and mud units with visible plant rootlets, and a third for mud units with no rootlets (Hamilton and Shennan, 2005a; Shennan et al., 2014b). We assess goodness of fit between each fossil sample and the modern dataset with a dissimilarity coefficient, using the 20th percentile of the dissimilarity values for the modern samples as the cut-off between 'close' and 'poor' modern analogues for fossil samples, and the 5th percentile as the threshold for defining 'good' modern analogues. For reconstruction of the elevation at which the fossil sediment accumulated, termed paleo-marsh surface elevation, PMSE, we present sample-specific 95.4% (2σ) error terms.

The addition of further samples to the modern training set available for transfer function methods, following each field season since the original study (Hamilton and Shennan, 2005a), raises a methodological debate regarding transfer function methods that we raised previously (Barlow et al., 2013; Watcham et al., 2013). A modern dataset dominated by modern samples from the local site, i.e. in the same marsh or estuary as the fossil core, will most likely provide the smallest error terms

for the youngest samples. In contrast, it may not provide good analogues for older samples. By definition, all our modern samples are from the postseismic period of the latest earthquake deformation cycle; therefore, we see no a priori reason to suppose that a local dataset will provide all modern analogues for our fossil sequences that may be thousands of years older and from different phases of an earthquake cycle. One effect of increasing the sample size is to increase the model error terms for RSL reconstructions (Table 2). The largest increase is within the upper elevation range, demonstrated in model 1, and reflects better sampling since 2005 of the diverse peat-forming environments in the transition from upper tidal marsh to freshwater environments. We also consider the reduction in number of components used in the model solution an improvement (Kemp and Telford, 2015).

We have always argued that model performance and their subsequent elevation predictions are judged not only by the size of the error term but also by an assessment of the goodness of fit between each fossil sample and the modern dataset (Hamilton and Shennan, 2005a), as outlined above. When we apply the new transfer function models to all of our fossil data collected across south-central Alaska, i.e. those from our previous studies and the new sites reported below, we see an increase in the number of good modern analogues and consider this an important step in improving our confidence in the reconstructions of elevation change. We therefore accept larger error terms in order to have more good and close modern analogues.

3.2 Summarising microfossil data and sea-level reconstructions

Microfossil-based reconstructions of relative sea level-change involve datasets that comprise multiple variables, species, and many samples. In the case of diatoms, samples through a section typically contain more than 100 different species. The data invariably show noise, some redundancy and internal correlations, and often contain outliers (Birks, 1995). These provide a challenge to illustrate, both for a reader familiar with diatom taxonomy and ecology, and for a wider audience who know much less about diatoms, but need to see how an author reached an interpretation or quantitative estimate of sea-level change. Published examples, including those within supplementary information files, range from all species plotted, to only a summary of species abundance based upon a classification scheme.

Figure 6 illustrates an example somewhere between these two extremes. The left hand part shows the changes in frequency of the most abundant species, colour coded by their classification based on salinity preference. The first summary diagram includes all the diatom abundances based on salinity preference. This is probably the most widely used summary classification in diatom-based studies. These provide a simple visual summary, with some important qualifications. First, the assignment of

a species to a salinity group will depend upon the database or literature source used (Atwater and Hemphill-Haley, 1997; Atwater et al., 1995; Beyens and Denys, 1982; Denys, 1991; Karlin and Abella, 1996; Patrick and Reimer, 1966, 1975; Sawai, 2001b; Sawai et al., 2004; Van der Werff and Huls, 1958-1974; Zong and Sawai, 2015) yet the modern environments may be rather different to the study region. For example, a species' classification could date back to nineteenth century observations in Europe. Second, assignment to a class may take no account of the tolerance of a species and its distribution along an environmental gradient. Some classification schemes attempt to allow for this by increasing the number of classes, but too many classes may lead to a less clear diagram. Finally, some sharp changes in the summary graph may result from changes of a single species. Although salinity-based grouping remain popular, the relationship between elevation and salinity need not be linear (Thomas and Varekamp, 1991; Varekamp et al., 1992), hence the caution required in describing the tendency of change observed, rather than a quantitative estimate (Nelson et al., 1996; Shennan, 1986).

The second summary plot and the four graphs on the right hand side of figure 6 reflect additional information based on numerical approaches. The summary plot is an alternative to the salinity classification, each diatom species is classified by their optimum elevation in the modern data set used for the transfer function models (Garrett et al., 2015b). The four graphs represent two transfer function methods of reconstructing elevation, WA-PLS and MAT, and two methods of illustrating these. Paleo-marsh surface elevation (PMSE) indicates the elevation of the sample with respect to the tidal frame at the time it formed, whereas RSL takes into account the depth of sediment accumulated since the time of formation.

The individual diatom species, both summary classifications and the quantitative reconstructions all illustrate two subduction-zone earthquakes at Girdwood, pre-seismic changes and interseismic changes (Shennan and Hamilton, 2006) and, within the upper peat layer, Little Ice Age glacial isostatic effects (Barlow et al., 2012). While the qualitative approaches, the two summary classifications, and the quantitative reconstructions of elevation estimated by two different transfer function models, show similar patterns for major changes, they differ with respect to smaller changes (Figure 7). WAPLS and MAT show very similar estimates for most samples, although the latter shows a little more level-to-level noise in part of the sequence. Both summary classification schemes also exhibit some level-to-level noise, with the salinity-based scheme seemingly exaggerating the degree of change compared to the other methods.

Given the qualifications outlined above regarding summary classification schemes, and their only broad relationship to elevation (Figure 8), we should exercise caution in using them to interpret other than rapid changes in sea level greater than approximately 0.5 m, and definitely be cautious

about level-to-level oscillations of less than 0.5 m (Figure 9). This example (Figure 9) suggests that, used in isolation, a change inferred between two samples has an even chance of showing the correct sign for a change of less than half a metre. Trends sustained over a number of contiguous samples are proportionally more likely to show the correct direction of change.

4. Tidal wetlands and different detection limits for recording paleoseismic evidence

The majority of the evidence for the multiple ruptures of the Prince William Sound segment (Section 2 and Figure 4) comes from just four sites, Ocean View at Anchorage, Girdwood, Portage, and Copper River Delta. Girdwood and Portage lie within the region of greatest subsidence in 1964, ~1.5 m excluding any additional subsidence due to ground shaking and sediment compaction. Copper River Delta lies within a broad area of uplift of a similar amount, or more, in 1964 (Plafker, 1969; Plafker et al., 1969). Multiple couplets spanning 4000 years or longer (Figure 4) suggest that subsidence and uplift of these magnitudes are clearly above the detection limit of tidal marshes to record earthquake induced marsh submergence and emergence. Ocean View at Anchorage provides a shorter record, ~2500 years, covering the period that includes three pre-1964 regional earthquakes (Figure 4). Importantly, at the time of EQ3 recorded at other sites in the Prince William Sound segment, sediments of that age show gradual accumulation during slow relative sea-level change, with no abrupt changes in lithostratigraphy (Hamilton et al., 2005; Shennan and Hamilton, 2006). This may be evidence of a different rupture mode. Scenarios B and C (Figure 5) predict different trends of subsidence along Turnagain Arm, between Portage and Anchorage, and transitions to no subsidence at sites to the southwest, along Cook Inlet out to Kodiak Island. In the following sub-sections we present additional evidence, first from sites within Turnagain Arm, then from Cook Inlet and Kodiak Island to evaluate whether tidal marshes can record evidence with sufficient resolution to illustrate spatial patterns of different amounts of subsidence or uplift, including the transition to zero change. Table 3 presents radiocarbon dated samples not previously published, with ages calibrated using OxCal 4.2 (Bronk Ramsey, 2009).

4.1 Bird Point

At Bird Point, approximately 10 km west of Girdwood, tidal flat and marshes occupy sheltered embayments between glacially eroded bedrock. Sediment outcrops and hand-driven cores reveal an extensive peat-mud couplet, typically 0.4 to 0.8 m below the present marsh surface, recording subsidence in 1964 (Witter et al., 2015). In contrast to Girdwood, the sediments beneath the marsh

rarely extend to more than 5 m depth before reaching bedrock. Although less widespread, three further peat-mud couplets occur beneath the 1964 couplet. All three have sharp contacts and large changes in diatom assemblages that reconstruct marsh subsidence of 1.82±0.97, 1.29±0.96 and 1.42±0.98 m (Figure 10). Ages for these couplets correlate well as maximum ages for regional earthquakes EQ1, EQ2 and EQ3.

4.2 Hope

Tidal marshes at Hope occur along fringes of the active delta of Resurrection Creek as it enters Turnagain Arm. Resurrection Creek was the centre of a gold rush in the late nineteenth and early twentieth century, adding to sediment discharge from the catchment to the delta. Outcrops along the marsh front and hand-driven cores reveal a complex stratigraphy of minerogenic beds, ranging from mud to gravel, close to the present creek and within the eastern part of the delta. Peat-mud couplets correlated between cores only occur west of Resurrection Creek (Figure 11). Sawn timber exposed in outcrop indicates the uppermost couplet represents marsh submergence following ~1.5 m regional coseismic subsidence in 1964 (Plafker et al., 1969). The borehole evidence reveals another couplet ~3 m below the surface with lateral continuity and a sharp peat-mud contact. Diatom analyses indicate 1.17±0.99 m rapid submergence and the radiocarbon age supports a correlation with regional earthquake EQ3 (Figure 11). Further couplets occur between 1 and 3 m depth but show less consistency between boreholes.

4.3 Kasilof

The Kasilof River drains 1,919 km^2 of the Kenai Peninsula with the potential of major flooding from the sea, snowmelt, rainfall or outburst from lakes impounded by Tustmena Glacier (Reger et al., 2007). Intertidal outcrops along the river and a series of cores towards the bluff reveal three peat-mud couplets close to the river (Figure 12). The site lies with the zone of submergence in 1964, although the estimate of ~0.5 m is an interpolation between points ~100 km apart (Plafker, 1969). For diatom analyses we classified the original counts of Hamilton (2003) from location 8 in line with the new transfer function models described above and undertook further analyses across the key sediment boundaries at location 1.

Radiocarbon ages indicate a record covering more than 6200 years, commencing with the transition from intertidal mud to the base of peat C. Peat C accumulated in close proximity to tidal sedimentation, indicated by the low but consistent frequencies of tidal flat and tidal marsh diatom species (Figure 12). Radiocarbon ages on the outer rings of tree stumps rooted within peat C and correlation of tephra layers (Combellick and Pinney, 1995; Combellick and Reger, 1994), from an

outcrop close to location 8, support an interpretation of gradual accumulation of peat C in the absence of any visible stratigraphic hiatus. Preliminary ^{137}Cs analysis at location 8 (Hamilton, 2003) indicated AD 1964 occurs within the mud unit well above the upper contact of peat A (Figure 12). To check this finding we sampled the top contact of peat A at location 1 and found no above background ^{137}Cs so confirm that the upper contact of peat A is not AD 1964.

In order to evaluate each peat-mud couplet as evidence of marsh submergence caused by coseismic subsidence we will consider in detail the diatom evidence across each couplet from locations 1 and 8 along with the other lines of evidence.

The contact at the top of peat C appears to fulfil the Nelson et al. (1996) criteria as evidence of submergence associated with coseismic subsidence. We can trace the contact laterally and it is always abrupt (Figure 12). Some diatom species show abrupt change across the contact with estimates of submergence as 0.56 ± 0.47 m at Site 8 and 0.62 ± 0.47 m at Site 1 (Figure 13). Radiocarbon ages from the contact and 1 cm below the contact correlate well as maximum ages for submergence indistinguishable from the age of regional earthquake EQ2. An alternative hypothesis is that local processes, including river flooding, could produce a similar couplet. The correlation with regional earthquake EQ2 does not prove a coseismic cause; rather it indicates that we should not reject the coseismic hypothesis. The gradual trend of relative sea-level fall through the mud and into peat B fits with a model of century-scale interseismic uplift following coseismic subsidence (Scenario B, figure 2) superimposed on longer-term sea-level rise illustrated in Figure 12.

The peat B top contact shows some subtle contrasts with the peat C top contact. It is sharp in some outcrop and cores, and gradual in others (Figure 12). Combellick and Reger (1994) also recorded it less sharp than contact C. At location 8, the sample from mud directly above the contact shows a diatom assemblage different to those above and below and give a sea-level reconstruction that appears as an outlier on a general trend of sea-level rise (Figures 12 and 13). In contrast, the diatom assemblages from the samples above and below are very similar to each other. At location 1, the samples across the contact indicate submergence of 0.48 ± 0.47 m. Radiocarbon ages from the top of peat B, leaf fragments from within the lowest 1 cm of the mud unit, and the base of peat A, some 0.3 m higher up-section, constrain the age of submergence to earlier than regional earthquake EQ1 (Figure 13).

The uppermost peat-mud couplet occurs across the whole transect of cores and is visible in outcrop for at least 200 m. The upper contact is sharp in all locations apart from one borehole. Diatom assemblages from a few centimetres either side of the contact record a clear rise in sea level (Figure 12), but the abrupt rise is not at the contact. The samples from the base of the mud unit and the top

of the peat at both location 1 and location 8 indicate no rise in sea level across the contact, with the rise occurring within the mud unit. Diatom species within the basal mud sample show a distinct change in assemblage compared to the peat sample immediately below, indicating a change in sedimentary environment but at a similar elevation within the tidal frame.

In order to suggest possible mechanism for these changes we must consider the sedimentary system as a whole. Aerial imagery of the ~8 km tidal section of Kasiof River shows a dynamic system with evidence of changes in meander patterns, undercutting of channel sides and packages of sediment deposited adjacent to the channel. Away from the channel, the marsh surface is relatively flat (Figure 12), with small changes in topography, <0.1 m, delimiting ponds of standing water from vegetated marsh. We envisage major floods, whether from snowmelt, rainfall or lake outbursts, may cause morphological changes that become recorded in the stratigraphy. These include a temporary pulse of minerogenic sedimentation, channel erosion and channel avulsion. Lateral erosion could undercut waterlogged marsh and ponds, leading to lowering of the local water table through drainage into the tidal channel. This would lead to peat compaction, allowing initial mud accumulation at a similar elevation. Continued compaction would produce relative sea-level rise, recorded within the mud unit.

The age of this episode of marsh submergence falls within a radiocarbon plateau, giving a range of 280 to 0 BP. As noted above, ^{137}Cs evidence shows that the couplet does not correlate with the 1964 earthquake (Figure 12). The coarse sampling interval for the ^{137}Cs samples, 8 cm, prevents a precise determination of AD 1964 other than the envelope shown in the figure. It is possible that the step change in reconstructed sea level, 0.21 ± 0.61 m, at the top of the envelope, is the record of marsh submergence in 1964.

The contrasts seen in the three couplets at Kasilof may indicate a detection limit of around 0.5 m for coseismic submergence at the site. This value is directly related to the scaling factor used in the modern training set to allow for different tidal ranges, so it is better to consider this vale as approximately 8% of the great diurnal range at the site (the difference between mean higher high water, MHHW, and mean lower low water, MLLW). We return to this topic in sections 5 and 6.

4.4 Homer

The road from Homer Township to Homer Spit runs along an embankment that separates Beluga Lake from Beluga Slough, an intertidal marsh with tidal channels behind a sand and gravel spit (Figure 14). Beluga Lake once extended across what is now Beluga Slough. During the early years of Homer Township a railway ran from coal mines 3 km west, along a spit across the mouth of Beluga Lake, and continued along Homer Spit to the east (Stone, 1906). The mines closed in 1903. Much of

the gravel for construction of the new road and embankment 1941-45 came from the spit (Soberg, 1991). It no longer formed a complete barrier and the 1946 USGS topographic map shows a creek flowing from the embankment to the coast. The 1964 earthquake caused ~0.6 m regional subsidence, with sediment compaction and slumping along Homer Spit leading to localised subsidence up to two metres (Waller, 1966).

Hand drilled cores from along the central axis of Beluga Wetlands (locations 8-12, figure 14) reveal thick, >5.5 m, freshwater peat that we could not bottom out. Near to the base, we found two thin mud/sand layers that we interpret as tephra. Surface peat floating on water prevented further coring close to the lake. Cores to the edge of the wetland close show intercalations of organic, limnic and minerogenic sediments, with no sequence of units that we could trace easily between cores. We interpret the coarse minerogenic sediments as slope wash from the bluff.

Cores from the marsh and tidal flats of Beluga Slough (locations 1-7, figure 14) reveal multiple peat-mud alternations, usually with a sharp upper contact of the peat, and quite often with a sharp lower contact too. We find it difficult to correlate these thin, multiple couplets between boreholes. Figure 14 shows our best interpretation of the field data, suggesting five couplets, A to E, which we feel we have some confidence in their continuity, based on the lithology of the organic and minerogenic layers that form the couplet and their stratigraphic position. Radiocarbon ages indicate a 4000-year record and therefore potential evidence of multiple 1964-style earthquakes.

Sawn timber within outcrops along the intertidal channel of Beluga Slough, adjacent to cores 1 and 2, indicate a twentieth century age for couplet A. Absence of ^{137}Cs for samples across the contact suggest a pre-1964 age. The abundance of *Fragilaria construens* var. *venter* and *Fragilariforma virescens,* planktonic diatom species indicative of standing water (Denys, 1991; Patrick and Reimer, 1966), suggest a change in hydrological conditions and sediment input. Transfer function reconstructions show no change in relative sea level (Figure 15). We suggest that couplet A likely formed as the result of changes to the gravel spit across the mouth of wetland. Extraction of gravel from the spit for road construction and lowering the water table for the building of the Beluga Lake embankment in 1941-45 is a possible explanation.

Couplet B comprises a thin peat, with a sharp upper contact, traceable across all cores from Beluga Slough. At core 4 the diatoms include the standing water species mentioned above, marsh species, no abrupt changes across the contact and no change in reconstructed sea level. At core 5, diatom assemblages show no abrupt changes at the contact, but trends below and above. The sea-level reconstructions indicate a rise commencing within peat B and continuing across the contact. The radiocarbon ages at the two cores differ.

The radiocarbon ages from couplet C suggest reworking of an older peat at core 4. At core 5 the diatom assemblages in both the peat and mud units suggest standing water throughout, with a change in depositional environment across the contact and an increase in species reflecting lower elevations or higher salinity. The reconstructions estimate a rise in sea level of 0.22 ± 0.58 m. The radiocarbon age from core 5 matches the age of regional earthquake EQ3.

Couplet D has differences in both age and diatom assemblages between cores 4 and 5. If both cores record synchronous submergence the older age at core 4 would imply some erosion of peat. The age from core 4 does not correlate with a regional earthquake, whereas that from core 5 fits with EQ4. The diatom assemblages and sea-level reconstructions indicate gradual changes and sea-level rise within the peat and a more abrupt change across the contact, estimating a slight fall in sea level, 0.18 ± 0.55 m.

Couplet E also has differences in age and diatom assemblages between cores 4 and 5. Core 4 shows the older age, slight sea-level fall across the contact, and then a more abrupt sea-level rise within the mud unit. Core 5 records sea-level rise across the contact, 0.27 ± 0.58 m. The age could indicate a maximum age for marsh submergence correlated with regional earthquake EQ6.

Diatom species reflecting standing water, especially *Fragilaria construens* var. *venter* and *Fragilariforma virescens*, occur in each couplet (Figure 15). In our modern data, their optima and tolerances are 0.40 ± 0.25 and 0.68 ± 0.22 m MHHW respectively, although they never account for more than 10% in any sample. We have a poor analogue for many of the fossil samples containing much higher abundances. High abundances of these species suggest standing water, such as a lagoon or lake behind a gravel spit or barrier, such as that described pre-1903 to carry a railroad (Stone, 1906). The present tidal regime shows low water behind the spit just below MHHW level in the open water of Cook Inlet (Figure 16). The elevation of low water and ponding behind the barrier will vary according to the dynamics of the barrier, as will the supply of sediment into the tidal system. The diatom assemblages suggest that peat-mud couplets indicate sedimentation above MHHW. We suggest that non-seismic, dynamic changes in the spit across the mouth of Beluga Slough offer an alternative explanation to coseismic subsidence for abrupt changes in lithology and diatom biostratigraphy. We return to the evaluation of these alternatives in the discussion of testing models of different rupture modes, section 5, and in section 6, regarding the wider implications with respect to detection limits of different sedimentary environments.

4.5 Kalsin Bay

A recent study of tidal marshes in the northeast of Kodiak Island reports evidence of marsh submergence and deposition of sediments by tsunami in AD 1964 and 1788, the latter including correlation of Bayesian age modelling of radiocarbon ages with historical accounts, and an earlier earthquake ~500 BP (Shennan et al., 2014a). Observations from 1964 indicate 1.4 ± 0.3 m subsidence (Plafker, 1969; Plafker and Kachadoorian, 1966) and diatom-based reconstructions estimate submergence of 0.41 ± 0.26 m in 1788. The marshes used for that study also provide evidence of tidal flat and marsh sediments that extend further back in time. We summarise these older data to illustrate the short, fragmentary records available from the Kodiak segment, and how they constrain analyses of rupture modes.

While the evidence for the 1788 earthquake extends across much of the marsh area at Kalsin Bay, sediment sequences extending back more than 2000 years occur in isolated patches. The most coherent of these, in that they show some lateral continuity of peat-mud couplets and sand layers at the contact, occur within a small depression behind a fossil beach ridge, ~700 m from the coast and close to the main river into the bay.

In addition to peat-mud couplet A, attributed to the 1788 earthquake, two earlier couplets occur at location 5 and some of the adjacent ones (Figure 17). Couplet B includes a sand layer on the top of the peat unit. Diatoms show a slight increase in sea level across the couplet. The age does not correlate with the earthquake ~500 BP elsewhere in Kodiak. At least three possible hypotheses remain: a small amount of coseismic subsidence during an earthquake not yet recorded beyond the site; a tsunami from a distant source and gradual non-seismic sea-level rise; sand deposition during a flood from the tidal reach of the river between ~500 BP and AD 1788.

Peat-mud couplet C further illustrates the difficulty of assessing paleoseimic evidence where the amount of submergence appears to be less than ~0.5 m. First, it is difficult to trace the lateral extent of the couplet, even with cores only 10 m apart. Second, the change in diatoms, and therefore the reconstructed sea level, comes from primarily two species, *Fragilaria construens* var. *venter* and *Fragilariformis virescens*, the same two species discussed above at Homer. These illustrate a temporary change in sedimentation, and given the diatom species, may be a local change in hydrology behind the active spit at that time. Alternatively, we can hypothesise that a seismic process drove this local change. These alternatives can be assessed when evaluating different modes of rupture and their proposed spatial patterns of surface displacement.

Finally, we should note that the base of the sequence at this part of Kalsin Bay is ~2500 BP, but contains no more peat-mud couplets traced across multiple cores.

4.6 Anton Larson Bay

Mashes at the head of Anton Larson Bay, on the northeast peninsula of Kodiak Island, provide limited evidence of Late Holocene fluvial, deltaic, tidal flat and marsh sedimentation. The Katmai tephra, AD 1912, is up to 0.8 m thick in some cores and tidal channel outcrops. Coarse gravel from rivers form deltas at the mouths of streams and rivers, and limit total depth of hand-driven cores. The field stratigraphy reveals three couplets, all with limited lateral extent (Figure 18). Above the Katmai tephra, a number of cores show a coarse sand layer directly above the tephra, while a small area at the head of the marsh has a thin peat, <0.01 m, with an eroded upper contact, between the tephra and coarse sand with gravel. We interpret this as record of the 1964 earthquake and tsunami. Diatom changes between the peat and the organic mud above the coarse sand indicate a rise in sea level of 0.74 ± 0.33 m.

A second peat-mud couplet occurs a few decimetres below the Katmai tephra along transect B-B' and isolated cores on transect A-A' (Figure 18). Ages from two cores, 4 and 9, correlate the couplet with the 1788 earthquake (Shennan et al., 2014a), on the assumption that both contacts provide maximum ages for the same event. Both cores estimate submergence, 0.38 ± 0.32 m at core 4 (figure 18) and 0.07 ± 40 m at core 9. [

A third peat-mud couplet, recorded at only two cores, is significant in that it reveals gradual sea-level rise over at least 2000 years. Although there are abrupt changes in diatoms and lithology, there are no abrupt changes in sea level. Unless there are hiatuses in the sequence, this record of gradual, uninterrupted sea-level rise covers the time in which three regional earthquakes occurred in the Prince William Sound segment (Figure 18).

5. Testing displacement predictions for different rupture modes

Eighteen locations provide records of pre-1964 tidal wetland submergence or emergence for testing model predictions of cosesimic displacement for different rupture scenarios (Figure 19). Other locations record episodes of marsh submergence (Hutchinson and Crowell, 2007) but we exclude them from this analysis as they either show insufficient evidence of lateral continuity of the local stratigraphy, such as the large delta of Fox River (Combellick and Reger, 1994) or their age control relies on radiocarbon dating of bulk peat samples. Initial attempts to correlate possible paleoseismic evidence around Cook Inlet reported significant differences in the ages of peat-mud couplets between sites (Combellick, 1991, 1994; Combellick and Reger, 1994). Subsequent studies from Cook Inlet demonstrated the potential of contamination of bulk peat samples by older carbon, such as coal deposits in the catchment (Hamilton et al., 2005; Shennan et al., 2014c). In the following sections, we compare the evidence of coseismic displacements with predictions for different

earthquake ruptures (Section 2), first for 1964-type ruptures, second, ruptures extending beyond the 1964 eastern limit, and third, smaller ruptures within the 1964 limits.

5.1 Evaluating 1964-type rupture modes

One interpretation of the paleoseismic evidence from the eighteen sites (Figure 19) is that no earthquake in the last 6000 years caused a spatial pattern of uplift and subsidence earthquake the same as 1964 (Scenario A in figure 5). The validity of this interpretation lies on three lines of argument:

- the length of records available at each site,
- the continuity of each record,
- the extent to which alternative explanations of the evidence remain possible, i.e. the evidence available does not reject a number of working hypotheses.

The reasoning requires close consideration of the evidence for absence of rapid submergence or emergence, along with consideration of the absence of evidence. All of the sites bar two in the 1964 rupture (involving the Kodiak, Kenai and Prince William Sound segments, Figure 19) provide stratigraphic evidence of relative subsidence or uplift in 1964 in terms of peat-mud couplets or mud-peat couplets respectively. The spatial extent of the evidence varies within each site, with only part of the intertidal environment falling within the elevation zone that will record the amount of coseismic subsidence or uplift as a change in lithology. Outside of this elevation zone, the change may still be recorded, without a change in sediment lithology and therefore much harder to detect. In the part of the Kasilof River studied (section 4.3), any record of the 1964 earthquake falls within a predominantly mud unit. ^{137}Cs and diatom reconstructions of relative sea-level change record an abrupt change around this time, but they come from the only profile analysed in sufficient detail. At Homer, the sedimentary setting was disturbed by road construction and gravel extraction from the spit in the decades prior to 1964 (section 4.4), and the pre-20th sediments indicate a quite different sedimentary setting compared to 1964 and since. In this situation, we have a poor modern equivalent at the site itself and need to consider the relationship between past environmental changes using possible modern equivalents from elsewhere.

In considering the evidence of absence of abrupt elevation change during previous earthquakes, we first evaluate the continuity of each record, and then the alternative explanations for observed changes. At Hope, deltaic processes mask much of the record, with coarse-grained sedimentation and channel migration raising the creation and preservation thresholds such that a fragmentary record remains. At Puffy Slough the field investigation was exploratory (Shennan et al., 2014c) and the absence of a record for EQ2 may reflect the small number of boreholes made. In contrast, from

~6200 to ~1500 BP both Kenai River (Hamilton and Shennan, 2005b) and Kasilof River (Section 4.3), 20 km apart, record a single peat horizon, with no mud layers and no visible breaks in sedimentation. Both sites have tephra layers within the peat unit, correlated with an eruption of Mount Hayes ~3600 BP (Combellick and Pinney, 1995). All the age determinations, radiocarbon ages from in situ herbaceous macrofossils at the upper and lower boundaries, from two locations at Kenai and two at Kasilof, and further radiocarbon ages on tree stumps rooted within the peat layer at each site (Combellick and Reger, 1994), and the Hayes tephra, fall in chronological order. In the absence of any evidence for any hiatuses in peat accumulation, we next ask whether peat accumulation took place at an elevation within the zone susceptible for recording abrupt relative sea-level rise resulting from coseismic subsidence with EQ3 to EQ9. Diatom-based reconstructions indicate peat accumulation below the level of Highest Astronomical Tides (HAT) throughout at Kasilof (Figure 20). At Kenai the mean estimates are just below HAT. On the present marsh at Kenai, intertidal mud accumulation occurs up to ~1.2 m MHHW at which point high marsh grades to bog communities. We suggest that these reconstructions and the stratigraphy indicate that any rapid submergence in the order of 0.1 m at Kasilof and 0.3 m at Kenai should have been recorded by diatom assemblage changes and probably mud accumulation. This interpretation would imply that Kenai and Kasilof only indicate rapid submergence associated with earthquakes in AD 1964 and EQ2, ~1500 BP and that the patterns of deformation in the other earthquakes recorded in the Prince William Sound segment differ. This interpretation also assumes no localised uplift on upper plate structures during great earthquakes to offset regional subsidence. Movement along splay faults caused additional localised uplift in 1964 and other Holocene earthquakes (Chapman et al., 2014; Chapman et al., 2011; Plafker, 1969; Shennan et al., 2014c), but none of these is near to Kenai or Kasilof. Koehler et al. (2012) record the most recent surface deformation from faults near these sites as more than 1.6 million years ago. An alternative interpretation of the Kenai and Kasilof evidence is that all of the regional earthquakes produced subsidence below the creation threshold for recording rapid submergence at those river estuary sites. The creation threshold would be in the order of 0.1 to 0.3 m.

In order to support a 1964-type rupture the data from Homer should indicate submergence (Figure 21 – scenario A), whereas the stratigraphy, radiocarbon results and diatom reconstructions offer little support for interpretations involving coseismic subsidence (section 4.4). For Homer, the alternative interpretation is that the spit, prior to human interference, provided a barrier and lagoon environment that was insensitive to small coseismic ground motions. Changes in the hydrology of the lagoon and sediment input vary through time but the causes could equally be non-seismic, such as major storms superimposed on Late Holocene net sea-level rise.

The record for 1964-type deformation in Kodiak is patchy. At both Kalsin Bay and Anton Larson Bay sediments older than 800 BP occur across only small areas, <50 m radius. Neither offer supporting evidence for rapid submergence coincident with EQ1, EQ2 or EQ3, even though they have sediments of similar ages and diatoms indicating inter-tidal environments that should be sensitive to relative sea-level change. An alternative interpretation is that the field evidence fails to show sufficient evidence of the lateral continuity of different units. Without lateral continuity we may not distinguish between the absence of rapid change and the absence of evidence due to sediment erosion and hiatuses. Evidence from Sitkinak indicates uplift around the time of EQ1, in contrast to subsidence in 1964 at the same site, but, as noted by Briggs et al. (2014), present uncertainties are too large to correlate this uplift with simultaneous rupture of the Prince William Sound segment.

5.2 Evaluating rupture modes extending to the east

Paleoseismic evidence from the coast of the Gulf of Alaska, beyond the eastern limit of deformation in 1964, record coseismic uplift that correlates in age with EQ1 and EQ2 (Shennan et al., 2009). The greater extent eastwards and amounts of deformation compared to those observed in AD 1899 (Plafker and Thatcher, 2008) and 1964 support the hypothesis of simultaneous rupture of adjacent segments of the megathrust and the Yakutat microplate. The alternative hypothesis is that the segments ruptured separately, during a time interval within the radiocarbon age error terms, a few decades or less. This alternative hypothesis, however, less easily explains the patterns of uplift at Cape Suckling and along the Yakataga coast (Shennan, 2009; Shennan et al., 2009). Bayesian age modelling produces a strong correlation with EQ1 and EQ2 (Shennan et al., 2014c). Comparisons of the estimates of submergence and emergence with model predictions of coseismic subsidence and uplift show good agreement for the Prince William Sound segment and Yakataga (Figure 21 – scenario D), but not for the Kenai and Kodiak segments, subject to the alternative interpretations discussed in the preceding section. The palaeoseismic evidence suggest a rupture mode not presently modelled, comprising the western Yakutat and Prince William Sound segments, and possibly part of the Kenai segment.

5.3 Evaluating smaller ruptures within the 1964 limits

Interpretations of zero coseismic subsidence in Kodiak, Homer, Kasilof and Kenai (section 5.1) imply a different pattern of rupture to 1964, such as scenarios B and C (Figure 5 and Nicolsky et al., 2013; Nicolsky et al., 2014). Both scenarios illustrate Mw 8.8 earthquakes, with a deeper slip distribution in Scenario C (Table 1) producing subsidence further to the west (Figure 21).

Relative sea-level reconstructions of marsh submergence and emergence across the region broadly show good fits with rupture modes that comprise the Prince William Sound segment and part of the

Kenai segment. The pattern of marsh submergence and emergence for EQ1 matches closest with Scenario B, but indicates a rupture that extend further east (section 5.2). The pattern for EQ3 broadly matches closest with scenario B, but also with the extension east, and for EQ2 with scenario C (Figure 21). In detail, however, certain aspects suggest further work is required to match better the model predictions and reconstructions. For example, the models predict an axis of maximum subsidence along Turnagain Arm around Hope, not seen in the reconstructions of marsh submergence (Figure 22), although localised sediment compaction will potentially influence each marsh differently and possibly obscure such trends in the reconstruction data. More important is the trend to zero submergence at Anchorage in EQ3 (Hamilton et al., 2005). The evidence of increasing submergence from Hope to Portage and the lack of any evidence of emergence, contrasts with the transition from subsidence to uplift suggested by Scenario C. To attribute the model-to-reconstruction differences as simply a result of sediment compaction requires greater amounts of compaction than those interpreted for 1964 (Plafker, 1969; Plafker and Kachadoorian, 1966; Plafker et al., 1969).

5.4 Variable rupture modes and seismic hazard assessment

On the balance of evidence, we infer that the reconstructions of marsh submergence and emergence reflect different patterns of rupture mode in great earthquakes. EQ1 and EQ2, ~850 and ~1500 BP respectively probably ruptured the Prince William Sound segment, at least part of the Kenai segment, and the western part of the Yakutat microplate. The western extent of submergence with EQ2 would indicate a deeper slip distribution.

The pattern of submergence and emergence for EQ3, ~2100 BP, is consistent with a modelled rupture of just the Prince William Sound and part of the Kenai segment (Figure 21). Although restricted to fewer sites (figure 19), the evidence of no submergence at Kenai, Kasilof and Homer would indicate Scenario B or C-type ruptures of the Prince William Sound and Kenai segments.

For the southwestern part of the 1964 rupture area, a number of studies conclude that the Kodiak segment of the megathrust ruptures independently of the Prince William Sound segment (Briggs et al., 2014; Carver and Plafker, 2008; Gilpin, 1995; Sauber et al., 2006; Shennan et al., 2014a). These include the AD 1788 earthquake, described in historical documents (Soloviev, 1990) and recorded in tidal marsh stratigraphy on Kodiak Island and Sitkinak Island, and another one ~500 BP (Briggs et al., 2014; Shennan et al., 2014a). Tsunami sediments on Chirikof Island, only 125 km further west of Sitkinak record the AD 1788 earthquake but show no correlation with those ~500 BP on Kodiak Island and EQ1 in the Prince William Sound segment (Nelson et al., 2015).

Current hazard assessment studies model a single segment rupture of the Kodiak segment, Mw ~8.8 (Suleimani et al., 2002; Wesson et al., 2007; Wesson et al., 2008), although paleoseismic evidence also suggest a possible rupture scenario of the Kodiak segment and at least part of the Kenai segment (Kelsey et al., 2015). Some of the alternative interpretations of the sedimentary evidence from Kasilof, Homer and Kalsin Bay (Sections 4.3 to 4.5) could support a hypothesis of a co-rupture of the Kodiak segment and a western part of the Kenai segment. The most abundant evidence relates to marsh submergence ~1100 BP recorded at Kasilof (figure 13), that could correlate with maximum ages of submergence recorded at Homer (Figure 14) and Kalsin Bay (Figure 17) and a minimum age for uplift at Sitkinak (Briggs et al., 2014). In contrast, Anton Larson Bay records gradual sea-level rise at that time.

The growing body of evidence of variable rupture modes provides considerable challenges in revising and updating the hazard model for the megathrust (Mueller et al., 2015; Wesson et al., 2008). Briggs et al. (2014) argue for a re-evaluation of 2007 segmented megathrust model (Wesson et al., 2007), with fixed segment boundaries. The analyses presented above support this call, to include both variable rupture modes and variable recurrence times. Creation and preservation thresholds limit the resolution of displacement recorded at each site. Rather than focus on this limit at each site, say ~0.3 m, we judge the fit between model predictions and paleoseismic reconstructions based on the spatial differences across numerous sites, ranging from the areas of large change, greater than say ~0.3 m, to areas with evidence of no change. If we see a spatial pattern of misfits that cannot be resolved, either we focus on the local site processes, which may explain the absence of evidence for coseismic uplift or subsidence across those sites, or infer that the model parameters need reassessing.

6. Identifying coseismic subsidence and uplift in tidal-wetland stratigraphic sequences

Considering the number of twenty-first century megathrust ruptures of unexpected magnitude and location (e.g., 2004 M_w 9.2 Sumatra-Andaman; 2010 M_w 8.8 Maule, Chile; 2011 M_w 9.0 Tohoku-Oki, Japan) it is time for new thinking on megathrust earthquake recurrence, segmentation and geometry (Mueller et al., 2015). This is potentially significant for practical reasons, earthquake and tsunami hazard assessment, and scientific understanding, of how megathrust earthquakes vary in time and location. Even in Japan, where written accounts extend back more than a thousand years, paleoseismic studies of coastal wetland provide information which, with hindsight, could have better informed hazard assessments (Goto et al., 2011; Minoura et al., 2001; Sawai et al., 2008). The most

comprehensive assessments of hazards are likely to be based on records that span multiple cycles of strain accumulation and release on the megathrust.

Both underestimates and overestimates of the number of paleoearthquakes are critical issues and may arise from incorrectly interpreting field evidence (McCalpin and Nelson, 2009; Nelson et al., 2015). Since peat-mud and mud-peat couplets are not uniquely a product of great earthquakes, there must be criteria to distinguish couplets that result from great earthquakes from those resulting from other processes. In quantitative terms, this equates to equation [2] described in section 1. With the geographical expansion of coastal paleoseismology studies, particularly since the 2004 M_w 9.2 Sumatra-Andaman earthquake and tsunami, much has been written about different types of evidence, the use of new methods, and their interpretation. These developments should lead to modifications, improved quantification and additions to the original criteria to identify coseismic subsidence (Nelson et al., 1996).

We see no dramatic paradigm shift, rather evolutions in the cutting-edge research literature, which we use to amend the criteria and to reflect usage in identifying coseismic uplift as well as subsidence (Table 4). We add additional criteria that may be present at some sites: liquefaction sediments (Atwater et al., 2001; Malik et al., 2011; Martin and Bourgeois, 2012; Obermeier and Dickenson, 2000; Walsh et al., 1995) and tree ring analysis (Yamaguchi et al., 1997). Newly applied analytical methods include stable carbon isotope and geochemical proxies (Bender et al., 2015; Dura et al., 2011; Engelhart et al., 2013; Hawkes et al., 2011; Witter et al., 2016). The last decade has also seen a lot written on identifying sediments deposited by tsunami (Alam et al., 2012; Chagué-Goff et al., 2011; Dura et al., 2015; Engel and Brückner, 2011; Garrett et al., 2013; Goff et al., 2011a; Goff et al., 2011b; Goto et al., 2011; Grand Pre et al., 2012; Kortekaas and Dawson, 2007; Morton et al., 2007; Nelson et al., 2015; Okal et al., 2011; Pilarczyk et al., 2014; Shanmugam, 2012; Witter et al., 2016).

In applying the criteria to address the questions outlined in the introduction, especially the extent of past great earthquake ruptures (a proxy for magnitude), the identification of the boundaries between rupture segments and the persistence of these boundaries over multiple earthquake cycles, three significant advances emerge. First, in assessing the amount of submergence or emergence; second, assessing the age of past earthquakes, including their correlation between sites; and third, analysis of the spatial patterns of submergence and emergence against model predictions.

6.1 Assessing the amount of vertical motion

Approaches to quantifying coseismic submergence and emergence are probably the most noticeable and widely adopted advance in the last 20 years. The original criteria promoted the accepted and

robust methods of geological practice and these remain the standard. Since then, advances in numerical techniques and the development of new proxy methods provide additional opportunities to quantify estimates of coseismic submergence and emergence. The most widely used of these advances relate to quantitative reconstructions based on microfossil approaches (section 3.1), although other approaches, such as geochemical proxies, also provide quantitative estimates (Bender et al., 2015).

Nelson et al. (1996) noted that combinations of sediment stratigraphy, plant macrofossils and microfossil analyses had a detection threshold of approximately 0.5 m, below which it was difficult to distinguish between coseismic and non-seismic marsh submergence, recorded by evidence of relative sea-level rise. Quantitative estimates for abrupt submergence at the sites discussed in section 4 range from ~0.25 to 1.00 m, which could be taken as a lack of progress. On the contrary, these estimates reflect a 95% probability range, although this is difficult to represent in graphs of relative sea-level change. A reader can judge the sample-to-sample changes in the microfossil assemblages and associated quantitative estimates in the peat and mud units below and above a stratigraphic contact, and contrast these with the changes directly across the contact. We suggest that multiple estimates across the same stratigraphic contact improves confidence in being able to infer that a change is abrupt and its possible coseismic cause (Shennan and Hamilton, 2006), and not only where the estimated change is less than the 95% uncertainty range (Shennan et al., 2014c). At Kalsin Bay, Kodiak Island, estimates for marsh submergence during the AD 1788 earthquake from six different cores range from 0.18 ± 0.26 to 0.67 ± 0.29 m, an average of 0.41 ± 0.26 m (Shennan et al., 2014c). All six estimates indicated submergence rather than a random distribution of mean values either side of zero.

While these separate estimates of less than 0.5 m elevation change from Kalsin Bay, and others of less than 0.5 m discussed in section 4, suggest a modest reduction in the detection limit of abrupt submergence or emergence as a result of scientific advances, it is important first to make the comparison with respect to tidal range. For comparison, 0.5 m vertical change in Cascadia, where the Nelson et al. (1996) framework was established, is ~17-22% of the Great Diurnal Range (NOAA, 2016). The examples in section 4 and those previously reported (Shennan et al., 2014a; Shennan et al., 2014b; Shennan et al., 2014c) suggest an achievable detection limit in the region of 10-15% of the Great Diurnal Range or better. While the 95% error term for reconstructing paleomarsh surface elevations for individual samples may be 10-15% of the Great Diurnal Range, a combination of multiple lines of evidence provides a more robust test of smaller magnitude coseismic submergence or emergence. If a site shows all the following features, the effective detection limit may be as low as perhaps 0.1 to 0.2 m:

- laterally extensive peat-mud or mud-peat couplet with a sharp contact at each outcrop or core,
- for multiple locations along the couplet, sudden elevation change determined by assessing the change across the contact in comparison with the changes below and above the contact,
- for multiple locations along the couplet, quantitative estimates of elevation change across the contact all indicating the same sign (emergence or submergence) rather than a random distribution of mean values either side of zero.

Coseismic motions below the detection limit should fail to meet the combination of these three criteria.

6.2 Additions to assessing the age of the earthquake and synchroneity between sites

Advances in numerical modelling of sediment-sample ages provide new approaches to evaluate contrasting interpretations and hypotheses of between-site correlations of paleoseismic evidence. While the careful consideration of what constraint each sample age places on an inferred earthquake, such as a minimum limiting age above a contact or a maximum limiting age from below a contact, remains unaltered, Bayesian age modelling provides a range of options by which to assess age correlation and intervals between inferred earthquakes (Berryman et al., 2012; Bronk Ramsey, 2008, 2009; Clark et al., 2015; DuRoss et al., 2011; Kelsey et al., 2015; Lienkaemper and Bronk Ramsey, 2009; Nelson et al., 2015; Shennan et al., 2014a; Shennan et al., 2014c; Witter et al., 2016). Integrating samples from areas of uplift, samples from areas of subsidence, samples for maximum ages of earthquakes, and samples for minimum ages of earthquakes into a Bayesian age model provides an age estimate for each hypothesised earthquake based on the correlation of palaeoseismic evidence at different sites across the proposed rupture segment or segments. The likelihood distribution and probability density functions (e.g. Figure 19) provide a good visual summary of the confidence we have in different events. There will likely be tighter constraints on more recent events, not least because we have more data. These model outputs also provide a framework in which to target material to help constrain the less well-known events.

Application of such age-modelling approaches also requires caution. Correlation of stratigraphic evidence between sites and correlation of sample ages does not always mean they are of the same event and careful consideration of the geological evidence alongside models of earthquake rupture should be taken into account rather than drawing simple chronological correlation. An example of this would be radiocarbon dating the 1899 Yakutat Bay earthquakes (Plafker and Thatcher, 2008), where two earthquakes six days apart may appear as the same event in a palaeoseismic record.

Though very likely related, grouping these two earthquakes into one may have differing implications for seismic hazard assessment.

6.3 Spatial constraints

In the early phase of coastal paleoseismology many studies were implicitly inductive, depending on inferences and reasoning. As research progresses and more data from more sites become available, it becomes easier to frame the research to test multiple working hypotheses, which may include predictions of surface displacement derived from geophysical models (e.g. Figure 21). Although described as geological-based criteria for identifying regional coseismic subsidence (Nelson et al., 1996), in testing geophysical models of surface displacement we use these criteria to refute one or more models. The emphasis on the importance of different criteria may change as our knowledge of a tectonic region increases. As we test models for subduction zone ruptures in segments of variable length in different earthquakes we anticipate that sites close together within a segment ought to show the same coseismic inference. If one site has a buried peat with the age tightly constrained by radiocarbon dated samples but with weak criteria (e.g. amount of vertical change across the contact), the lack of a correlation in age to nearby buried peats with strong coseismic criteria is a good indication that the dated peat with weak criteria may be of non-coseismic origin. By comparison, in a less well-studied region, in a setting far removed from an established earthquake chronology the same sort of peat, buried peat of well-constrained age but with weak criteria, the criterion of age correlation well established earthquakes elsewhere on the margin is no longer a justifiable criterion to evaluate whether coseismic submergence formed the peat. This criterion increases in importance as the number of sites studied increases, alongside the geographical context of hypothesised rupture length and spatial pattern of associated coseismic surface deformation.

The spatial attributes of the field-based evidence of coseismic submergence and emergence provide evidence for testing, calibrating and refining tectonic models, in an iterative process similar to those followed at tectonically stable locations with models of glacial isostatic adjustment. Geological estimates of coseismic change can constrain the modelled boundaries or transitions between regions of uplift, subsidence and no vertical change. We must, however, be aware of the discussed detection thresholds, including creation thresholds that may be ~10-15% of the tidal range and for different preservation thresholds that vary according to site location with respect to rupture location and dimensions (Figure 2). These must be considered before rejecting a particular hypothesis.

Notable residuals between the geophysical model predictions and field-based reconstructions can define a framework to target sites for further work to explore for evidence of coseismic change. Analysis of the spatial pattern of residuals should also include an investigation of site-specific

reasons for coseismic evidence not being evident; and alongside this, there should be further efforts to quantify the rates of background non-seismic RSL change that may provide an explanation for the lack of coseismic change (Barlow et al., 2012; Garrett et al., 2015a). In all cases, uncertainties in the reconstructions should be clearly stated and ideally given at the 2-sigma range so that modelling efforts know the range in which they should attempt to work.

7. Conclusions

The original criteria for identifying coseismic subsidence in tidal-wetland stratigraphic sequences at the Cascadia subduction zone have stood the test of time very well in two different respects. On the one hand, the detailed range of evidence and inferences summarised in the original paper (Table 2 in Nelson et al., 1996) provided a guide for the types of evidence assessed in later studies. We have expanded this to reflect numerous new techniques, observations and inferences used over the intervening time (Table 4). On the other hand, the five criteria neatly summarised, 1 - lateral extent of peat-mud couplets with sharp contacts; 2 - suddenness of submergence; 3 - amount of vertical motion; 4 - presence of tsunami deposited sediments directly above the peat horizon, and, 5 - synchroneity with other sites, provided a valuable means to frame the research in a number of later studies (e.g. Briggs et al., 2014; Clark et al., 2015; Dura et al., 2015; Dura et al., 2016; Dura et al., 2011; Engelhart et al., 2013; Garrett et al., 2015b; Grand Pre et al., 2012; Hamilton and Shennan, 2005a; Hayward et al., 2015; Kelsey et al., 2015; Leonard et al., 2004; Nelson et al., 2009; Nelson et al., 2006; Shennan et al., 2009; Witter et al., 2003). In order to reflect developments in research over the past twenty years, for paleoseismological studies of tidal wetland sediment sequences an approach framed around such are criteria is better summarised as assessing the following:

1 – lateral extent of peat-mud or mud-peat couplets with sharp contacts

2 – suddenness of submergence or emergence, replicated a multiple locations within a site

3 – amount of vertical motion, quantified with 95% error terms, replicated at multiple locations within a site

4 – syncroneity of submergence and emergence based on statistical age modelling

5 – spatial pattern of submergence and emergence

6 – possible additional evidence of coseismic motions, including tsunami or liquefaction concurrent with submergence or emergence.

Application of these criteria to tidal wetland evidence across a range of palaeo-seismic locations has the potential to improve understanding of how megathrust earthquakes vary in time and space, and

the growing body of evidence of variable rupture modes provides considerable challenges in revising and updating seismic and tsunami hazard models.

FIGURE CAPTIONS

Figure 1: a) Peat-mud couplet representing the AD 1964 earthquake at Girdwood, Alaska, and ~0.5 m sediment accumulation since (Photograph September 2006). The peat layer represents the freshwater marsh that subsided at least 1.5 m in AD 1964, regional subsidence 1.5 m and locally up to an additional 0.9 m from sediment compaction (Plafker et al., 1969). b) Mud-peat couplet at Katalla, represent coseismic uplift of unvegetated tidal flat ~870 BP and colonisation by freshwater peat-forming communities (Shennan et al., 2014c). c) Ghost forest at Girdwood, with trees killed following subsidence in AD 1964 and subsequent tidal sedimentation. Tree stump from the penultimate great earthquake in the region, ~870 BP, is rooted in a peat-mud couplet a few decimetres below the surface and its top extends to the peat unit of the AD 1964 peat-mud couplet (Photograph May 2006).

Figure 2: Schematic summary of a subduction earthquake cycle, showing the three primary processes (in *italics*) following a subduction earthquake (after Wang et al., 2012), the key features of observed deformation (after Wang, 2007) and six scenarios to illustrate preservation thresholds for records of multiple earthquake cycles. Here postseismic indicates a few years to a few decades after a great earthquake and interseismic is a few decades to centuries after the earthquake. The distance from the trench to the volcano is ~400 km. Arrows at the top show the sense of vertical and horizontal motions of the Earth's surface, the latter relative to distant parts of the upper plate. Length of arrow indicates relative magnitude at coastal locations, a and b, and locations more distant from the trench, c and d.

Figure 3: Figure 3: Zones of coseismic uplift and subsidence in AD 1964 (after Plafker, 1969), present-day velocities (http://www.gps.alaska.edu/jeff/Chapman_GPS_velocities.html accessed 13 July, 2015) and location of coastal marsh sites providing paleoseismic records (circles).

Figure 4: Probability density functions for earthquake ages from sites in the Prince William Sound segment (data from Shennan et al., 2014b; 2014c).

Figure 5: Vertical deformation of ocean floor and adjacent coastal regions for earthquake scenarios summarised in Table 1 and location of sites with paleoseismic evidence. Deformation estimates redrawn from Nicolsky et al. (2013).

Figure 6: Summary microfossil data from Girdwood, original data Shennan & Hamilton (2006), and reconstructions of paleo marsh surface elevations (PMSE) and relative sea level (RSL) from two transfer function model methods, weighted-averaging partial least squares (WAPLS) and modern analogue technique (MAT). Salinity classes are based on the halobian scheme (Karlin and Abella,

1996). Environment classes determined by their mean elevation (defined by the bootstrap species coefficient from the WAPLS transfer function model) in the modern data set.

Figure 7: Comparison of quantitative and qualitative representations of sample elevations for the data from the Girdwood core shown in figure 6.

Figure 8: Comparison of qualitative diatom classification schemes against elevation. Data from the modern training set from south-central Alaska (2015, Table 2).

Figure 9: Comparison of change in summary salinity classification against elevation. We should expect a rise in surface elevation reflected by a fall in the percentage of marine and brackish water diatoms. The shaded quadrants indicate the regions where the diatom changes show the opposite change to that expected. Samples for elevation changes greater than 0.5 m not shown; they all plot in the unshaded quadrants, reflecting the expected direction of change. Data from the modern training set from south-central Alaska (2015, Table 2) based on stratified sampling, measuring change between random pairs stratified by site.

Figure 10: Paleoseismic evidence from Bird Point. A) borehole locations (Google Earth image). B) borehole stratigraphy. C) summary diatom data from borehole 09/1, showing only those species >10% of the assemblage. Species and summary groups, classified by environment (classes determined by their mean elevation (defined by the bootstrap species coefficient from the WAPLS transfer function model: dark blue = ~tidal flat elevations; mid blue = tidal marsh; light blue = upper marsh to freshwater; white = insufficient abundance of species sent in modern data set. The right-hand graph shows the changes in relative sea level (RSL), with 95% confidence limits. D) Probability density functions for earthquake ages (black) from sites in the Prince William Sound segment (Figure 4) and radiocarbon ages (red) from the tops of peat layers (details in Table 3).

Figure 11: Paleoseismic evidence from Hope. A) borehole locations (Google Earth image). B) borehole stratigraphy. C) summary diatom data from borehole 09/1, showing only those species >10% of the assemblage. Species and summary groups, classified by environment (classes determined by their mean elevation (defined by the bootstrap species coefficient from the WAPLS transfer function model: dark blue = ~tidal flat elevations; mid blue = tidal marsh; light blue = upper marsh to freshwater; white = insufficient abundance of species sent in modern data set. The right-hand graph shows the changes in relative sea level (RSL), with 95% confidence limits. D) Probability density functions for earthquake ages (black) from sites in the Prince William Sound segment (Figure 4) and radiocarbon age (red) from the top of the peat layer in C (details in Table 3).

Figure 12: Paleoseismic evidence from Kasilof. A) outcrop and borehole locations (Google Earth image). B) outcrop (upper sections at 1 and 8) and borehole stratigraphy. C) outcrop at 8, summary

diatom changes based on salinity (Σ marine and brackish species) and environment (Σ tidal flat and tidal marsh species), changes in relative sea level (RSL), with 95% confidence limits, stratigraphic position of radiocarbon samples (Table 3), and ^{137}Cs concentrations in upper mud unit.

Figure 13: Paleoseismic evidence from Kasilof. Summary diatom data and RSL change, (A) upper section, and (B) lower section. Species and summary groups, classified by environment (classes determined by their mean elevation (defined by the bootstrap species coefficient from the WAPLS transfer function model: dark blue = ~tidal flat elevations; mid blue = tidal marsh; light blue = upper marsh to freshwater; white = insufficient abundance of species sent in modern data set. The right-hand graph shows the changes in relative sea level (RSL), with 95% confidence limits. C) Probability density functions for earthquake ages (black) from sites in the Prince William Sound segment (Figure 4) and radiocarbon age (red) from the top of the peat C (details in Table 3). C) Probability density functions for earthquake ages (black) from sites in the Prince William Sound segment (Figure 4) and radiocarbon ages from peat A and B and the mud unit between (details in Table 3).

Figure 14: Paleoseismic evidence from Homer. A) borehole locations (Google Earth image). B) borehole stratigraphy. C) Probability density functions for earthquake ages (black) from sites in the Prince William Sound segment (Figure 4) and radiocarbon ages (red and blue) from the tops of the peat layers in boreholes 4 and 5 (details in Table 3).

Figure 15: Homer diatom data and relative sea-level change. Summary diatom data, showing only those species >10% of the assemblage. Species and summary groups, classified by environment (classes determined by their mean elevation (defined by the bootstrap species coefficient from the WAPLS transfer function model: dark blue = ~tidal flat elevations; mid blue = tidal marsh; light blue = upper marsh to freshwater; white = insufficient abundance of species sent in modern data set. The right-hand graph shows the changes in relative sea level (RSL), with 95% confidence limits.

Figure 16: Water levels in Cook Inlet (NOAA tide station at Seldovia) and Homer (waterlogger in Beluga Slough, data from Steve Baird, Kachemak Research Reserve, Homer) for May and June 2011; mean and ranges of paleo marsh surface elevation reconstructions for fossil peat and mud samples in figure 15.

Figure 17: Paleoseismic evidence from Kalsin Bay. A) borehole locations (Google Earth image) and surface transect. B) borehole stratigraphy. C) summary diatom data from borehole 5, showing only those species >10% of the assemblage. Species and summary groups, classified by environment (classes determined by their mean elevation (defined by the bootstrap species coefficient from the WAPLS transfer function model: dark blue = ~tidal flat elevations; mid blue = tidal marsh; light blue = upper marsh to freshwater; white = insufficient abundance of species sent in modern data set. The

right-hand graph shows the changes in relative sea level (RSL), with 95% confidence limits. D) Probability density functions for earthquake ages (black) from sites in the Prince William Sound segment (Figure 4) and radiocarbon age (red) from the tops of peat layers and the base of the sequence (details in Table 3).

Figure 18: Paleoseismic evidence from Anton Larson Bay. A) borehole locations (Google Earth image). B) borehole stratigraphy. C) summary diatom data from borehole 4, showing only those species >10% of the assemblage. Species and summary groups, classified by environment (classes determined by their mean elevation (defined by the bootstrap species coefficient from the WAPLS transfer function model: dark blue = ~tidal flat elevations; mid blue = tidal marsh; light blue = upper marsh to freshwater; white = insufficient abundance of species sent in modern data set. The right-hand graph shows the changes in relative sea level (RSL), with 95% confidence limits. D) Probability density functions for earthquake ages (black) from sites in the Prince William Sound segment (Figure 4) and radiocarbon ages (red) from peat A (78-117 cm) and peat B (146-170 cm, details in Table 3).

Figure 19: Probability density functions for earthquake ages from sites in the Prince William Sound (PWS) segment, 1964 and EQ1 to EQ9 (black lines and blue shading), length of sedimentary record at 18 sites (brown) in four segments of the megathrust, and presence of evidence of coseismic submergence or emergence (black) that correlates with the PWS ages. Grey shading, Homer and Kasilof: see discussion in the text.

Figure 20: Reconstructed paleo-marsh surface elevations 6500-1500 BP at Kenai and Kasilof, m Mean Higher High Water (MHHW), and Highest Astronomical Tide (HAT).

Figure 21: Comparisons of paleoseismic evidence (circles) for three late Holocene earthquakes (EQ1, ~850 BP; EQ2, ~1500 BP; EQ3, ~2100 BP) with estimates of coseismic displacement from models of four modes of rupture (Scenarios A – D, Table 1 and figure 5). Estimates of displacement derived from (Nicolsky et al., 2013); paleoseismic evidence interpreted as coseismic submergence (blue), coseismic emergence (red) and no coseismic change is relative land/sea level (white).

Figure 22: Predicted coseismic displacement at sites along Turnagain Arm, approximately perpendicular to the megathrust, for three modes of rupture, compared with reconstructed coseismic relative land-level change at five sites during EQ3, ~2100 BP. At Anchorage there is evidence for no rapid change, inferred from sediment stratigraphy and diatom assemblages within the tidal flat sediments of that were accumulating at that time. Colours and site locations as shown in Figure 21. Horizontal scale: Anchorage to Portage = 65 km.

TABLE CAPTIONS

Table 1: Summary of tectonic models used to predict coseismic surface deformation. Model parameters and deformation estimates from Nicolsky et al. (2013); their figures 10, 14 and 15.

Table 2: Summary statistics for weighted-averaging partial least squares transfer function models used to reconstruct paleo marsh surface elevations. The 2005 models use modern samples only from upper Cook Inlet, 2013 and 2015 use modern samples from sites across south-central Alaska.

Table 3: Radiocarbon dated samples, not previously published. All samples less than 0.01 m.

Table 4: Stratigraphic, sedimentologic, paleontologic, and age evidence from tidal-marsh stratigraphic sequences for coastal subsidence or uplift during great earthquakes at subduction zones

Table Footnote: Inferences are made from evidence and comments are about evidence. Papers evaluated include those cited in the original version (Nelson et al., 1996) and these additional ones (Alam et al., 2012; Atwater et al., 2005; Atwater et al., 2001; Bender et al., 2015; Carver and Plafker, 2008; Chagué-Goff et al., 2011; Dura et al., 2015; Dura et al., 2016; Dura et al., 2011; Engel and Brückner, 2011; Engelhart et al., 2013; Garrett et al., 2013; Goff et al., 2011a; Grand Pre et al., 2012; Kelsey et al., 2002; Martin and Bourgeois, 2012; McCalpin and Carver, 2009; Morton et al., 2007; Nelson et al., 2015; Nelson et al., 2006; Obermeier and Dickenson, 2000; Pilarczyk et al., 2014; Shennan, 2009; Shennan et al., 2014a; Shennan et al., 2014c; Walsh et al., 1995; Witter et al., 2003; Yamaguchi et al., 1997)

Acknowledgements

Work supported by the U.S. Geological Survey earthquake hazards project awards G13AP00051, G12AP20084, G10AP00075 and G09AP00105 (The views and conclusions contained in this document are those of the authors and should not be interpreted as necessarily representing the official policies, either expressed or implied, of the U.S. Government) and NERC Radiocarbon Allocations 935.0901 and 1339.1008. Barlow thanks The Royal Society Dudley Stamp Memorial Fund, The Royal Geographical Society Monica Cole Research Grant and Department of Geography, Durham University for financial support whilst undertaking fieldwork at Hope and Bird Point. Brian Atwater, Julius Jara-Muñoz and Alan Nelson for comments on a previous version.

References

Alam, E., Dominey-Howes, D., Chagué-Goff, C., Goff, J., 2012. Tsunamis of the northeast Indian Ocean with a particular focus on the Bay of Bengal region—A synthesis and review. Earth-Science Reviews 114, 175-193.

Atwater, B.F., 1987. Evidence for great Holocene earthquakes along the outer coast of Washington State. Science 236, 942-944.

Atwater, B.F., Hemphill-Haley, E., 1997. Recurrence intervals for great earthquakes of the past 3,500 years at northeastern Willapa Bay, Washington. U.S. Geological Survey Professional Paper 1576, 1-108.

Atwater, B.F., Musumi-Rokkaku, S., Satake, K., Tsuji, Y., Ueda, K., Yamaguchi, D.K., 2005. The Orphan Tsunami of 1700—Japanese Clues to a Parent Earthquake in North America. U.S. Geological Survey Professional Paper 1707, 1-144.

Atwater, B.F., Nelson, A.R., Clague, J.J., Carver, G.A., Yamaguchi, D.K., Bobrowsky, P.T., Borgeois, J., Darienzo, M.E., Grant, W.C., Hemphill-Haley, E., Kelsey, H.M., Jacoby, G.C., Nishenko, S.P., Palmer, S.P., Peterson, C.D., Reinhart, M.A., 1995. Summary of coastal geologic evidence for past great earthquakes at the Cascadia subduction zone. Earthquake Spectra 11, 1-18.

Atwater, B.F., Yamaguchi, D.K., Bondevik, S., Barnhardt, W.A., Amidon, L.J., Benson, B.E., Skjerdal, G., Shulene, J.A., Nanayama, F., 2001. Rapid resetting of an estuarine recorder of the 1964 Alaska earthquake. Geological Society of America Bulletin 113, 1193-1204.

Barlow, N.L.M., Shennan, I., Long, A.J., 2012. Relative sea-level response to Little Ice Age ice mass change in south central Alaska: Reconciling model predictions and geological evidence. Earth and Planetary Science Letters 315-316, 62-75.

Barlow, N.L.M., Shennan, I., Long, A.J., Gehrels, W.R., Saher, M.H., Woodroffe, S.A., Hillier, C., 2013. Salt marshes as late Holocene tide gauges. Global and Planetary Change 106, 90-110.

Bender, A.M., Witter, R.C., Rogers, M., 2015. Testing the use of bulk organic δ13C, δ15N, and Corg:Ntot ratios to estimate subsidence during the 1964 great Alaska earthquake. Quaternary Science Reviews 113, 134-146.

Bernhardt, C.E., Willard, D.A., 2015. Pollen and spores of terrestrial plants, Handbook of Sea-Level Research. John Wiley & Sons, Ltd, pp. 218-232.

Berryman, K.R., Cochran, U.A., Clark, K.J., Biasi, G.P., Langridge, R.M., Villamor, P., 2012. Major Earthquakes Occur Regularly on an Isolated Plate Boundary Fault. Science 336, 1690-1693.

Beyens, L., Denys, L., 1982. Problems in diatom analysis of deposits: allochthonous valves and fragmentation. Geologie en Mijnbouw 61, 159-162.

Birks, H.J.B., 1995. Quantitative palaeoenvironmental reconstructions, In: Maddy, D., Brew, J.S. (Eds.), Statistical modelling of Quaternary Science data. Quaternary Research Association., Cambridge, pp. 161-254.

Brain, M.J., 2015. Compaction, Handbook of Sea-Level Research. John Wiley & Sons, Ltd, pp. 452-469.

Briggs, R.W., Engelhart, S.E., Nelson, A.R., Dura, T., Kemp, A.C., Haeussler, P.J., Corbett, D.R., Angster, S.J., Bradley, L.-A., 2014. Uplift and subsidence reveal a nonpersistent megathrust rupture boundary (Sitkinak Island, Alaska). Geophysical Research Letters, 2014GL059380.

Bronk Ramsey, C., 2008. Deposition models for chronological records. Quaternary Science Reviews 27, 42-60.

Bronk Ramsey, C., 2009. Bayesian analysis of radiocarbon dates. Radiocarbon 51, 337-360.

Carver, G., Plafker, G., 2008. Paleoseismicity and Neotectonics of the Aleutian Subduction Zone - An Overview, In: Freymueller, J.T., Haeussler, P.J., Wesson, R., Ekstrom, G. (Eds.), Active tectonics and seismic potential of Alaska. American Geophysical Union, Washington, pp. 43-63.

Chagué-Goff, C., Schneider, J.-L., Goff, J.R., Dominey-Howes, D., Strotz, L., 2011. Expanding the proxy toolkit to help identify past events — Lessons from the 2004 Indian Ocean Tsunami and the 2009 South Pacific Tsunami. Earth-Science Reviews 107, 107-122.

Chapman, J.B., Elliott, J., Doser, D.I., Pavlis, T.L., 2014. Slip on the Suckling Hills splay fault during the 1964 Alaska earthquake. Tectonophysics 637, 191-197.
Chapman, J.B., Worthington, L.L., Pavlis, T.L., Bruhn, R.L., Gulick, S.P., 2011. The Suckling Hills Fault, Kayak Island Zone, and accretion of the Yakutat microplate, Alaska. Tectonics 30, TC6011, doi:6010.1029/2011TC002945.
Charman, D.J., 2015. Testate amoebae, Handbook of Sea-Level Research. John Wiley & Sons, Ltd, pp. 281-294.
Cisternas, M., Atwater, B.F., Torrejon, F., Sawai, Y., Machuca, G., Lagos, M., Eipert, A., Youlton, C., Salgado, I., Kamataki, T., Shishikura, M., Rajendran, C.P., Malik, J.K., Rizal, Y., Husni, M., 2005. Predecessors of the giant 1960 Chile earthquake. Nature 437, 404-407.
Clark, K.J., Hayward, B.W., Cochran, U.A., Wallace, L.M., Power, W.L., Sabaa, A.T., 2015. Evidence for Past Subduction Earthquakes at a Plate Boundary with Widespread Upper Plate Faulting: Southern Hikurangi Margin, New Zealand. Bulletin of the Seismological Society of America 105, 1661-1690.
Combellick, R.A., 1991. Palaeoseismicity of the Cook Inlet region, Alaska: Evidence from peat stratigraphy in Turnagain and Knik Arms. Alaska Division of Geological and Geophysical Surveys Professional Report 112, 1-52.
Combellick, R.A., 1994. Investigation of peat stratigraphy in tidal marshes along Cook Inlet, Alaska, to determine the frequency of 1964-style great earthquakes in the Anchorage region. Alaska Division of Geological and Geophysical Surveys Report of Investigations 94-7, 1-24.
Combellick, R.A., Pinney, D.S., 1995. Radiocarbon age of probable Hayes tephra, Kenai Peninsula, Alaska, In: Combellick, R.A., Tannian, F. (Eds.), Short notes on Alaskan geology 1995. Professional report 117. State of Alaska Department of Natural Resources, pp. 1-9.
Combellick, R.A., Reger, R.D., 1994. Sedimentological and radiocarbon age data for tidal marshes along eastern and upper Cook Inlet, Alaska. Alaska Division of Geological and Geophysical Surveys Report of Investigations 94-6, 1-60.
Cronin, T.M., 2015. Ostracods and sea level, Handbook of Sea-Level Research. John Wiley & Sons, Ltd, pp. 249-257.
Davies, J., Sykes, L., House, L., Jacob, K., 1981. Shumagin Seismic Gap, Alaska Peninsula: History of great earthquakes, tectonic setting, and evidence for high seismic potential. Journal of Geophysical Research: Solid Earth 86, 3821-3855.
Denys, L., 1991. A checklist of the diatoms in the Holocene deposits of the western Belgian coastal plain with a survey of their apparent ecological requirments. Belgian Geological Survey Professional Paper 1991/2 246, 1-41.
Dura, T., Cisternas, M., Horton, B.P., Ely, L.L., Nelson, A.R., Wesson, R.L., Pilarczyk, J.E., 2015. Coastal evidence for Holocene subduction-zone earthquakes and tsunamis in central Chile. Quaternary Science Reviews 113, 93-111.
Dura, T., Hemphill-Haley, E., Sawai, Y., Horton, B.P., 2016. The application of diatoms to reconstruct the history of subduction zone earthquakes and tsunamis. Earth-Science Reviews 152, 181-197.
Dura, T., Rubin, C.M., Kelsey, H.M., Horton, B.P., Hawkes, A., Vane, C.H., Daryono, M., Pre, C.G., Ladinsky, T., Bradley, S., 2011. Stratigraphic record of Holocene coseismic subsidence, Padang, West Sumatra. Journal of Geophysical Research: Solid Earth 116, B11306.
DuRoss, C.B., Personius, S.F., Crone, A.J., Olig, S.S., Lund, W.R., 2011. Integration of Paleoseismic Data from Multiple Sites to Develop an Objective Earthquake Chronology: Application to the Weber Segment of the Wasatch Fault Zone, Utah. Bulletin of the Seismological Society of America 101, 2765-2781.
Edwards, R., Wright, A., 2015. Foraminifera, Handbook of Sea-Level Research. John Wiley & Sons, Ltd, pp. 191-217.
Engel, M., Brückner, H., 2011. The identification of palaeo-tsunami deposits–a major challenge in coastal sedimentary research. Coastline Reports 17, 65-80.

Engelhart, S.E., Horton, B.P., Vane, C.H., Nelson, A.R., Witter, R.C., Brody, S.R., Hawkes, A.D., 2013. Modern foraminifera, δ13C, and bulk geochemistry of central Oregon tidal marshes and their application in paleoseismology. Palaeogeography, Palaeoclimatology, Palaeoecology 377, 13-27.
Garrett, E., Barlow, N.L.M., Cool, H., Kaufman, D.S., Shennan, I., Zander, P.D., 2015a. Constraints on regional drivers of relative sea-level change around Cordova, Alaska. Quaternary Science Reviews 113, 48-59.
Garrett, E., Shennan, I., Watcham, E.P., Woodroffe, S.A., 2013. Reconstructing paleoseismic deformation, 1: modern analogues from the 1960 and 2010 Chilean great earthquakes. Quaternary Science Reviews 75, 11-21.
Garrett, E., Shennan, I., Woodroffe, S.A., Cisternas, M., Hocking, E.P., Gulliver, P., 2015b. Reconstructing paleoseismic deformation, 2: 1000 years of great earthquakes at Chucalén, south central Chile. Quaternary Science Reviews 113, 112-122.
Gilpin, L.M., 1995. Holocene paleoseismicity and coastal tectonics of the Kodiak Islands, Alaska. University of California Santa Cruz, Santa Cruz, p. 358.
Goff, J., Chagué-Goff, C., Dominey-Howes, D., McAdoo, B., Cronin, S., Bonté-Grapetin, M., Nichol, S., Horrocks, M., Cisternas, M., Lamarche, G., Pelletier, B., Jaffe, B., Dudley, W., 2011a. Palaeotsunamis in the Pacific Islands. Earth-Science Reviews 107, 141-146.
Goff, J., Lamarche, G., Pelletier, B., Chagué-Goff, C., Strotz, L., 2011b. Predecessors to the 2009 South Pacific tsunami in the Wallis and Futuna archipelago. Earth-Science Reviews 107, 91-106.
Goldfinger, C., Nelson, C.H., Morey, A.E., Johnson, J.E., Patton, J.R., Karabanov, E., Gutiérrez-Pastor, J., Eriksson, A.T., Gràcia, E., Dunhill, G., Enkin, R.J., Dallimore, A., Vallier, T., 2012. Turbidite event history - Methods and implications for Holocene paleoseismicity of the Cascadia subduction zone. U.S. Geological Survey Professional Paper 1661-F, 1-170.
Goto, K., Chagué-Goff, C., Fujino, S., Goff, J., Jaffe, B., Nishimura, Y., Richmond, B., Sugawara, D., Szczuciński, W., Tappin, D.R., Witter, R.C., Yulianto, E., 2011. New insights of tsunami hazard from the 2011 Tohoku-oki event. Marine Geology 290, 46-50.
Grand Pre, C.A., Horton, B.P., Kelsey, H.M., Rubin, C.M., Hawkes, A.D., Daryono, M.R., Rosenberg, G., Culver, S.J., 2012. Stratigraphic evidence for an early Holocene earthquake in Aceh, Indonesia. Quaternary Science Reviews 54, 142-151.
Guilbault, J., Clague, J.J., Lapointe, M., 1996. Foraminiferal evidence for the amount of coseismic subsidence during a late Holocene earthquake on Vancouver island, west coast of Canada. Quaternary Science Reviews 15, 913-937.
Guilbault, J.P., Clague, J.J., Lapointe, M., 1995. Amount of subsidence during a late Holocene earthquake - evidence from fossil tidal marsh foraminifera at Vancouver Island, west coast of Canada. Palaeogeography, Palaeoclimatology, Palaeoecology 111, 49-71.
Hamilton, S., Shennan, I., 2005a. Late Holocene relative sea-level changes and the earthquake deformation cycle around upper Cook Inlet, Alaska. Quaternary Science Reviews 24, 1479-1498.
Hamilton, S., Shennan, I., Combellick, R., Mulholland, J., Noble, C., 2005. Evidence for two great earthquakes at Anchorage, Alaska and implications for multiple great earthquakes through the Holocene. Quaternary Science Reviews 24, 2050-2068.
Hamilton, S.L., 2003. Late Holocene relative sea-level changes and earthquakes around the upper Cook Inlet, Alaska, USA. , Geography. Durham University.
Hamilton, S.L., Shennan, I., 2005b. Late Holocene great earthquakes and relative sea-level change at Kenai, southern Alaska. Journal of Quaternary Science 20, 95-111.
Hawkes, A.D., Horton, B.P., Nelson, A.R., Vane, C.H., Sawai, Y., 2011. Coastal subsidence in Oregon, USA, during the giant Cascadia earthquake of AD 1700. Quaternary Science Reviews 30, 364-376.
Hayward, B.W., Grenfell, H.R., Sabaa, A.T., Carter, R., Cochran, U., Lipps, J.H., Shane, P.R., Morley, M.S., 2006. Micropaleontological evidence of large earthquakes in the past 7200 years in southern Hawke's Bay, New Zealand. Quaternary Science Reviews 25, 1186-1207.

Hayward, B.W., Grenfell, H.R., Sabaa, A.T., Cochran, U.A., Clark, K.J., Wallace, L., Palmer, A.S., 2015. Salt-marsh foraminiferal record of 10 large Holocene (last 7500 yr) earthquakes on a subducting plate margin, Hawkes Bay, New Zealand. Geological Society of America Bulletin.
Horton, B.P., Edwards, R.J., Lloyd, J.M., 1999. A foraminiferal-based transfer function: Implications for sea-level studies. Journal of Foraminiferal Research 29, 117-129.
Hughes, J.F., Mathewes, R.W., Clague, J.J., 2002. Use of pollen and vascular plants to estimate coseismic subsidence at a tidal marsh near Tofino, British Columbia. Palaeogeography, Palaeoclimatology, Palaeoecology 185, 145-161.
Hutchinson, I., Crowell, A.L., 2007. Recurrence and Extent of Great Earthquakes in Southern Alaska During the Late Holocene from an Analysis of the Radiocarbon Record of Land-Level Change and Village Abandonment. Radiocarbon 49, 1323-1385.
Imbrie, J., Kipp, N.G., 1971. A new micropaleontological method for quantitative paleoclimatology: application to a Late Pleistocene Caribbean core, In: Turekian, K.K. (Ed.), The Late Cenozoic Glacial Ages. Yale University Press, New Haven, pp. 71-181.
Karlin, R.E., Abella, S.E.B., 1996. A history of Pacific Northwest earthquakes recorded in Holocene sediments from Lake Washington. Journal of Geophysical Research 101, 6137-6150.
Kelsey, H.M., 2015. Geomorphological indicators of past sea levels, Handbook of Sea-Level Research. John Wiley & Sons, Ltd, pp. 66-82.
Kelsey, H.M., Witter, R.C., Engelhart, S.E., Briggs, R., Nelson, A., Haeussler, P., Corbett, D.R., 2015. Beach ridges as paleoseismic indicators of abrupt coastal subsidence during subduction zone earthquakes, and implications for Alaska-Aleutian subduction zone paleoseismology, southeast coast of the Kenai Peninsula, Alaska. Quaternary Science Reviews.
Kelsey, H.M., Witter, R.C., Hemphill-Haley, E., 2002. Plate-boundary earthquakes and tsunamis of the past 5500 years, Sixes River estuary, southern Oregon. Bulletin of the Geological Society of America 114, 298-314.
Kemp, A.C., Telford, R.J., 2015. Transfer functions, Handbook of Sea-Level Research. John Wiley & Sons, Ltd, pp. 470-499.
Koehler, R.D., Farrell, R.E., Burns, P.A.C., Combellick, R.A., 2012. Quaternary faults and folds in Alaska: A digital database. Alaska Division of Geological & Geophysical Surveys Miscellaneous Publication 141, 1-31.
Kortekaas, S., Dawson, A., 2007. Distinguishing tsunami and storm deposits: an example from Martinhal, SW Portugal. Sedimentary Geology 200, 208-221.
Leonard, L.J., Hyndman, R.D., Mazzotti, S., 2004. Coseismic subsidence in the 1700 great Cascadia earthquake: Coastal estimates versus elastic dislocation models. Geological Society of America Bulletin 116, 655-670.
Lienkaemper, J.J., Bronk Ramsey, C., 2009. OxCal: Versatile tool for developing paleoearthquake chronolgies - A primer. Seismological Research Letters 80, 431-434.
Long, A.J., Shennan, I., 1993. Holocene relative sea-level and crustal movements in southeast and northeast England, U.K, In: Owen, L.A., Stewart, I., Vita-Finzi, C. (Eds.), Neotectonics: Recent Advances. Quaternary Proceedings No.3, Quaternary Research Association, Cambridge, pp. 15-19.
Long, A.J., Shennan, I., 1994. Sea-level changes in Washington and Oregon and the 'earthquake deformation cycle'. Journal of Coastal Research 10(4), 825-838.
Long, A.J., Shennan, I., 1998. Models of rapid relative sea-level change in Washington and Oregon, USA. The Holocene 8, 129-142.
Malik, J.N., Shishikura, M., Echigo, T., Ikeda, Y., Satake, K., Kayanne, H., Sawai, Y., Murty, C.V.R., Dikshit, O., 2011. Geologic evidence for two pre-2004 earthquakes during recent centuries near Port Blair, South Andaman Island, India. Geology 39, 559-562.
Martin, M.E., Bourgeois, J., 2012. Vented sediments and tsunami deposits in the Puget Lowland, Washington – differentiating sedimentary processes. Sedimentology 59, 419-444.
McCalpin, J., P, Carver, G., 2009. Paleoseismology of compressional tectonic environments, In: McCalpin, J., P (Ed.), Paleoseismology, 2nd ed. Academic Press, Burlington, pp. 315 - 419.

McCalpin, J.P., Nelson, A., 2009. Introduction to Paleoseismology, In: McCalpin, J.P. (Ed.), Paleoseismology, 2nd ed. Academic Press, Burlington, pp. 1-27.
Minoura, K., Imamura, F., Sugawara, D., Kono, Y., Iwashita, T., 2001. The 869 Jōgan tsunami deposit and recurrence interval of large-scale tsunami on the Pacific coast of noertheast Japan. Journal of Natural Disaster Science 23, 83-88.
Morton, R.A., Gelfenbaum, G., Jaffe, B.E., 2007. Physical criteria for distinguishing sandy tsunami and storm deposits using modern examples. Sedimentary Geology 200, 184-207.
Mueller, C.S., Briggs, R.W., Wesson, R.L., Petersen, M.D., 2015. Updating the USGS seismic hazard maps for Alaska. Quaternary Science Reviews 113, 39-47.
Nelson, A.R., 2015. Coastal sediments, Handbook of Sea-Level Research. John Wiley & Sons, Ltd, pp. 47-65.
Nelson, A.R., Atwater , B.F., Bobrowski, P.T., Bradley, L.A., Clague, J.J., Carver, G.A., Darienzo, M.E., Grant, W.C., Krueger, H.W., Sparks, R., Stafford, T.W.J., Stuvier, M., 1995. Radiocarbon evidence for extensive plate-boundary rupture about 300 years ago at the Cascadia subduction zone. Nature 378, 371-374.
Nelson, A.R., Briggs, R.W., Dura, T., Engelhart, S.E., Gelfenbaum, G., Bradley, L.-A., Forman, S.L., Vane, C.H., Kelley, K.A., 2015. Tsunami recurrence in the eastern Alaska-Aleutian arc: A Holocene stratigraphic record from Chirikof Island, Alaska. Geosphere.
Nelson, A.R., Kashima, K., Bradley, L.-A., 2009. Fragmentary Evidence of Great-Earthquake Subsidence during Holocene Emergence, Valdivia Estuary, South Central Chile. Bulletin of the Seismological Society of America 99, 71-86.
Nelson, A.R., Kelsey, H.M., Witter, R.C., 2006. Great earthquakes of variable magnitude at the Cascadia subduction zone. Quaternary Research 65, 354-365.
Nelson, A.R., Shennan, I., Long, A.J., 1996. Identifying coseismic subsidence in tidal-wetland stratigraphic sequences at the Cascadia subduction zone of western North America. Journal of Geophysical Research 101, 6115-6135.
Nicolsky, D.J., Suleimani, E.N., Haeussler, P.J., Ryan, H.F., Koehler, R.D., Combellick, R.A., Hansen, R.A., 2013. Tsunami inundation maps of Port Valdez, Alaska. Alaska Division of Geological & Geophysical Surveys Report of Investigation 2013-1, 1-77.
Nicolsky, D.J., Suleimani, E.N., Koehler, R.D., 2014. Tsunami inundation maps of Cordova and Tatitlek, Alaska. Alaska Division of Geological & Geophysical Surveys Report of Investigation 2014-1, 1-49.
Nishenko, S.P., Jacob, K.H., 1990. Seismic potential of the Queen Charlotte - Alaska - Aleutian seismic zone. Journal of Geophysical Research 95, 2511-2532.
NOAA, 2016. Tides and Currents https://tidesandcurrents.noaa.gov/products.html, Silver Spring, MD, USA, p. Center for Operational Oceanographic Products and Services.
Obermeier, S.F., Dickenson, S.E., 2000. Liquefaction Evidence for the Strength of Ground Motions Resulting from Late Holocene Cascadia Subduction Earthquakes, with Emphasis on the Event of 1700 A.D. Bulletin of the Seismological Society of America 90, 876-896.
Okal, E.A., Borrero, J.C., Chagué-Goff, C., 2011. Tsunamigenic predecessors to the 2009 Samoa earthquake. Earth-Science Reviews 107, 128-140.
Patrick, R., Reimer, C.W., 1966. The Diatoms of the United States. Volume 1. Monographs of The Academy of Natural Sciences of Philadelphia No 13. Academy of Natural Sciences of Philadelphia, Philadelphia.
Patrick, R., Reimer, C.W., 1975. The Diatoms of the United States. Volume 2, Part 1. Monographs of The Academy of Natural Sciences of Philadelphia No 13. The Academy of Natural Sciences of Philadelphia, Philadelphia.
Pilarczyk, J.E., Barber, D.C., 2015. Mollusca, Handbook of Sea-Level Research. John Wiley & Sons, Ltd, pp. 258-267.

Pilarczyk, J.E., Dura, T., Horton, B.P., Engelhart, S.E., Kemp, A.C., Sawai, Y., 2014. Microfossils from coastal environments as indicators of paleo-earthquakes, tsunamis and storms. Palaeogeography, Palaeoclimatology, Palaeoecology 413, 144-157.
Plafker, G., 1969. Tectonics of the March 27, 1964, Alaska earthquake. U.S. Geological Survey Professional Paper 543-I, 74.
Plafker, G., Hudson, T., Rubin, M., Dixon, K., L., 1982. Holocene marine terraces and uplift history in the Yakataga seismic gap near Icy Cape, Alaska. U.S. Geological Survey Circular 844, 111-115.
Plafker, G., Kachadoorian, R., 1966. Geologic effects of the March 1964 earthquake and associated seismic sea waves on Kodiak and nearby islands, Alaska. U.S. Geological Survey Professional Paper 543-D, 46.
Plafker, G., Kachadoorian, R., Eckel, E.B., Mayo, L.R., 1969. Effects of the earthquake of march 27, 1964 on various communities. US Geological Survey Professional Paper 542-G, 1-50.
Plafker, G., Thatcher, W., 2008. Geological and geophysical evaluation of the mechanisms of the Great 1899 Yakutat Bay Earthquakes, In: Freymueller, J.T., Haeussler, P.J., Wesson, R., Ekström, G. (Eds.), Active Tectonics and Seismic Potential of Alaska. AGU, Washington, DC, pp. 215-236.
Reger, R.D., Sturmann, A.G., Berg, E.E., Burns, P.A.C., 2007. A guide to the late Quaternary history of northern and western Kenai Peninsula, Alaska. State of Alaska Department of Natural Resources, Division of Geological & Geophysical Surveys Guidebook 8, 1-112.
Sauber, J., Carver, G., Cohen, S., King, R., 2006. Crustal deformation and the seismic cycle across the Kodiak Islands, Alaska. Journal of Geophysical Research: Solid Earth 111, B02403.
Sawai, Y., 2001b. Distribution of living and dead diatoms in tidal wetlands of northern Japan: relations to taphonomy. Palaeogeography, Palaeoclimatology, Palaeoecology 173, 125-141.
Sawai, Y., Satake, K., Kamataki, T., Nasu, H., Shishikura, M., Atwater, B.F., Horton, B.P., Kelsey, H.M., Nagumo, T., Yamaguchi, M., 2004. Transient uplift after a 17th-Century earthquake along the Kuril subduction zone. Science 306, 1918-1920.
Sawai, Y., Shishikura, M., Komatsubara, J., 2008. A study on paleotsunami using hand corer in Sendai plain (Sendai City, Natori City, Iwanuma City, Watari Town, Yamamoto Town), Miyagi, Japan. Annual Report on Active Fault and Paleoearthquake Researches 8, 17-70.
Scholz, C.H., 2014. Holocene Earthquake History of Cascadia: A Quantitative Test. Bulletin of the Seismological Society of America 104, 2120-2124.
Shanmugam, G., 2012. Process-sedimentological challenges in distinguishing paleo-tsunami deposits. Natural Hazards 63, 5-30.
Shennan, I., 1982. Interpretation of Flandrian sea-level data from the Fenland, England. Proceedings of the Geologists' Association 93, 53-63.
Shennan, I., 1986. Flandrian sea-level changes in the Fenland II. Tendencies of sea-level movement, altitudinal changes and local and regional factors. Journal of Quaternary Science 1, 155-179.
Shennan, I., 2009. Late Quaternary sea-level changes and palaeoseismology of the Bering Glacier region, Alaska. Quaternary Science Reviews 28, 1762-1773.
Shennan, I., Barlow, N., Carver, G., Davies, F., Garrett, E., Hocking, E., 2014a. Great tsunamigenic earthquakes during the past 1000 yr on the Alaska megathrust. Geology 42, 687-690.
Shennan, I., Barlow, N.L.M., Combellick, R., Pierre, K., Stuart-Taylor, O., 2014b. Late Holocene paleoseismology of a site in the region of maximum subsidence during the 1964 Mw 9.2 Alaska earthquake. Journal of Quaternary Science 29, 343-350.
Shennan, I., Bruhn, R., Barlow, N., Good, K., Hocking, E., 2014c. Late Holocene great earthquakes in the eastern part of the Aleutian megathrust. Quaternary Science Reviews 84, 86-97.
Shennan, I., Bruhn, R., Plafker, G., 2009. Multi-segment earthquakes and tsunami potential of the Aleutian megathrust. Quaternary Science Reviews 28, 7-13.
Shennan, I., Hamilton, S., 2006. Coseismic and pre-seismic subsidence associated with great earthquakes in Alaska. Quaternary Science Reviews 25, 1-8.

Shennan, I., Long, A.J., Rutherford, M.M., Green, F.M., Innes, J.B., Lloyd, J.M., Zong, Y., Walker, K., 1996. Tidal marsh stratigraphy, sea level change and large earthquakes, I: A 5000 year record in Washington USA. Quaternary Science Reviews 15, 1023-1059.
Shennan, I., Milne, G., Bradley, S., 2011. Late Holocene vertical land motion and relative sea-level changes: lessons from the British Isles. Journal of Quaternary Science 27, 64-70.
Shennan, I., Scott, D.B., Rutherford, M., Zong, Y., 1999. Microfossil analysis of sediments representing the 1964 earthquake, exposed at Girdwood Flats, Alaska, USA. Quaternary International 60, 55-73.
Soberg, R., 1991. Bridging Alaska: from the Big Delta to the Kenai. Hardscratch Press, Walnut Creek, CA.
Soloviev, S.L., 1990. Sanak-Kodiak tsunami of 1788. Science of Tsunami Hazards 8, 34-30.
Stone, R.W., 1906. Coal fields of the Kachemak Bay region. Bulletin of the United States Geological Survey 277, 53-73.
Suito, H., Freymueller, J.T., 2009. A viscoelastic and afterslip postseismic deformation model for the 1964 Alaska earthquake. Journal of Geophysical Research: Solid Earth 114, B11404.
Suleimani, E.N., Hansen, R.A., Combellick, R.A., Carver, G.A., Kamphaus, R.A., Newman, J.C., Venturato, A.J., 2002. Tsunami hazard maps of the Kodiak area, Alaska. Alaska Division of Geological & Geophysical Surveys Report of Investigation 2002-1, 1-16.
Thomas, E., Varekamp, J.C., 1991. Paleo-Environmental Analyses of Marsh Sequences (Clinton, Connecticut): Evidence for Punctuated Rise in Relative Sealevel During the Latest Holocene. Journal of Coastal Research 11, 125-158.
Tooley, M.J., 1974. Sea-level changes during the last 9000 years in northwest England. The Geographical Journal 140, 18-42.
Tooley, M.J., 1976. Flandrian sea-level changes in West Lancashire and their implications for the 'Hillhouse Coastline'. Geological Journal 11, 137-152.
Tooley, M.J., 1978. Sea-level changes in north-west England during the Flandrian Stage. Clarendon Press, Oxford.
Van der Werff, A., Huls, H., 1958-1974. Diatomeeenflora van Nederland. 8 parts. Published privately, De Hoef, The Netherlands.
Varekamp, J.C., Thomas, E., van de Plassche, O., 1992. Relative Sea-Level Rise and Climate Change Over the Last 1500 Years. Terra Nova 4, 293-304.
Waller, R.M., 1966. Effects of the earthquake of March 27, 1964 in the Homer area, Alaska. US Geological Survey Professional Paper 542-D, 1-28.
Walsh, T.J., Combellick, R.A., Black, G.L., 1995. Liquefaction features from a subduction zone earthqauke: preserved examples from the 1964 Alaska earthquake. Washington Division of Geology and Earth Resources Report of Investigations 32, 1-80.
Wang, K., 2007. Elastic and viscoelastic models of subduction earthquake cycles, In: Dixon, T.H., Moore, J.C. (Eds.), The Seismogenic Zone of Subduction Thrust Faults. Columbia University Press, New York, pp. 540-575.
Wang, K., Hu, Y., He, J., 2012. Deformation cycles of subduction earthquakes in a viscoelastic Earth. Nature 484, 327-332.
Watcham, E.P., Shennan, I., Barlow, N.L.M., 2013. Scale considerations in using diatoms as indicators of sea-level change: lessons from Alaska. Journal of Quaternary Science 28, 165-179.
Wesson, R.L., Boyd, O.S., Mueller, C.S., Bufe, C.G., Frankel, A.D., Petersen, M.D., 2007. Revision of time-independent probabilistic seismic hazard maps for Alaska, U.S. Geological Survey Open-File Report, pp. 1-33.
Wesson, R.L., Boyd, O.S., Mueller, C.S., Frankel, A.D., 2008. Challenges in making a seismic hazard map for Alaska and the Aleutians, In: Freymueller, J.T., Haeussler, P.J., Wesson, R., Ekström, G. (Eds.), Active Tectonics and Seismic Potential of Alaska. AGU, Washington, DC, pp. 385-397.
Witter, R.C., 2015. Pre-fieldwork surveys, Handbook of Sea-Level Research. John Wiley & Sons, Ltd, pp. 27-46.

Witter, R.C., Briggs, R.W., Engelhart, S.E., Gelfenbaum, G., Koehler, R.D., Barnhart, W.D., 2014. Little late Holocene strain accumulation and release on the Aleutian megathrust below the Shumagin Islands, Alaska. Geophysical Research Letters, 2014GL059393.
Witter, R.C., Carver, G.A., Briggs, R.W., Gelfenbaum, G., Koehler, R.D., La Selle, S., Bender, A.M., Engelhart, S.E., Hemphill-Haley, E., Hill, T.D., 2015. Unusually large tsunamis frequent a currently creeping part of the Aleutian megathrust. Geophysical Research Letters, 2015GL066083.
Witter, R.C., Carver, G.A., Briggs, R.W., Gelfenbaum, G., Koehler, R.D., La Selle, S., Bender, A.M., Engelhart, S.E., Hemphill-Haley, E., Hill, T.D., 2016. Unusually large tsunamis frequent a currently creeping part of the Aleutian megathrust. Geophysical Research Letters 43, 76-84.
Witter, R.C., Kelsey, H.M., Hemphill-Haley, E., 2003. Great Cascadia earthquakes and tsunamis of the past 6700 years, Coquille River estuary, southern coastal Oregon. Geological Society of America Bulletin 115, 1289-1306.
Yamaguchi, D.K., Atwater, B.F., Bunker, D.E., Benson, B.E., Reid, M.S., 1997. Tree-ring dating the 1700 Cascadia earthquake. Nature 389, 922.
Zong, Y., Horton, B.P., 1999. Diatom-based tidal-level transfer functions as an aid in reconstructing Quaternary history of sea-level movements in the UK. Journal of Quaternary Science 14, 153-167.
Zong, Y., Sawai, Y., 2015. Diatoms, Handbook of Sea-Level Research. John Wiley & Sons, Ltd, pp. 233-248.
Zong, Y., Shennan, I., Combellick, R.A., Hamilton, S.L., Rutherford, M.M., 2003. Microfossil evidence for land movements associated with the AD 1964 Alaska earthquake. The Holocene 13, 7-20.

Table 1

Table 1: Summary of tectonic models used to predict co-seismic surface deformation. Model parameters and deformation estimates from Nicolsky et al. (2013, which includes full descriptions of the slip partitioningfor each model); their figures 10, 14 and 15.

Scenario	**Earthquake magnitude**	**Segmentation**
Scenario A	Mw 9.2	1964 rupture, Prince William Sound, Kenai and Kodiak segments
Scenario B	Mw 8.8	Prince William Sound and Kenai segments; slip distribution 15-25 km depth
Scenario C	Mw 8.8	Prince William Sound and Kenai segments; slip distribution 17-30 km depth
Scenario D	Mw 9.3	Multi-segment rupture, 1964 segments and the western part of the Yakutat microplate

Table 2

Table 2: Summary statistics for weighted average partial-least squares transfer function models used to reconstruct paleo marsh surface elevations. The 2005 models use modern samples only from upper Cook Inlet, 2013 and 2015 use modern samples from sites across south-central Alaska.

	Model 1			Model 2			Model 3		
Lithology of fossil sample to which the model can be applied	Peat			Mud with herbaceous rootlets OR peat			Any, including mud, no visible rootlets or laminated mud & fine sand		
Year	2005	2013	2015	2005	2013	2015	2005	2013	2015
Number of samples in modern training set	72	100	103	129	206	256	154	255	304
Number of components in weighted averaging partial least squares model[1]	2	2	1	3	2	2	2	2	2
Squared correlation between bootstrap predicted and observed values (r^2)	0.74	0.75	0.56	0.81	0.68	0.66	0.68	0.76	0.77
Root mean squared error of prediction (bootstrap RMSEP)	2.95	6.31	4.74	7.79	11.27	10.66	21.98	17.48	15.23
Improvement in RMSEP over next lower component model	7.17%	14.70%	-	6.70%	11.40%	7.87%	8.56%	10.50%	10.33%
RMSEP scaled to tidal range at Girdwood (m)	0.10	0.21	0.16	0.26	0.38	0.36	0.75	0.59	0.52
RMSEP scaled to tidal range at Kasilof (m)	0.09	0.18	0.14	0.23	0.33	0.31	0.64	0.51	0.44
RMSEP scaled to tidal range at Homer (m)	0.07	0.16	0.12	0.19	0.28	0.26	0.54	0.43	0.38

[1] We assess model performance using boot-strapped r^2, scatterplots of observed and predicted values, and RMSEP, with the best models being those with the highest r^2 value, a linear distribution

of observed plotted against predicted values, and the lowest RMSEP, but only if the RMSEP was improved by at least 5% with the addition of an extra component.

Table 3

Table 3: Radiocarbon dated samples, not previously published. All samples less than 0.01 m.

Code	Core / outcrop	Stratigraphic context	Material	depth (cm) below surface	^{14}C age and 1σ		Calibrated age: median, years BP	95% age range	
Anton Larson Bay									
Beta - 295547	ALB10/9	Top of peat	Herbaceous macrofossil leaves/stems	57	180	30	181	1	297
Beta - 287205	ALB10/4	Top of peat	Herbaceous macrofossil leaves/stems	78.5	370	40	426	315	504
Beta - 295546	ALB10/4	Base of peat	Herbaceous macrofossil leaves/stems	117	1320	30	1264	1183	1297
Beta - 287206	ALB10/4	Top of peat	Herbaceous macrofossil leaves/stems	146	2260	40	2239	2154	2348
Bird Point									
SUERC-22673	BP08/6	Top of peat	Herbaceous macrofossil leaves/stems	191	991	35	909	796	964
SUERC-22676	BP08/6	1 cm below top of peat	Herbaceous macrofossil leaves/stems	192	1060	37	969	924	1056
Beta-266420	BP09/1	Top of peat	Herbaceous macrofossil leaves/stems	338	1580	20	1467	1412	1528
Beta-266421	BP09/1	Top of peat	Herbaceous macrofossil leaves/stems	429	2170	20	2252	2116	2305
Homer									
OS-112093	BS13/4	Top of peat	Stem and probable root material	171.5	1230	20	1174	1072	1257
OS-112094	BS13/4	Top of peat	Small twig	382.5	2680	25	2778	2751	2844
OS-112095	BS13/4	Top of peat	Woody stem fragments	412.5	2880	20	3003	2945	3072
OS-112096	BS13/4	Top of peat	Small intact leaves	423.5	2740	25	2825	2772	2915
OS-112097	BS13/4	Top of peat	*Triglochin* stem bases	452.5	3540	20	3837	3724	3891
OS-112098	BS13/4	Base of peat	*Triglochin* stem bases	460.5	3830	20	4214	4151	4346
OS-109768	BS13/5	Top of peat	Stem fragments and 1 seed	169.5	1120	20	1018	970	1062
OS-109769	BS13/5	Top of peat	Stem fragments and 9 seeds	372.5	2130	20	2116	2011	2293
OS-109770	BS13/5	Top of peat	Stem fragments	389	2250	20	2229	2159	2339
OS-109771	BS13/5	Top of peat	2 stem fragments	406	2550	20	2726	2519	2748
OS-109772	BS13/5	Top of peat	1cm long wood fragment	441.5	3390	25	3633	3576	3693
OS-109773	BS13/5	Base of peat	Grass and stem fragments	452.5	3670	25	4007	3920	4086
Hope									
Beta-266423	HP09/8	Top of peat	Herbaceous macrofossil leaves/stems	326	2040	20	1992	1929	2100

Kalsin Bay									
Beta - 357771	KB13/5	Base of peat below Katmai tephra	Herbaceous macrofossil leaves/stems	77	180	40	177	1	301
Beta - 356266	KB13/5	Top of peat	Herbaceous macrofossil leaves/stems	92	10	30	0	0	0
Beta - 357408	KB13/5	Top of peat	Herbaceous macrofossil leaves/stems	116	200	30	180	1	303
Beta - 356268	KB13/5	Top of peat	Herbaceous macrofossil leaves/stems	131.5	1070	30	974	929	1054
Beta - 356269	KB13/5	Base of organic sequence	Herbaceous macrofossil leaves/stems	184	2460	30	2564	2365	2707
Kasilof									
OS-110179	KS13/1	Top of peat	Stem and leaf fragments	45.5	150	20	180	3	282
OS-110178	KS13/1	Base of peat	Stem and leaf fragments	55	925	30	852	769	924
OS-110177	KS13/1	Silt - 1 cm above contact to peat	Herbaceous leaf fragments	99	1120	25	1019	960	1166
OS-110175	KS13/1	Top of peat	Single round stem	100	1050	20	952	927	1041
OS-110176	KS13/1	1cm below top of peat	*Sphagnum* stem and leaf fragments	100.5	1240	20	1211	1082	1263
OS-110042	KS13/1	Base of peat	Stem and leaf fragments	104	1270	20	1229	1180	1270
OS-110041	KS13/1	Top of peat	Stem	112	1540	20	1462	1376	1522
OS-110040	KS13/1	1cm below top of peat	Seeds, stem and leaf fragments	112.5	1630	25	1535	1416	1602
OS-110039	KS13/1	Base of peat	Stem and leaf fragments	190	5430	30	6240	6192	6290
CAMS-93965	KS01/8	Top of peat	*Sphagnum* stem and leaf fragments	95	1150	30	1061	979	1174
CAMS-93966	KS01/8	Top of peat	Herbaceous macrofossil leaves/stems	109	1570	35	1467	1386	1540

Table 4

Table 4: Stratigraphic, sedimentologic, paleontologic, and age evidence from tidal-marsh stratigraphic sequences for coastal subsidence or uplift during great earthquakes at subduction zones.

Type of Evidence		Inference or Comment
Suddenness of Submergence	***Suddenness of Emergence***	
Sequence of interbedded peat-mud couplets rather than thick peat	Sequence of interbedded mud-peat couplets rather than thick peat	Attributed to repeated, sudden changes in land level
More than half a meter of mud separating peat beds inferred to be tidal-wetland soils		Mud deposited over a period of many years and/or subsidence > thickness of mud
Peat-mud contacts are distinct above shallow bedrock at valley sides		Separation of peat beds suggests tectonic subsidence rather than local sediment compaction
Abrupt mud-over-peat contacts indicate sudden rises in sea level	Abrupt peat-over-mud contacts indicate sudden falls in sea level	Definitions of abrupt differ (Nelson et al., 1996)
Gradual mud-over-peat contacts indicate gradual rise in sea level	Gradual peat-over-mud contacts indicate slow rise or fall in sea level	Inferred to indicate a marked asymmetry in the rate of RSL change
Lamination or massive bedding of sediment directly overlying peat-mud contacts	Lamination or massive bedding of sediment directly underlying mud-peat contacts	Lack of sedimentary structures in massive beds attributed to high sedimentation rates, bioturbation or winter freezing processes
Soft mud overlying peat-mud contacts		Attributed to rapid deposition and minimal subaerial exposure,
Healthy outer rings in trees rooted in upper parts of buried wetland soils		Attributed to rapid tree death (less than a few years) from submergence
Plant stems rooted at tops of peat beds extend upward into mud or sand or flattened along top surface of peat		Attributed to rapid submergence and burial of wetland soil
Dramatic change in species composition of microfossil assemblages across peat-mud contacts	Dramatic change in species composition of microfossil assemblages across mud-peat contacts	Attributed to rapid submergence and burial of wetland soil, or rapid emergence of tidal flat and development of upper intertidal to supratidal wetland
Amount of Submergence	***Amount of Emergence***	
Peat overlain by mud		Attributed to change from higher to lower intertidal environment
	Mud overlain by peat	Attributed to change from lower to higher intertidal or supratidal environment
Peaty soil with remains of high-marsh plants buried by mud with plants typical of low marsh	Mud with plants typical of low marsh overlain by peaty soil with remains of high-marsh plants	Attributed to change in RSL of decimeters to a meter
Peaty soil with rooted tree stumps buried by mud with plants typical of low marsh		Attributed to rise in RSL of many decimeters to more than two meters
	Mud with plants typical of low marsh or laminations overlain by peat with macrofossils of freshwater plants including mosses	Attributed to fall in RSL of many decimeters to more than two meters
Qualitative diatom analysis (mud with brackish water or low	Qualitative diatom analysis (peat with freshwater or high intertidal	Attributed to change in RSL of decimeters to more than two

intertidal species over peat with freshwater or high intertidal species)	species over mud with brackish water or low intertidal species)	meters
Quantitative diatom, foraminifera, and/or pollen analysis (assemblages calibrated against modern environments)	Quantitative diatom, foraminifera, and/or pollen analysis (assemblages calibrated against modern environments)	May allow amount of RSL change to be estimated to within 0.5 m or less and give 95% error terms
Organic-rich sediment overlain by organic-poor sediment		Attributed to change from higher to lower intertidal environment
	Organic-poor sediment overlain by organic rich sediment	Attributed to change from lower to higher intertidal environment
Qualitative or quantitative analysis of geochemical proxies (C:N, TOC, $\delta^{13}C$, $\delta^{15}N$)		Attributed to change in RSL of decimeters to two meters
Sediment with low percentage of sand overlain by sediment with high percentage of sand		Applicability highly dependent on distance to and character of sand source
Lateral Extent of Peat-Mud Contacts	***Lateral Extent of Mud-Peat Contacts***	
Contacts mapped in outcrop for hundreds of meters	Contacts mapped in outcrop for hundreds of meters	Except in southern Washington, Copper River Delta and south central Chile, largely limited to youngest 1-2 buried soils
Contacts correlated between cores spaced 10-50 m apart for hundreds of meters	Contacts correlated between cores spaced 10-50 m apart for hundreds of meters	Cores with this spacing initially limited to a few sites, now typical of most studies
Contacts correlated between cores spaced >50 m apart	Contacts correlated between cores spaced >50 m apart	Core spacing typical of most studies pre 1996
Distinctive peat and mud stratigraphy correlated over several sites in the same estuary	Distinctive peat and mud stratigraphy correlated over several sites in the same estuary	Correlation within an estuary described by almost all studies
Distinctive peat and mud stratigraphy correlated between estuaries > 30 km apart		Correlations most convincing in northern Oregon and southern Washington
Synchroneity of Submergence	***Synchroneity of Emergence***	
Peat ^{14}C ages suggest peat-mud contacts formed within a few hundred years of one another	Peat ^{14}C ages suggest mud-peat contacts formed within a few hundred years of one another	Total errors on calibrated conventional ages typically > 300 years
Multiple AMS ^{14}C ages suggest peat-mud contacts formed within 200 years of one another	Multiple AMS ^{14}C ages suggest mud-peat contacts formed within 200 years of one another	Total errors on calibrated means of 6-8 ages typically < 200 years
Age modelling to calculate probability density functions for hypothesised earthquakes	Age modelling to calculate probability density functions for hypothesised earthquakes	Probability density function 95% ranges may be <100 years
Tree ring analysis suggests multiple trees rooted in a buried soil died within 10 years of each other.		Death attributed to submergence during regional coseismic subsidence. May be supported by high precision ^{14}C dating of tree rings.
Tsunami Concurrent With Submergence	***Tsunami Concurrent With Emergence***	
Laterally extensive sandy beds immediately overlie buried wetland soils and below intertidal mud	Laterally extensive sandy immediately overlie intertidal mud and lie below buried wetland soils	Attributed to surge of sandy water concurrent with submergence or emergence
Sandy beds not found within mud	Sandy beds not found within mud	Lack of other sand beds within

units	units	couplets suggests unusual depositional event
Sandy beds on buried wetland soils are sheets that thin and fine landward	Sandy beds on buried wetland soils are sheets that thin and fine landward	Bed geometry and grain-size changes indicate a marine source for sand
Sandy beds display erosive lower contacts and contain rip-up clasts	Sandy beds display erosive lower contacts and contain rip-up clasts	Attributed to high energy flow conditions
Sandy beds fine upward or are massive	Sandy beds fine upward or are massive	Attributed to deposition from suspension rather than currents
Sandy beds have discrete units, including lamination or interbedding	Sandy beds have discrete units, including lamination or interbedding	Attributed to closely spaced pulses of deposition, multiple tsunami waves or uprush and backflow
Sandy beds are separated by internal mud drapes and overlain by a mud cap	Sandy beds are separated by internal mud drapes and overlain by a mud cap	Attributed to quiescent periods between successive waves or after the final inundation
Rounding and mineralogy of heavy minerals in sandy beds is typical of marine sand	Rounding and mineralogy of heavy minerals in sandy beds is typical of marine sand	Attributed to deposition from a marine rather than a fluvial source
Sand layers contain elevated Na, S, Cl, Ca and Mg concentrations	Sand layers contain elevated Na, S, Cl, Ca and Mg concentrations	Attributed to inundation by saline water
Distribution and thickness of sand sheets along tidal channels suggests upchannel flow	Distribution and thickness of sand sheets along tidal channels suggests upchannel flow	Attributed to landward-directed surge
Sandy beds contain microfossils and macrofossils characteristic of marine or subtidal estuarine environments	Sandy beds contain microfossils and macrofossils characteristic of marine or subtidal estuarine environments	Attributed to deposition from a marine or deep estuarine source
Sandy beds contain mixed assemblages of microfossils characteristic of a range of different environments	Sandy beds contain mixed assemblages of microfossils characteristic of a range of different environments	Attributed to erosion and deposition of sediments from a range of different sub-, inter- and supratidal areas
Microfossils and macrofossils display elevated levels of abrasion, crushing and fracturing	Microfossils and macrofossils display elevated levels of abrasion, crushing and fracturing	Attributed to turbulent flow
Liquefaction Concurrent with Submergence	***Liquefaction Concurrent with Emergence***	
Sand dikes and sills seen in outcrop or subsurface sampling using pits or a sediment slicer	Sand dikes and sills seen in outcrop or subsurface sampling using pits or a sediment slicer	In cores, difficult to differentiate from possible tsunami deposit

Table Footnote: Inferences are made from evidence and comments are about evidence. Papers evaluated include those cited in the original version (Nelson et al., 1996) and these additional ones (Alam et al., 2012; Atwater et al., 2005; Atwater et al., 2001; Bender et al., 2015; Carver and Plafker, 2008; Chagué-Goff et al., 2011; Dura et al., 2015; Dura et al., 2016; Dura et al., 2011; Engel and Brückner, 2011; Engelhart et al., 2013; Garrett et al., 2013; Goff et al., 2011a; Grand Pre et al., 2012; Kelsey et al., 2002; Martin and Bourgeois, 2012; McCalpin and Carver, 2009; Morton et al., 2007; Nelson et al., 2015; Nelson et al., 2006; Obermeier and Dickenson, 2000; Pilarczyk et al., 2014; Shennan, 2009; Shennan et al., 2014a; Shennan et al., 2014c; Walsh et al., 1995; Witter et al., 2003; Yamaguchi et al., 1997)

Figure 1

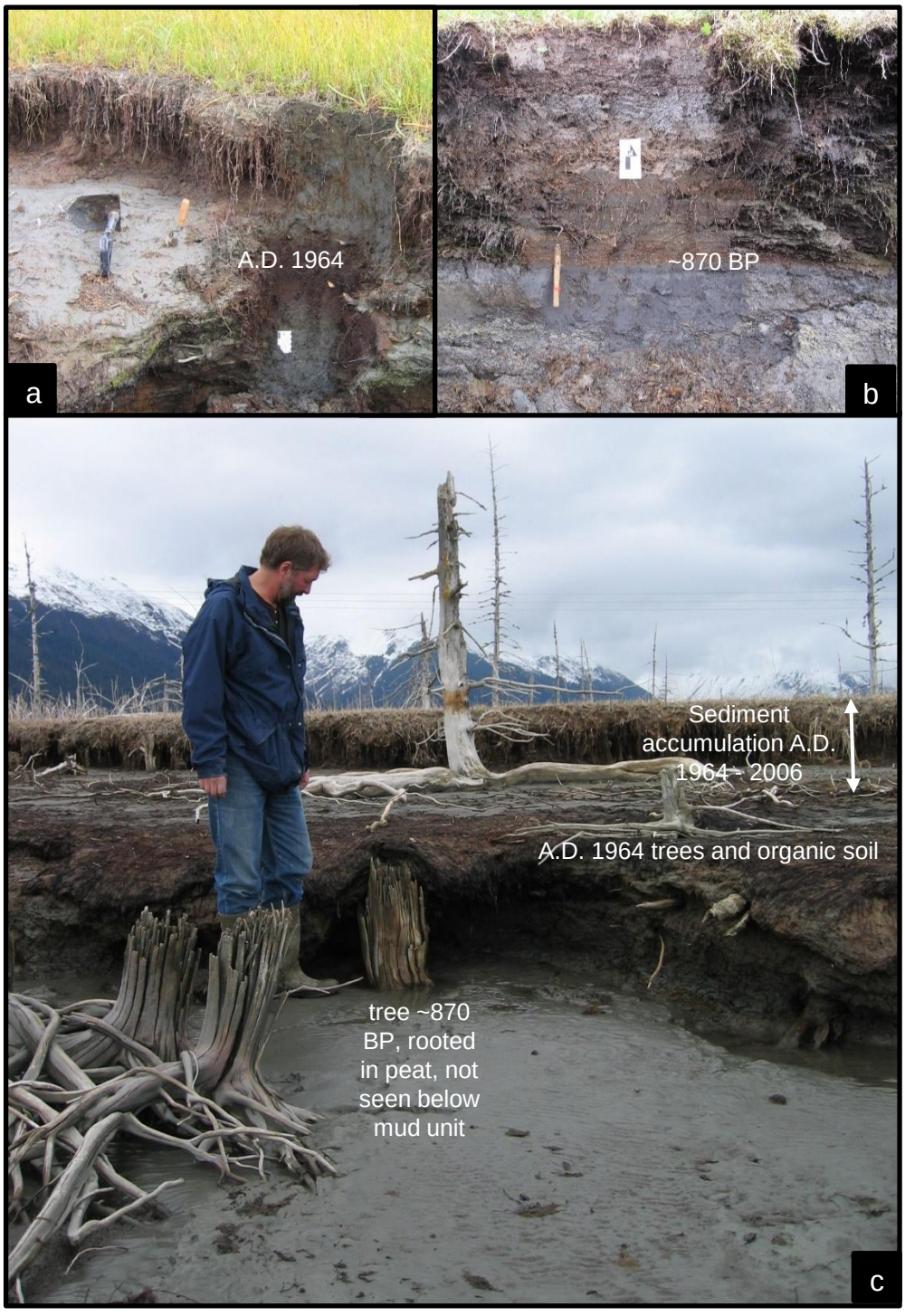
A.D. 1964
a
~870 BP
b
Sediment accumulation A.D. 1964 - 2006
A.D. 1964 trees and organic soil
tree ~870 BP, rooted in peat, not seen below mud unit
c

Figure 2

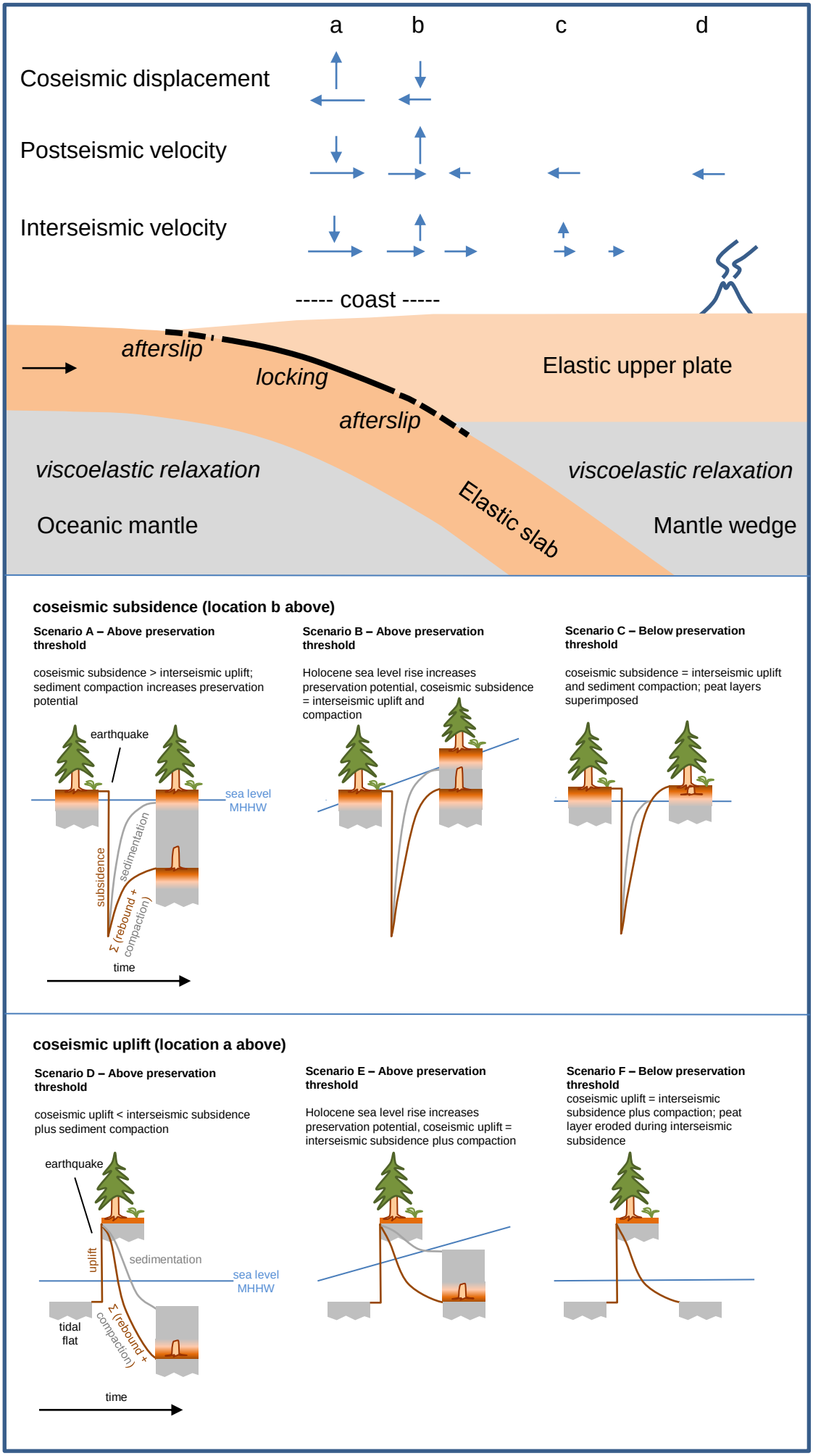
a
b
c
d
Coseismic displacement
Postseismic velocity
Interseismic velocity
----- coast -----
afterslip
locking
afterslip
Elastic upper plate
viscoelastic relaxation
viscoelastic relaxation
Oceanic mantle
Elastic slab
Mantle wedge
coseismic subsidence (location b above)
Scenario A – Above preservation threshold
coseismic subsidence > interseismic uplift; sediment compaction increases preservation potential
earthquake
sea level MHHW
subsidence
sedimentation
Σ (rebound + compaction)
time
Scenario B – Above preservation threshold
Holocene sea level rise increases preservation potential, coseismic subsidence = interseismic uplift and compaction
Scenario C – Below preservation threshold
coseismic subsidence = interseismic uplift and sediment compaction; peat layers superimposed
coseismic uplift (location a above)
Scenario D – Above preservation threshold
coseismic uplift < interseismic subsidence plus sediment compaction
earthquake
uplift
sedimentation
sea level MHHW
tidal flat
Σ (rebound + compaction)
time
Scenario E – Above preservation threshold
Holocene sea level rise increases preservation potential, coseismic uplift = interseismic subsidence plus compaction
Scenario F – Below preservation threshold
coseismic uplift = interseismic subsidence plus compaction; peat layer eroded during interseismic subsidence

Figure 3

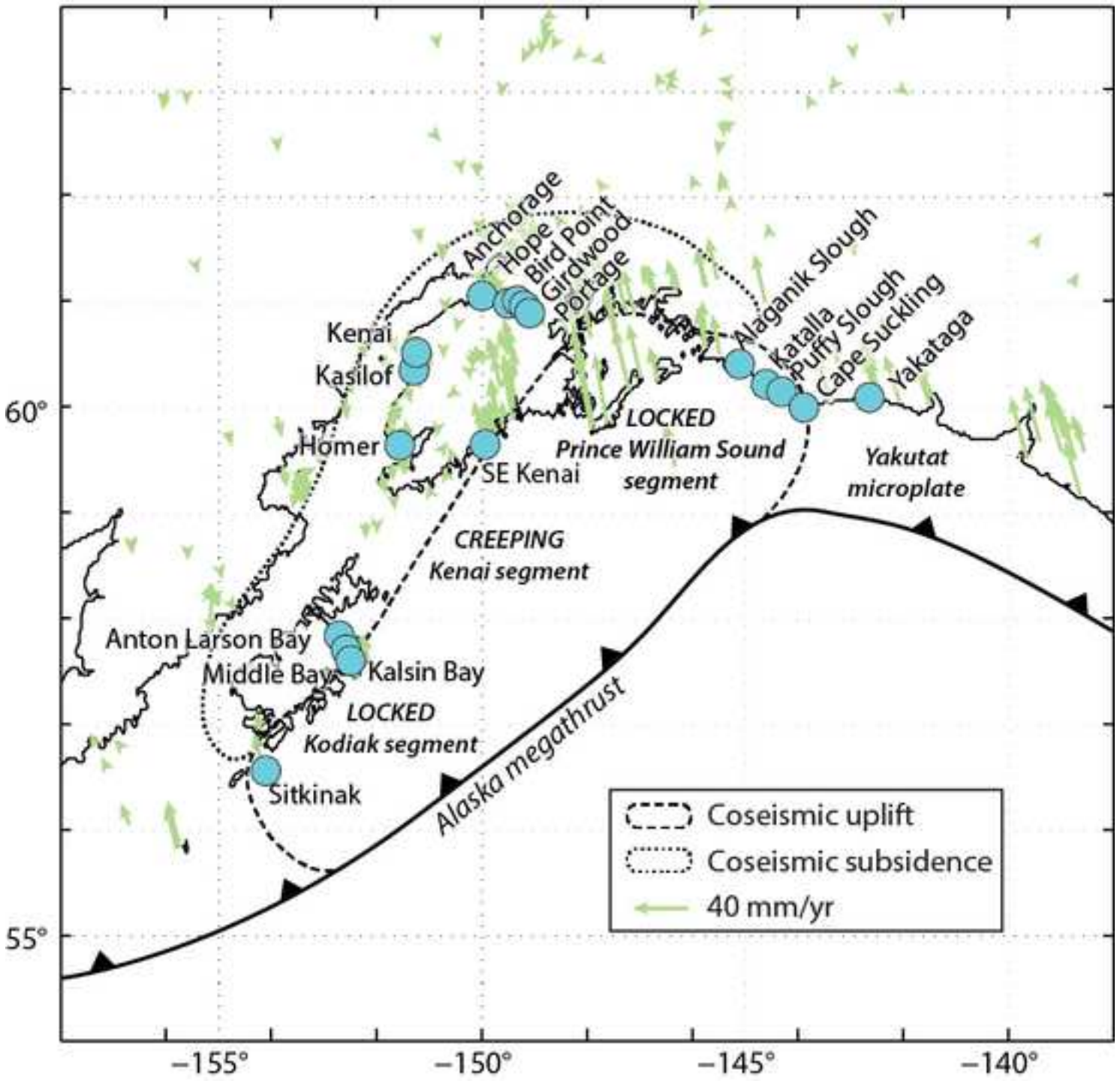
Anchorage
Hope
Bird Point
Girdwood
Portage
Kenai
Kasilof
Homer
SE Kenai
LOCKED
Prince William Sound
segment
Alaganik Slough
Katalla
Puffy Slough
Cape Suckling
Yakataga
Yakutat
microplate
CREEPING
Kenai segment
Anton Larson Bay
Middle Bay
Kalsin Bay
LOCKED
Kodiak segment
Sitkinak
Alaska megathrust
Coseismic uplift
Coseismic subsidence
40 mm/yr
60°
55°
−155°
−150°
−145°
−140°

Figure 4

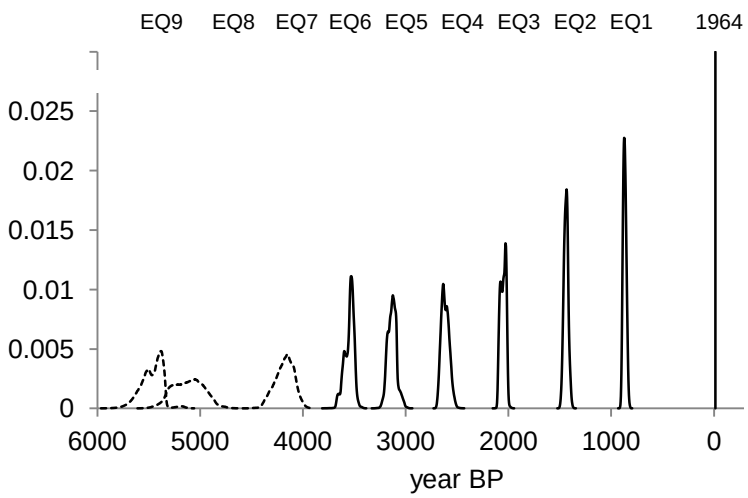
EQ9
EQ8
EQ7
EQ6
EQ5
EQ4
EQ3
EQ2
EQ1
1964
0.025
0.02
0.015
0.01
0.005
0
6000
5000
4000
3000
2000
1000
0
year BP

Figure 5

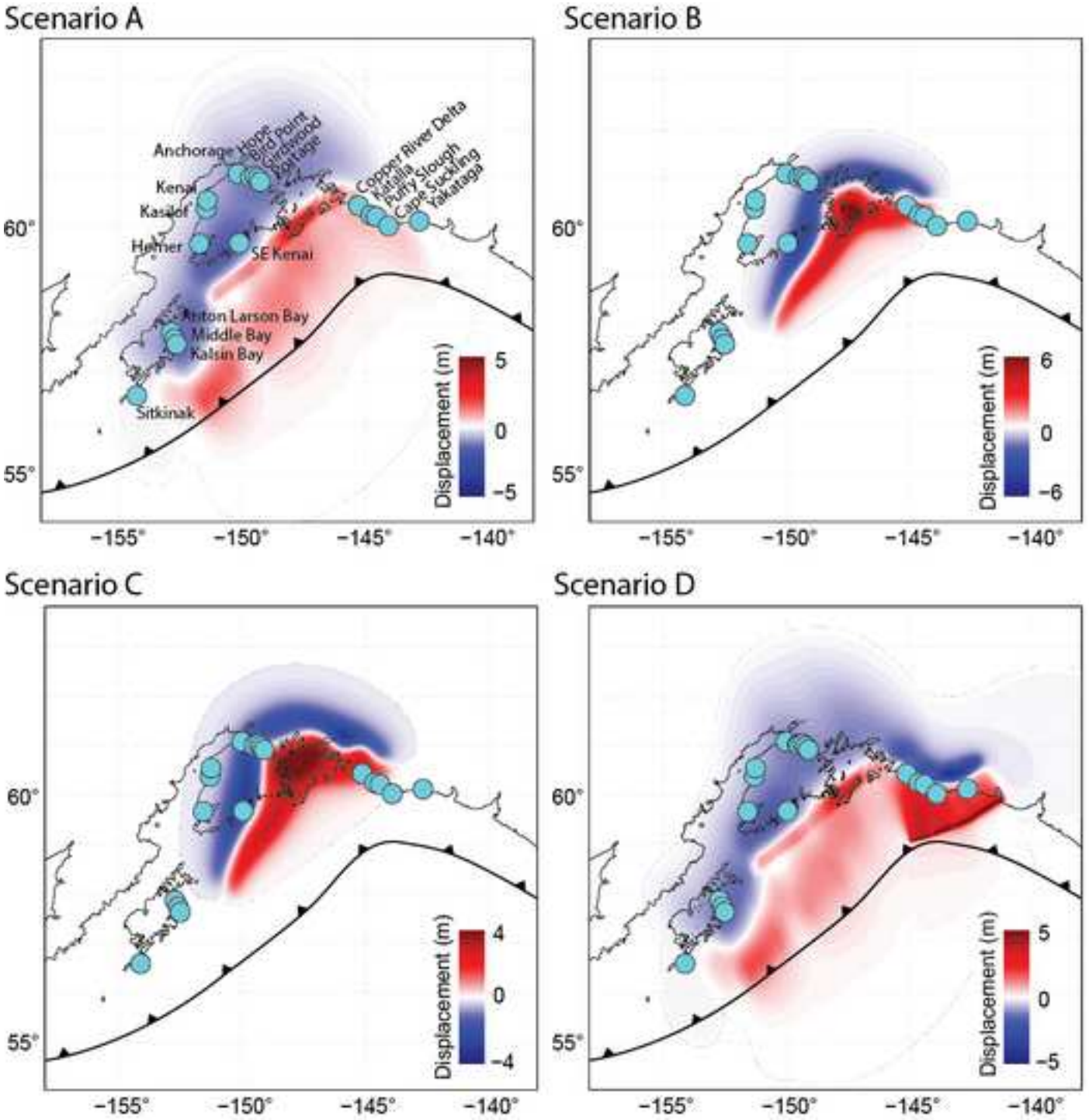
Scenario A
Scenario B
Scenario C
Scenario D
Anchorage
Hope
Bird Point
Girdwood
Portage
Kenai
Kasilof
Homer
SE Kenai
Copper River Delta
Katalla
Puffy Slough
Cape Suckling
Yakataga
Anton Larson Bay
Middle Bay
Kalsin Bay
Sitkinak
Displacement (m)
5
0
−5
6
−6
4
−4
60°
55°
−155°
−150°
−145°
−140°

Figure 6

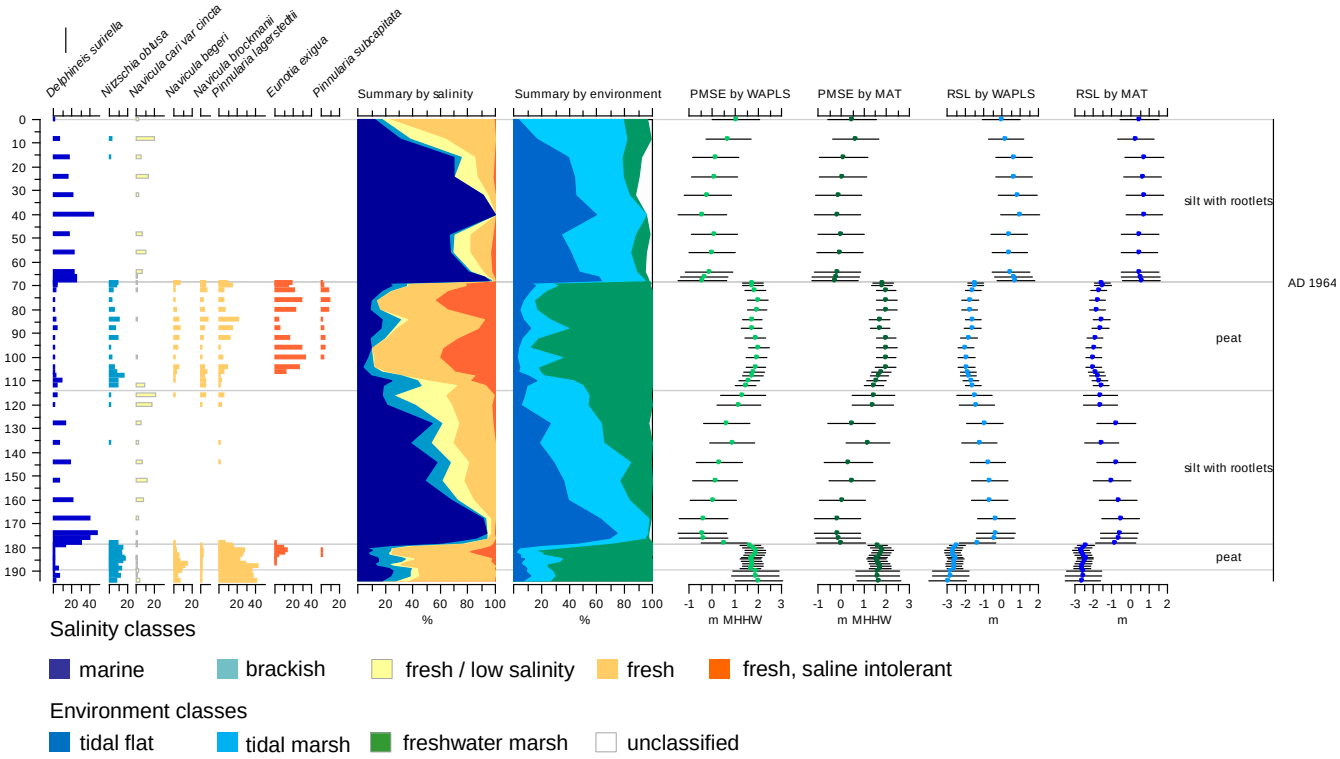
Delphineis surirella
Nitzschia obtusa
Navicula cari var cincta
Navicula begeri
Navicula brockmanii
Pinnularia lagerstedtii
Eunotia exigua
Pinnularia subcapitata
Summary by salinity
Summary by environment
PMSE by WAPLS
PMSE by MAT
RSL by WAPLS
RSL by MAT
silt with rootlets
peat
silt with rootlets
peat
AD 1964
%
%
m MHHW
m MHHW
m
m
Salinity classes
marine
brackish
fresh / low salinity
fresh
fresh, saline intolerant
Environment classes
tidal flat
tidal marsh
freshwater marsh
unclassified

Figure 7

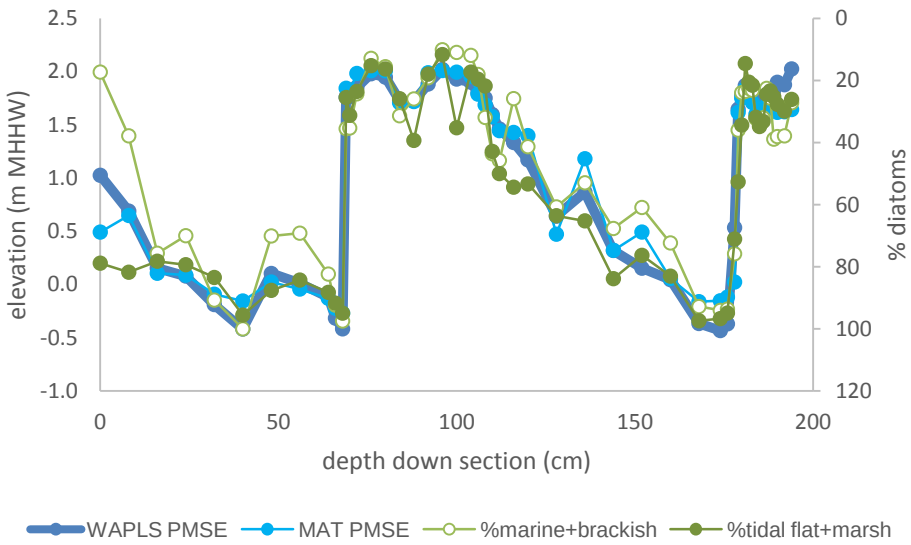
2.5
2.0
1.5
1.0
0.5
0.0
-0.5
-1.0
elevation (m MHHW)
0
20
40
60
80
100
120
% diatoms
0
50
100
150
200
depth down section (cm)
WAPLS PMSE
MAT PMSE
%marine+brackish
%tidal flat+marsh

Figure 8

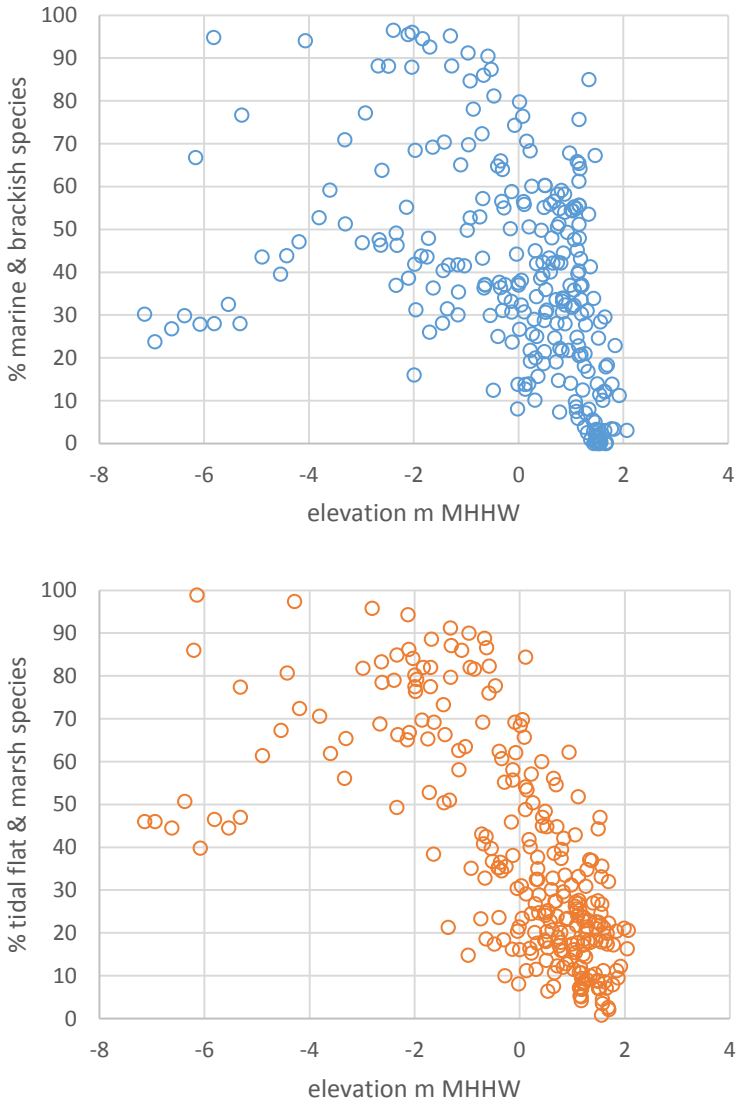
% marine & brackish species
100
90
80
70
60
50
40
30
20
10
0
-8
-6
-4
-2
0
2
4
elevation m MHHW
% tidal flat & marsh species
100
90
80
70
60
50
40
30
20
10
0
-8
-6
-4
-2
0
2
4
elevation m MHHW

Figure 9

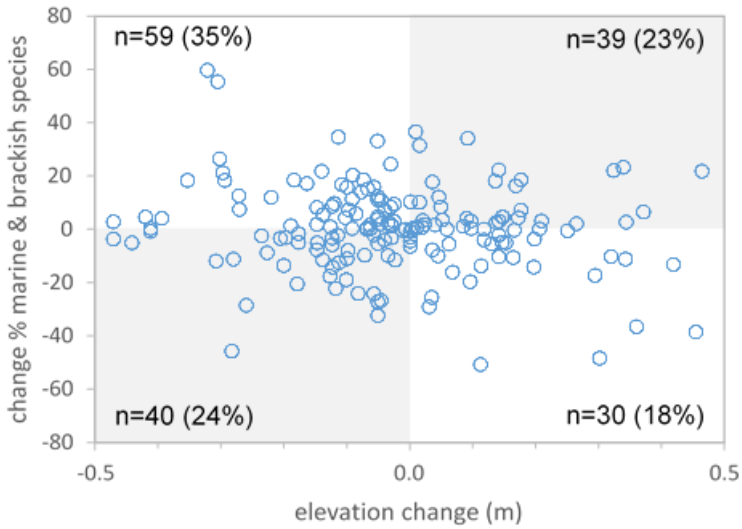
n=59 (35%)
n=39 (23%)
n=40 (24%)
n=30 (18%)
80
60
40
20
0
-20
-40
-60
-80
-0.5
0.0
0.5
change % marine & brackish species
elevation change (m)

Figure 10

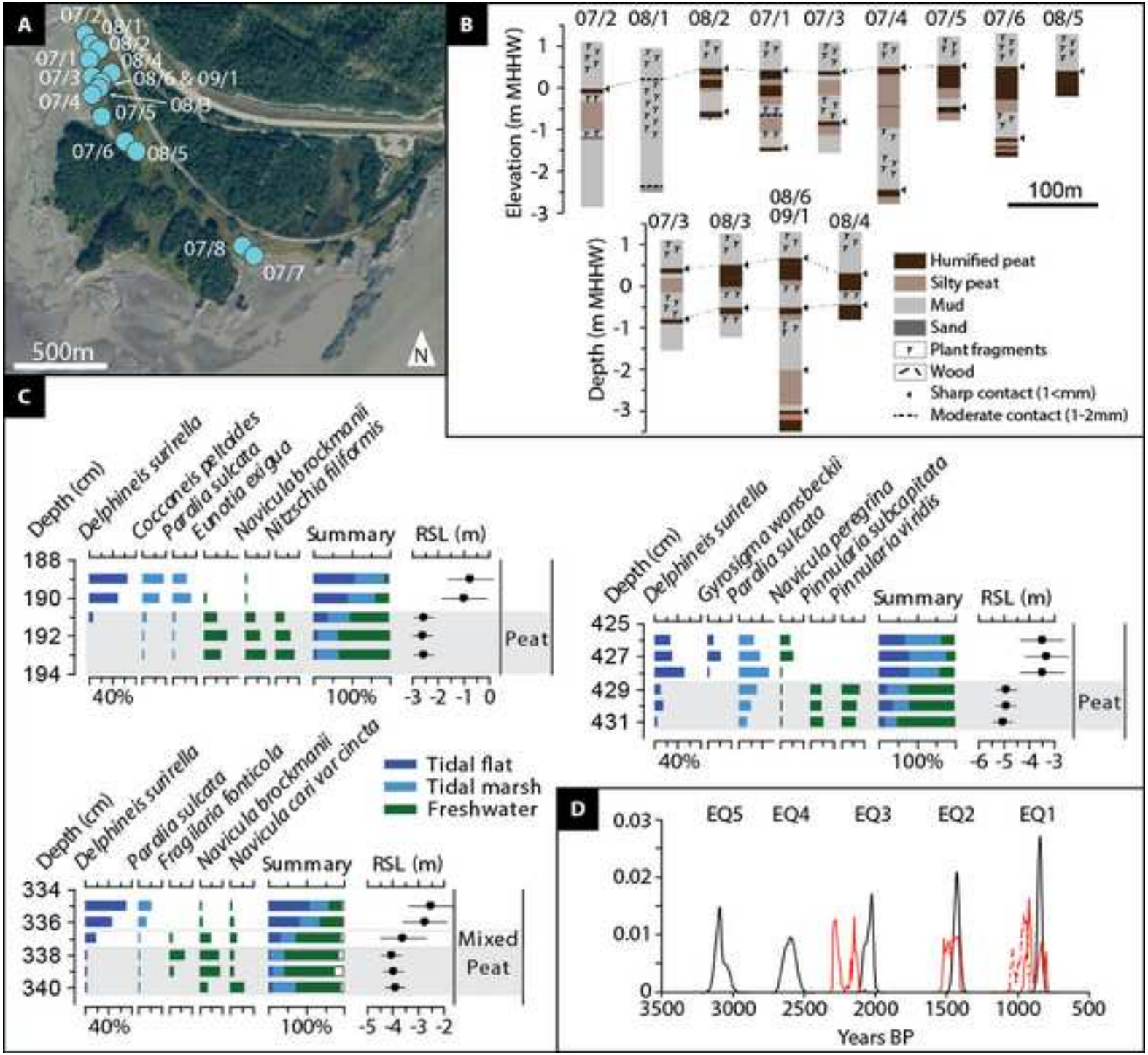
A
07/2
08/1
08/2
07/1
08/4
07/3
08/6 & 09/1
07/4
08/3
07/5
07/6
08/5
07/8
07/7
500m
N
B
07/2 08/1 08/2 07/1 07/3 07/4 07/5 07/6 08/5
Elevation (m MHHW)
100m
07/3 08/3 08/6 09/1 08/4
Depth (m MHHW)
Humified peat
Silty peat
Mud
Sand
Plant fragments
Wood
Sharp contact (1<mm)
Moderate contact (1-2mm)
C
Depth (cm)
Delphineis surirella
Cocconeis peltoides
Paralia sulcata
Eunotia exigua
Navicula brockmanii
Nitzschia filiformis
Summary
RSL (m)
188
190
192
194
Peat
40%
100%
-3 -2 -1 0
Depth (cm)
Delphineis surirella
Gyrosigma wansbeckii
Paralia sulcata
Navicula peregrina
Pinnularia subcapitata
Pinnularia viridis
Summary
RSL (m)
425
427
429
431
Peat
40%
100%
-6 -5 -4 -3
Tidal flat
Tidal marsh
Freshwater
Depth (cm)
Delphineis surirella
Paralia sulcata
Fragilaria fonticola
Navicula brockmanii
Navicula cari var cincta
Summary
RSL (m)
334
336
338
340
Mixed Peat
40%
100%
-5 -4 -3 -2
D
EQ5
EQ4
EQ3
EQ2
EQ1
0.03
0.02
0.01
0
3500
3000
2500
2000
1500
1000
500
Years BP

Figure 11

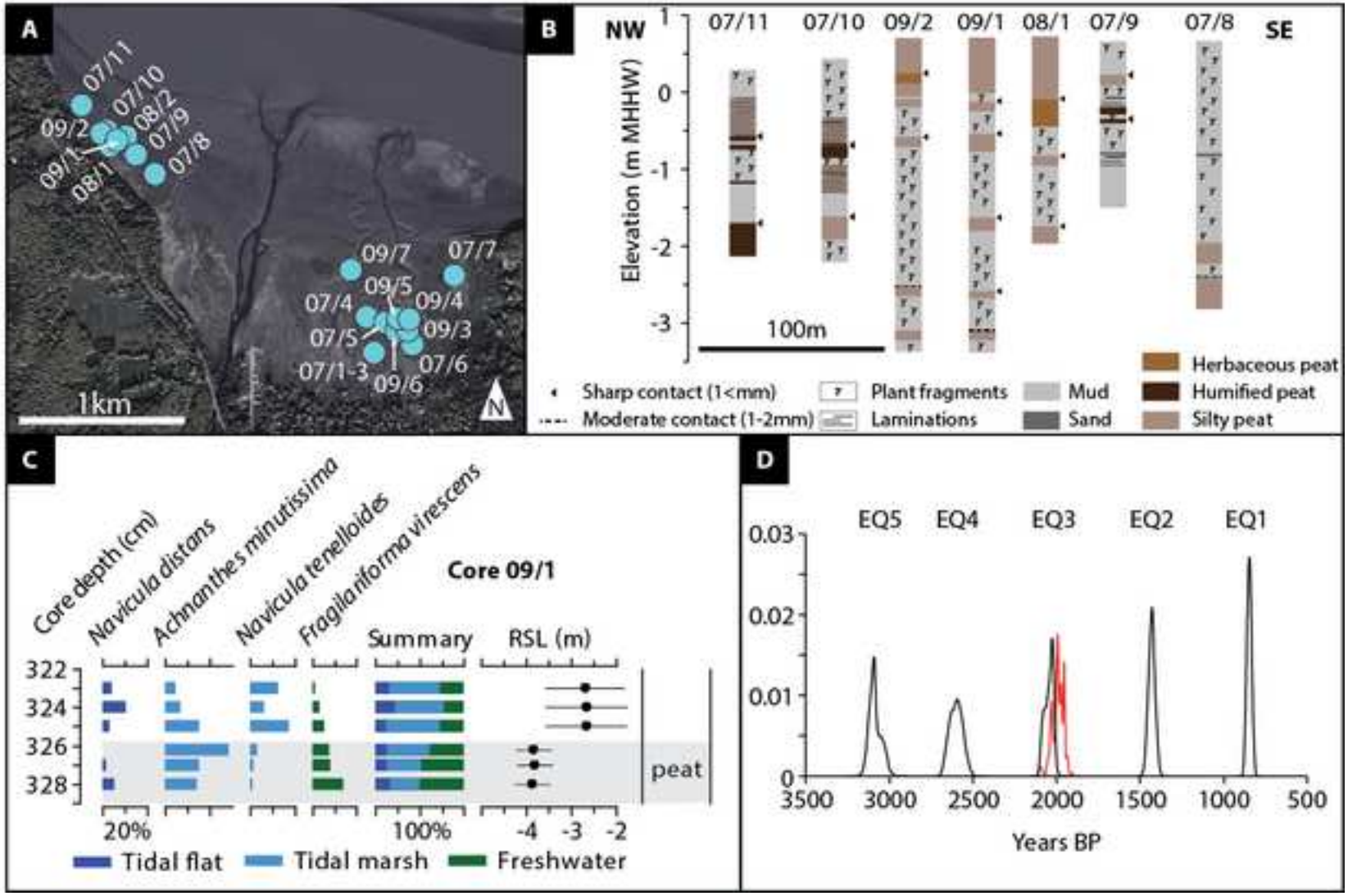
A
07/11
07/10
08/2
09/2
07/9
09/1
07/8
08/1
09/7
07/7
09/5
07/4
09/4
09/3
07/5
07/6
07/1-3
09/6
1km
N
B
NW
SE
07/11
07/10
09/2
09/1
08/1
07/9
07/8
Elevation (m MHHW)
100m
Sharp contact (1<mm)
Moderate contact (1-2mm)
Plant fragments
Laminations
Mud
Sand
Herbaceous peat
Humified peat
Silty peat
C
Core depth (cm)
Navicula distans
Achnanthes minutissima
Navicula tenelloides
Fragilariforma virescens
Core 09/1
Summary
RSL (m)
322
324
326
328
peat
20%
100%
-4
-3
-2
Tidal flat
Tidal marsh
Freshwater
D
EQ5
EQ4
EQ3
EQ2
EQ1
0.03
0.02
0.01
0
3500
3000
2500
2000
1500
1000
500
Years BP

Figure 12

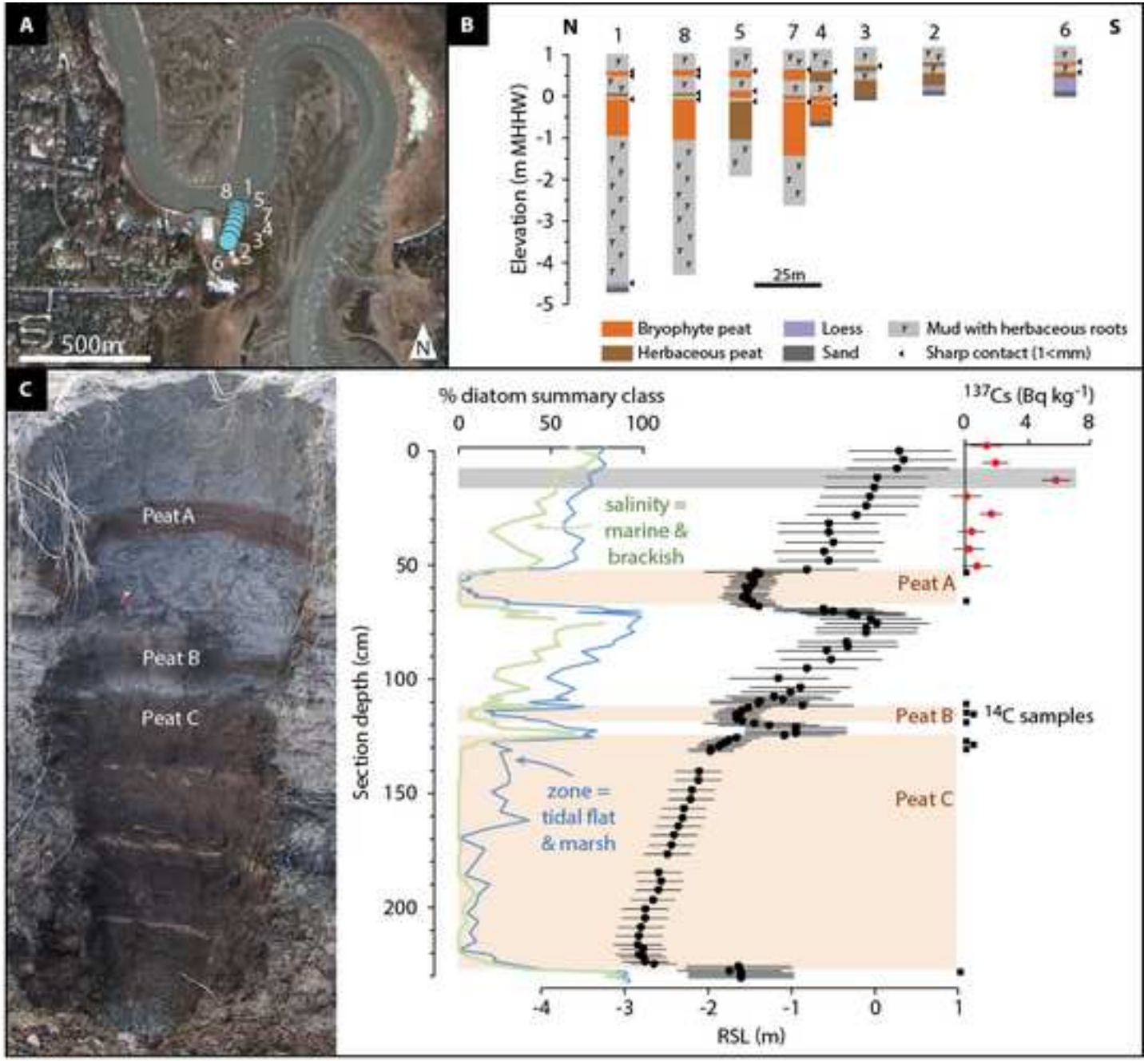
A
500m
N
B
N
S
1
8
5
7
4
3
2
6
Elevation (m MHHW)
25m
Bryophyte peat
Herbaceous peat
Loess
Sand
Mud with herbaceous roots
Sharp contact (1<mm)
C
Peat A
Peat B
Peat C
% diatom summary class
137Cs (Bq kg-1)
salinity = marine & brackish
zone = tidal flat & marsh
14C samples
Section depth (cm)
RSL (m)

Figure 13

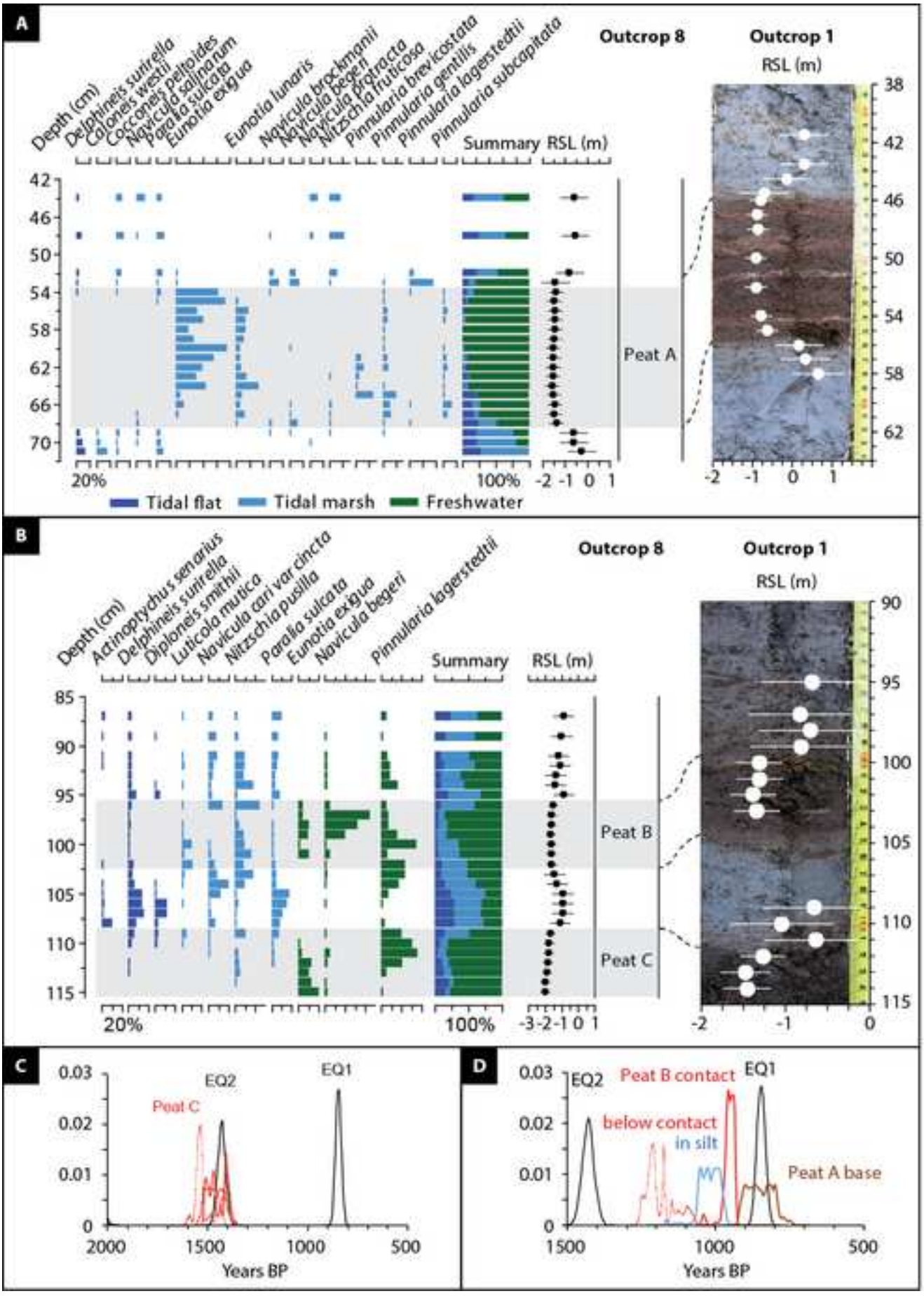
A
Depth (cm)
Delphineis surirella
Coloneis westii
Cocconeis peltoides
Navicula salinarum
Paralia sulcata
Eunotia exigua
Eunotia lunaris
Navicula brockmanii
Navicula begeri
Nitzschia fruticosa
Pinnularia gentilis
Pinnularia lagerstedtii
Pinnularia subcapitata
Summary
RSL (m)
Outcrop 8
Outcrop 1
RSL (m)
Peat A
20%
100%
Tidal flat
Tidal marsh
Freshwater
B
Depth (cm)
Actinoptychus senarius
Delphineis surirella
Diploneis smithii
Luticola mutica
Navicula cari var cincta
Nitzschia pusilla
Paralia sulcata
Eunotia exigua
Navicula begeri
Pinnularia lagerstedtii
Summary
RSL (m)
Outcrop 8
Outcrop 1
RSL (m)
Peat B
Peat C
20%
100%
C
EQ2
EQ1
Peat C
Years BP
D
EQ2
Peat B contact
EQ1
below contact
in silt
Peat A base
Years BP

Figure 14

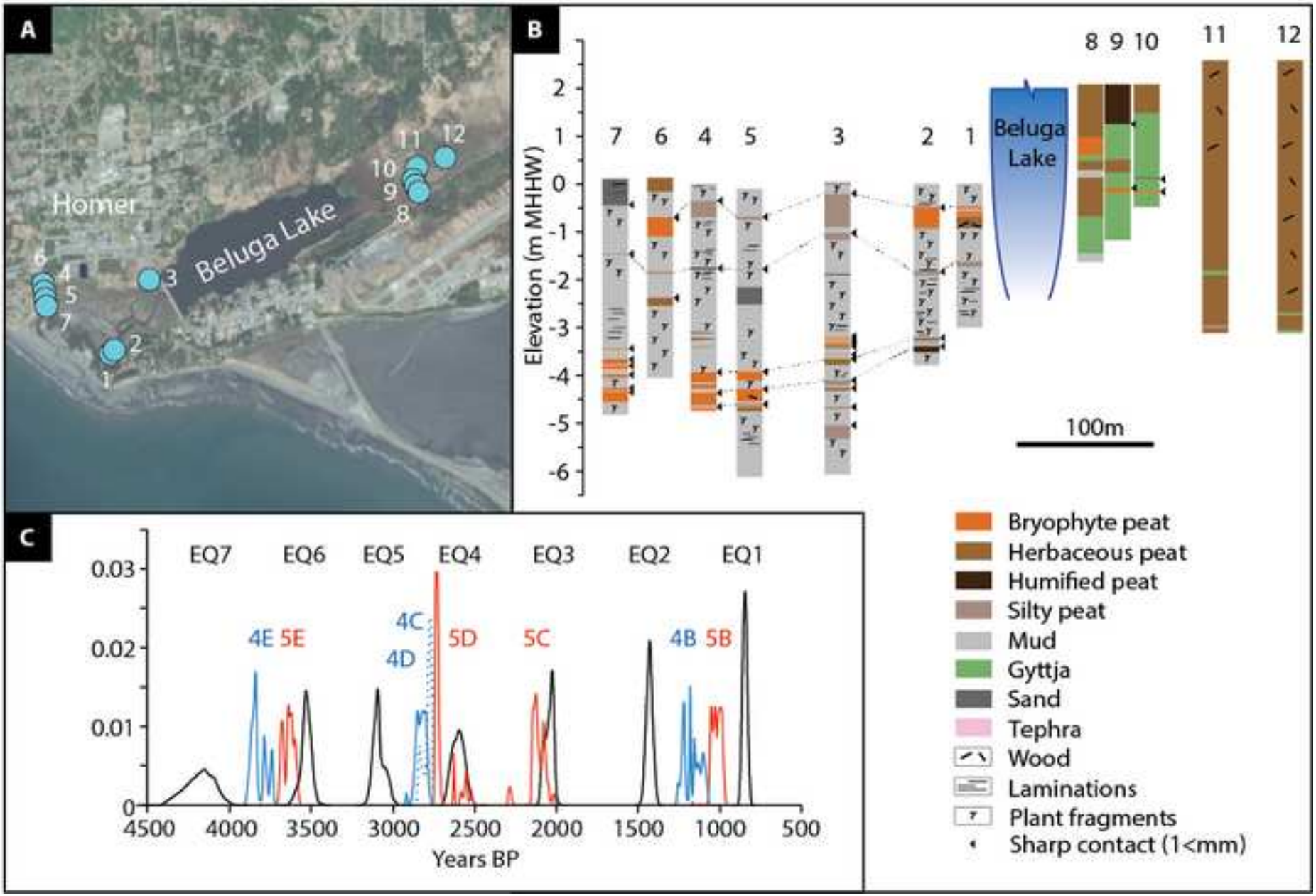
A
Homer
Beluga Lake
1
2
3
4
5
6
7
8
9
10
11
12
B
Elevation (m MHHW)
2
1
0
-1
-2
-3
-4
-5
-6
7
6
4
5
3
2
1
Beluga Lake
8 9 10
11
12
100m
C
EQ7
EQ6
EQ5
EQ4
EQ3
EQ2
EQ1
0.03
0.02
0.01
0
4E 5E
4C
4D
5D
5C
4B 5B
4500
4000
3500
3000
2500
2000
1500
1000
500
Years BP
Bryophyte peat
Herbaceous peat
Humified peat
Silty peat
Mud
Gyttja
Sand
Tephra
Wood
Laminations
Plant fragments
Sharp contact (1<mm)

Figure 15

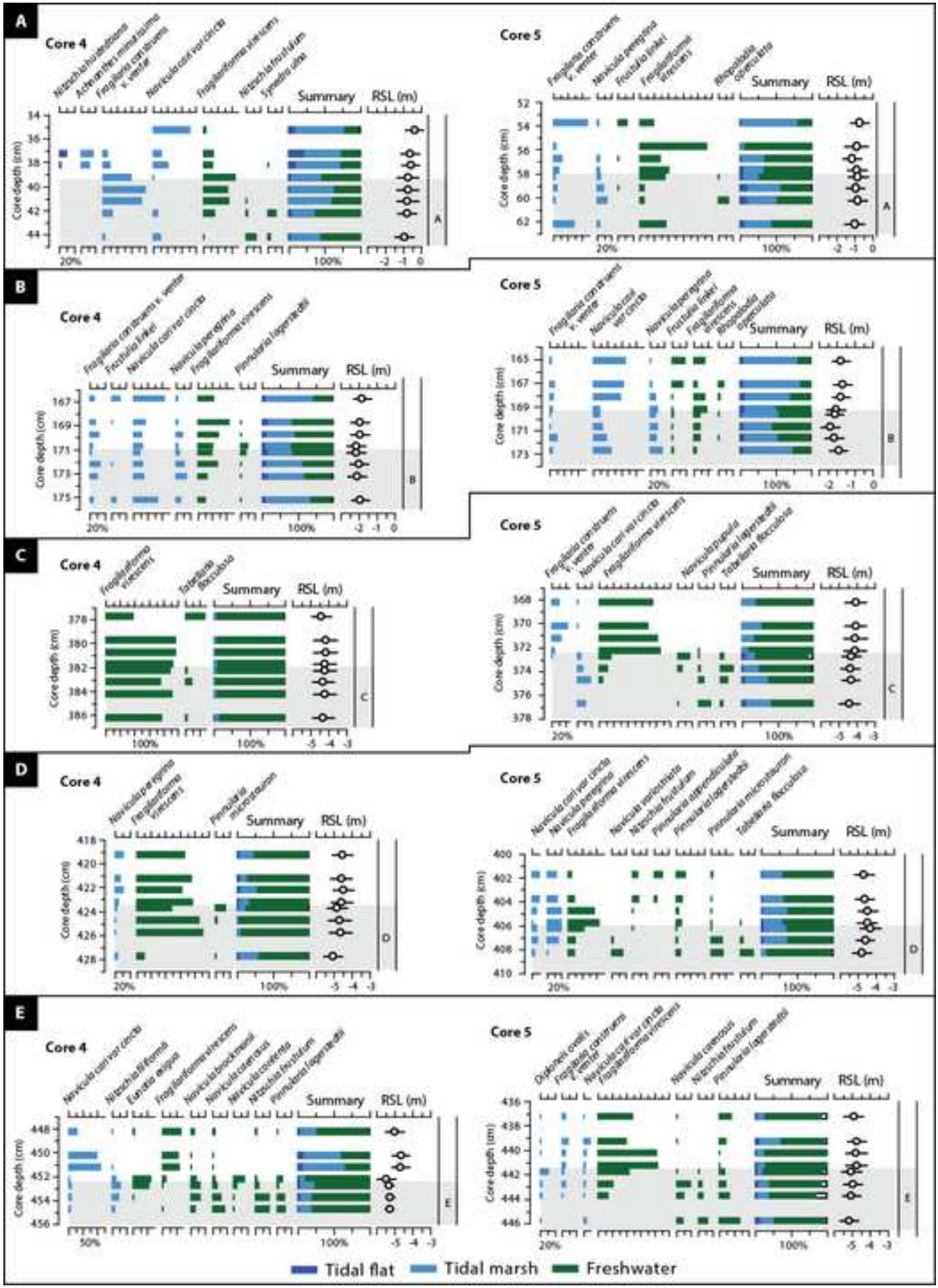
A
Core 4
Core 5
Summary
RSL (m)
Core depth (cm)
B
C
D
E
Tidal flat
Tidal marsh
Freshwater

Figure 16

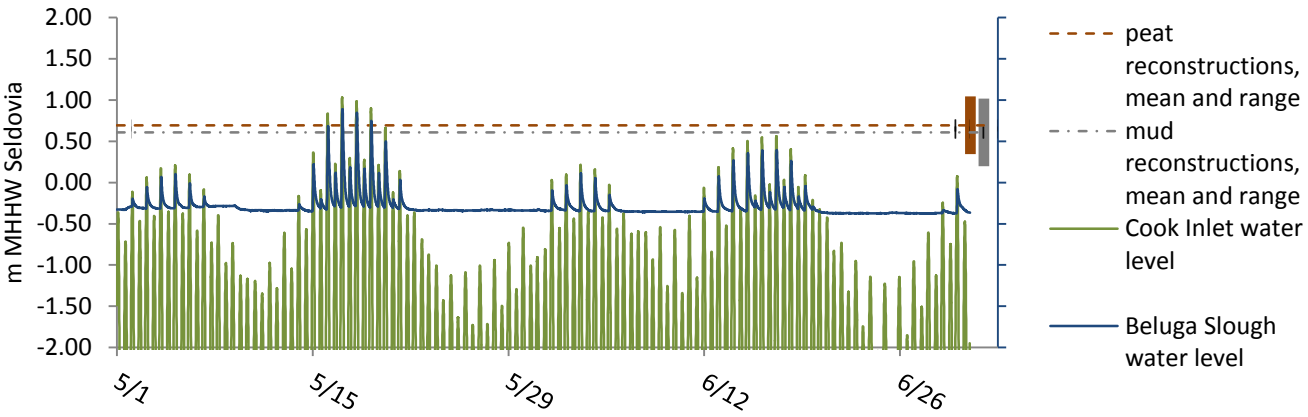
m MHHW Seldovia
2.00
1.50
1.00
0.50
0.00
-0.50
-1.00
-1.50
-2.00
5/1
5/15
5/29
6/12
6/26
peat reconstructions, mean and range
mud reconstructions, mean and range
Cook Inlet water level
Beluga Slough water level

Figure 17

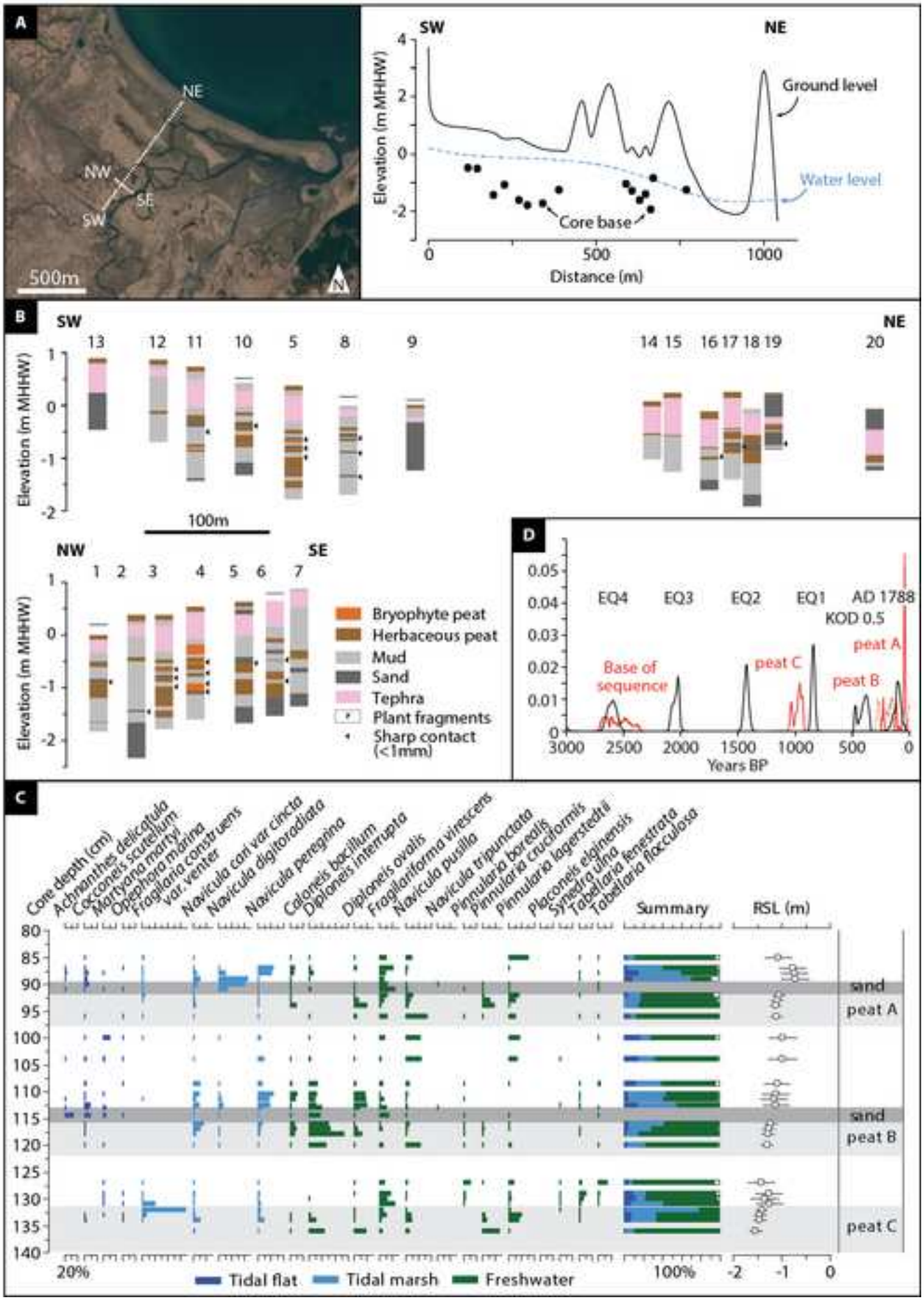
A
NE
NW
SE
SW
500m
N
SW
NE
Ground level
Water level
Core base
Elevation (m MHHW)
Distance (m)
B
SW
NE
13 12 11 10 5 8 9 14 15 16 17 18 19 20
100m
NW
SE
1 2 3 4 5 6 7
Bryophyte peat
Herbaceous peat
Mud
Sand
Tephra
Plant fragments
Sharp contact (<1mm)
D
EQ4 EQ3 EQ2 EQ1 AD 1788
KOD 0.5
peat A
peat B
peat C
Base of sequence
Years BP
C
Core depth (cm)
Achnanthes delicatula
Cocconeis scutellum
Martyana martyi
Opephora marina
Fragilaria construens var. venter
Navicula cari var cincta
Navicula digitoradiata
Navicula peregrina
Caloneis bacillum
Diploneis interrupta
Diploneis ovalis
Fragilariforma virescens
Navicula pusilla
Navicula tripunctata
Pinnularia borealis
Pinnularia cruciformis
Pinnularia lagerstedtii
Placoneis elginensis
Synedra ulna
Tabellaria fenestrata
Tabellaria flocculosa
Summary
RSL (m)
sand
peat A
sand
peat B
peat C
20%
100%
Tidal flat
Tidal marsh
Freshwater

Figure 18

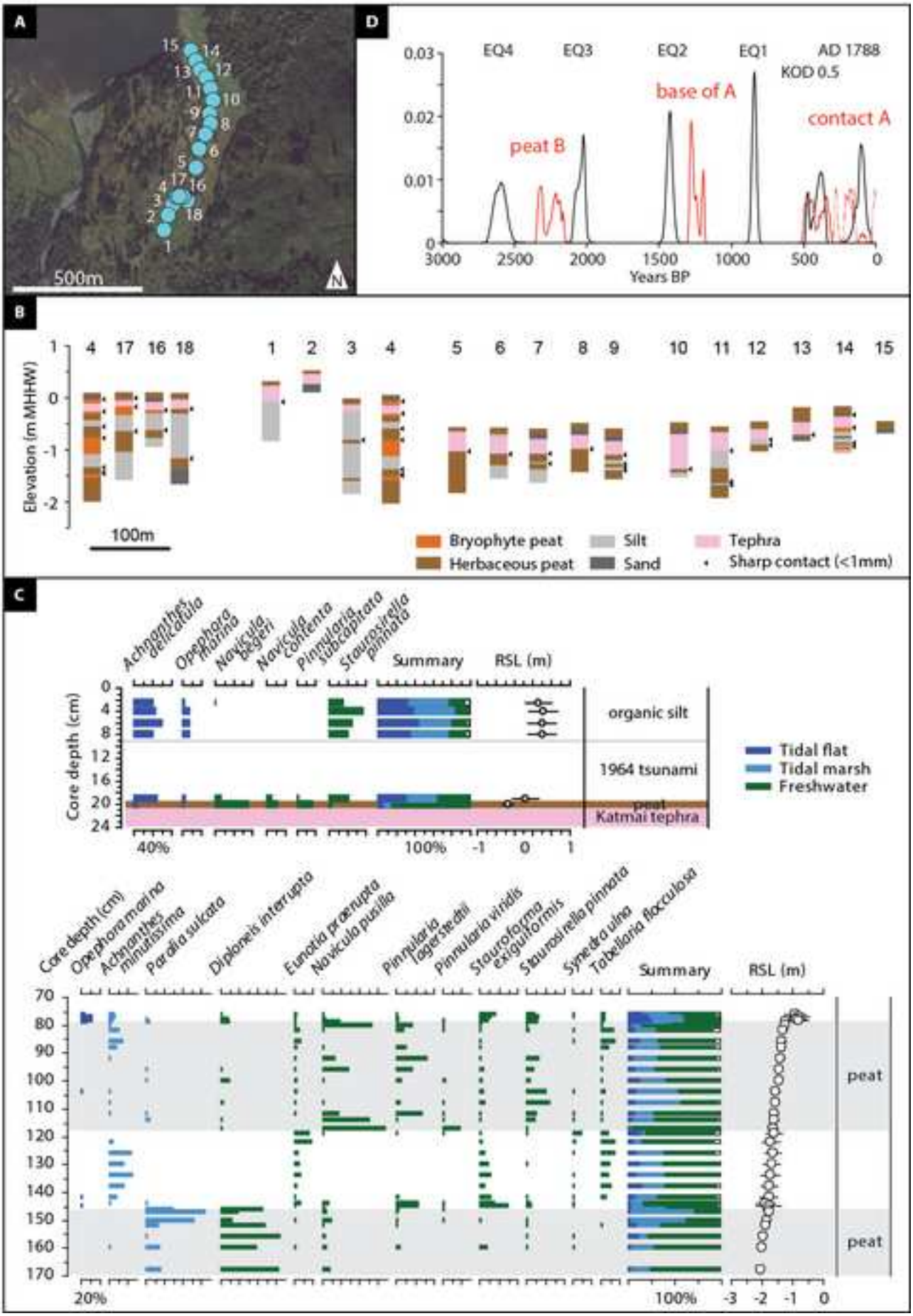
A
500m
N
D
EQ4
EQ3
EQ2
EQ1
AD 1788
KOD 0.5
base of A
contact A
peat B
Years BP
B
Elevation (m MHHW)
100m
Bryophyte peat
Herbaceous peat
Silt
Sand
Tephra
Sharp contact (<1mm)
C
Summary
RSL (m)
Core depth (cm)
organic silt
1964 tsunami
peat
Katmai tephra
Tidal flat
Tidal marsh
Freshwater
40%
100%
20%

Figure 19

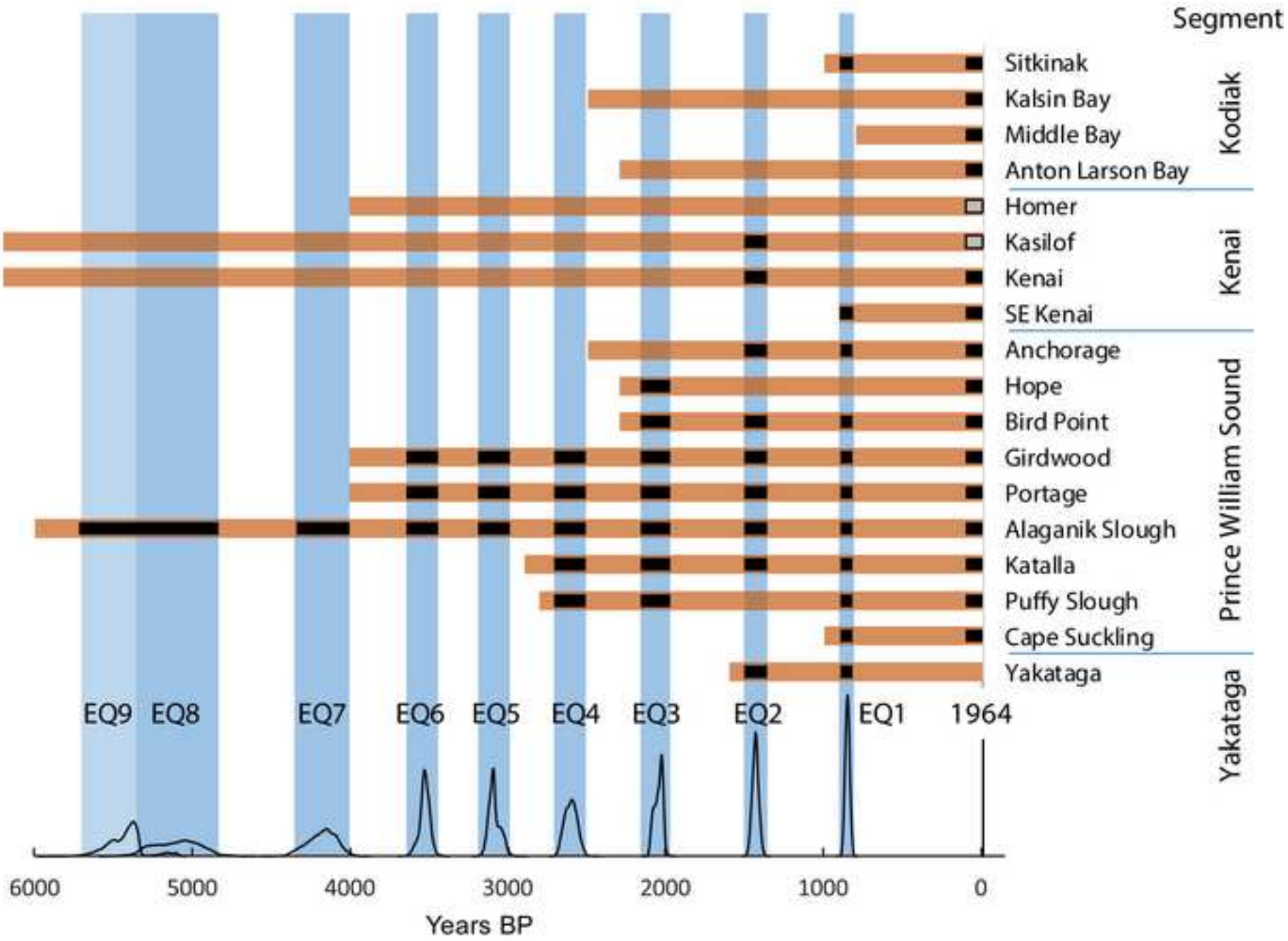
Segment
Sitkinak
Kalsin Bay
Middle Bay
Anton Larson Bay
Homer
Kasilof
Kenai
SE Kenai
Anchorage
Hope
Bird Point
Girdwood
Portage
Alaganik Slough
Katalla
Puffy Slough
Cape Suckling
Yakataga
Kodiak
Kenai
Prince William Sound
Yakataga
EQ9
EQ8
EQ7
EQ6
EQ5
EQ4
EQ3
EQ2
EQ1
1964
6000
5000
4000
3000
2000
1000
0
Years BP

Figure 20

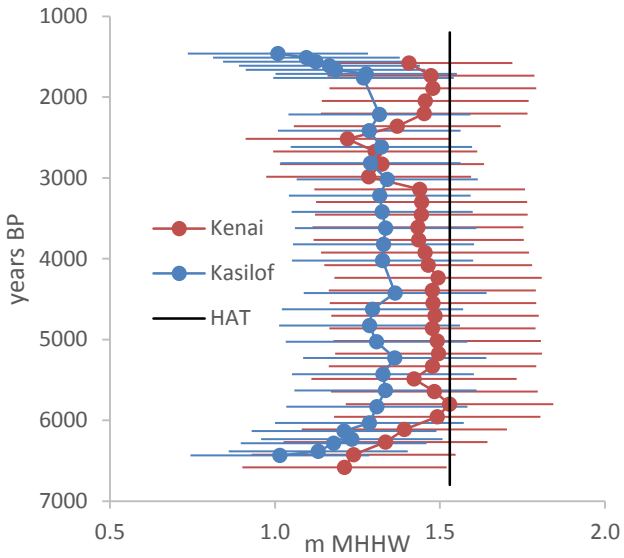
1000
2000
3000
4000
5000
6000
7000
years BP
Kenai
Kasilof
HAT
0.5
1.0
1.5
2.0
m MHHW

Figure 21

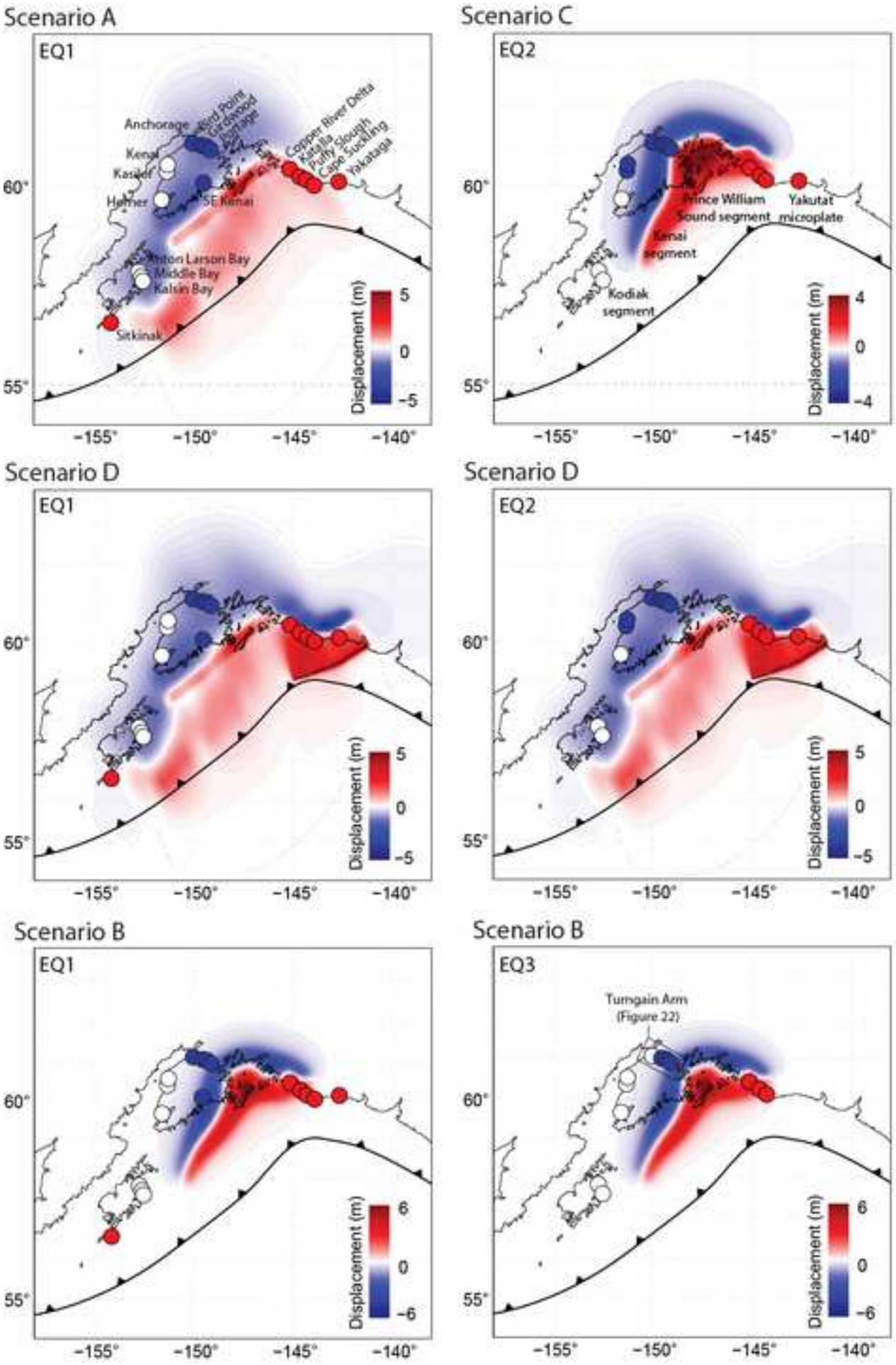
Scenario A
EQ1
Anchorage
Kenai
Kasilof
Homer
Bird Point
Girdwood
Portage
SE Kenai
Copper River Delta
Katalla
Puffy Slough
Cape Suckling
Yakataga
Anton Larson Bay
Middle Bay
Kalsin Bay
Sitkinak
Displacement (m)
5
0
-5
60°
55°
-155°
-150°
-145°
-140°
Scenario C
EQ2
Prince William
Sound segment
Yakutat
microplate
Kenai
segment
Kodiak
segment
Displacement (m)
4
0
-4
Scenario D
EQ1
Displacement (m)
5
0
-5
Scenario D
EQ2
Displacement (m)
5
0
-5
Scenario B
EQ1
Displacement (m)
6
0
-6
Scenario B
EQ3
Turnagain Arm
(Figure 22)
Displacement (m)
6
0
-6